Biopolymer nanocomposites for food and healthcare applications

Miss Tatiya Siripongpreda

A Dissertation Submitted in Partial Fulfillment of the Requirements
for the Degree of Doctor of Philosophy in Nanoscience and Technology
Inter-Department of Nanoscience and Technology
GRADUATE SCHOOL
Chulalongkorn University
Academic Year 2022

นาโนคอมพอสิตของพอลิเมอร์ชีวภาพสำหรับประยุกต์ใช้ด้านอาหารและสุขภาพ

น.ส.ตติยา ศิริพงศ์ปรีดา

วิทยานิพนธ์นี้เป็นส่วนหนึ่งของการศึกษาตามหลักสูตรปริญญาวิทยาศาสตรดุษฎีบัณฑิต
สาขาวิชาวิทยาศาสตร์นาโนและเทคโนโลยี สหสาขาวิชาวิทยาศาสตร์นาโนและเทคโนโลยี
บัณฑิตวิทยาลัย จุฬาลงกรณ์มหาวิทยาลัย
ปีการศึกษา 2565

Thesis Title	
By	Miss Tatiya Siripongpreda
Field of Study	Nanoscience and Technology
Thesis Advisor	Dr. NADNUDDA RODTHONGKUM

Accepted by the GRADUATE SCHOOL, Chulalongkorn University in Partial Fulfillment of the Requirement for the Doctor of Philosophy

.... Dean of the GRADUATE
SCHOOL
(Associate Professor YOOTTHANA
CHUPPUNNARAT, Ph.D.)

DISSERTATION COMMITTEE

.... Chairman
(Associate Professor Dr. VUDHICHAI PARASUK)
.... Thesis Advisor
(Dr. NADNUDDA RODTHONGKUM)
.... Examiner
(Assistant Professor Dr. RATTHAPOL RANGKUPAN)
.... Examiner
(Associate Professor Dr. NUTTHITA
CHUANKRERKKUL)
.... External Examiner
(Associate Professor Dr. Atitaya Siripinyanond)

ตติยา ศิริพงศ์ปรีดา : นาโนคอมพอสิตของพอลิเมอร์ชีวภาพสำหรับประยุกต์ใช้ด้านอาหารและสุขภาพ. (Biopolymer nanocomposites for food and healthcare applications) อ.ที่ปรึกษาหลัก : ดร.นาฏนัดดา รอดทองคำ

วิทยานิพนธ์นี้มุ่งเน้นที่การพัฒนาไบโอพอลิเมอร์โดยการใช้วัสดุนาโนเพื่อปรับปรุงคุณสมบัติของพอลิเมอร์บริสุทธิ์ในการพัฒนาประสิทธิภาพเพื่อใช้เป็นตัวรับรู้ทางเคมีและแมสสเปกโตรเมตรีสำหรับการควบคุมคุณภาพอาหาร การตรวจติดตามสุขภาพและการประยุกต์ใช้ด้านชีวการแพทย์ โดยวิทยานิพนธ์นี้แบ่งออกเป็น 4 ส่วน โดยส่วนที่ 1 พอลิแลคติคแอซิดและเซลลูโลสถูกนำมาใช้ในแพลตฟอร์มแบบคู่สำหรับตรวจวัดไบโอเจนิคเอมีนจากอาหารเสีย ฟิล์มพอลิแลคติคแอซิดที่มีรูพรุนสูงถูกเตรียมโดยการเพิ่มแคลเซียมคาร์บอเนตขนาดนาโนทำให้มีความสามารถในการกักเก็บสารสำหรับตัวรับรู้ในปริมาณสูง โดยอีกด้านหนึ่งของแพลตฟอร์ม เซลลูโลสบริสุทธิ์ถูกนำมาปรับปรุงโดยใช้แกรฟีนออกไซด์และใช้เป็นวัสดุรองรับสำหรับแมสสเปกโตรเมตรี โดยแพลตฟอร์มแบบคู่นี้ถูกนำไปใช้ในสำหรับการตรวจติดตามคุณภาพอาหาร ส่วนที่ 2 ไฮโดรเจลของแบคทีเรียนาโนเซลลูโลสที่มีความสามารถในการขยายตัวและอัตราการบวมตัวสูงถูกประดิษฐ์ขึ้นโดยการใช้คาร์บอกซีเมทิล เซลลูโลสดัดแปรโครงข่ายของนาโนเซลลูโลส และไฮโดรเจลที่ได้ถูกนำไปใช้สำหรับการวัดเชิงสีของความเป็นกรด-ด่างและกลูโคสในเหงื่อ ส่วนที่ 3 พื้นผิวของคอนแทคเลนส์ที่ขายในเชิงพาณิชย์ ถูกนำมาปรับปรุงโดยใช้นาโนคอมโพสิตที่ประกอบด้วยยาเลโวฟล็อกซาซินและเซลลูโลสนาโนไฟบริล เพื่อสร้างคอนแทคเลนส์ที่มีความสามารถในการรักษาและวินิจฉัยโรคในคราวเดียวกัน สำหรับโรคตาติดเชื้อ โดยเซลลูโลสนาโนไฟบริล ช่วยในการการกักเก็บยา ความชุ่มชื้น และเพิ่มความไวต่อค่าความเป็นกรด-ด่างให้กับคอนแทคเลนส์ โดยคอนแทคเลนส์ที่ได้สามารถที่จะปลดปล่อยยาเลโวฟล็อกซาซินในปริมาณที่เหมาะสมตามความรุนแรงของการติดเชื้อ คอนแทคเลนส์ที่มีความสามารถในการรักษาและวินิจฉัยโรคในคราวเดียวกันที่ถูกพัฒนาขึ้นยังสามารถบ่งบอกถึงความรุนแรงของการติดเชื้อโดยใช้การวัดเชิงสีความเป็นกรด-ด่าง สุดท้าย ส่วนที่ 4 ไคโตซานถูกรวมกับนาโนคอมโพสิตของไทเทเนียมไดออกไซด์และแกรฟีนออกไซด์ที่เจือด้วยไนโตรเจนเพื่อเพิ่มความสามารถในการดูดกลืนเลเซอร์และการคายการดูดซับเพื่อเพิ่มความสามารถในการแตกตัวเป็นไอออนของสารที่ต้องการวิเคราะห์โดยไม่ต้องใช้สารการดูดกลืนเลเซอร์เพิ่มเติมและนำใช้เป็นวัสดุรองรับชนิดใหม่ในสำหรับแมสสเปกโตรเมตรีสำหรับการตรวจวัดสารชีวโมเลกุล

สาขาวิชา	วิทยาศาสตร์นาโนและเทคโนโลยี	ลายมือชื่อนิสิต
		....
ปีการศึกษา	2565	ลายมือชื่อ อ.ที่ปรึกษาหลัก
		....

6087768420 : MAJOR NANOSCIENCE AND TECHNOLOGY
KEYWOR   Nanocomposites, Food, Healthcare, Nanomaterials, Biopolymers
D:

Tatiya Siripongpreda : Biopolymer nanocomposites for food and healthcare applications. Advisor: Dr. NADNUDDA RODTHONGKUM

This dissertation focuses on development of biopolymers by integrating nanomaterials to improve the properties of pristine polymers for enhancing the performances of chemical sensors and laser desorption/ionization mass spectroscopy (LDI-MS) applied for food quality control health monitoring and biomedical applications. The dissertation is divided into 4 parts: the first part, polylactic acid and cellulose were used for dual detection platform of biogenic amines for food spoilage indication. Highly porous PLA film is fabricated by adding nanosized calcium carbonate resulted in high sensing element entrapment. On another side of platform, pristine cellulose is modified with graphene oxide and exploited a substrate for LDI-MS. This dual platform is used for food quality monitoring. The second part, a bacterial nanocellulose hydrogel with reswelling ability and high swelling ratio is fabricated by introducing carboxymethyl cellulose into the nanocellulose network, and the obtained hydrogel is used as a colorimetric sensor for sweat pH and glucose. The third part, the surface of a commercial contact lens is modified with nanocomposite composed of levofloxacin and cellulose nanofibrils to create a theranostic contact lens for ocular infection, which the cellulose nanofibril helps improving drug entrapment, wettability and pH-sensitiveness to the pristine contact lens in order to control the releasing amount of levofloxacin depending on infection severity. The developed theranostic contact lens also indicates severity of infection by colorimetric pH sensor. Lastly, fourth part, chitosan is incorporated with developed titanium dioxide/nitrogen-doped graphene nanocomposites to enhance laser-absorbing and desorption property, leading to enhanced ionization efficiency of analytes without using an additional matrix, and utilizes as a novel substrate of LDI-MS for biomolecules determination.

CHULALONGKORN UNIVERSITY

Field of Study:	Nanoscience and Technology	Student's Signature ....
Academic Year:	2022	Advisor's Signature ....

ACKNOWLEDGEMENTS

TABLE OF CONTENTS

Page

จุฬาลงกรณ์มหาวิทยาลัย
CHULALONGKORN UNIVERSITY

TABLE OF FIGURES

จุฬาลงกรณ์มหาวิทยาลัย

CHULALONGKORN UNIVERSITY

LIST OF TABLES

CHAPTER I
INTRODUCTION

1.1 Introduction

Biopolymers are found to be useful in various applications, for example, food packaging and biomedical applications (e.g., drug delivery and sensors), because they are biocompatible and biodegradable. For example, polylactic acid has been used as an alternative bioplastic for food packaging [1] since it has proper rigidity, impact and tensile strength, barrier properties and biodegradability [2]. Cellulosic materials are one of the most abundant polymers in nature appear in many forms. Bacterial cellulose exhibits high mechanical strength, high water absorption capacity, and fine fiber networks [3] so, it can be used in food, cosmetics, biomedical and drug delivery industries [4]. Cellulose can be processed into cellulose nanofibrils having good mechanical properties, biocompatibility, and tailorable surface chemistry making it a potential material for biomedical including tissue engineering and wound dressings [5].

To increase their versatility of biopolymer utilization, one approach is a nanotechnology integration-the application of nanomaterials. The combination of biopolymers and nanomaterials have physical and chemical properties that are significantly different from the macroscale materials, that can improve or change the properties of the polymer matrices. This is able to fabricate the novel biocompatible polymers having attractive properties with desired physical and chemical properties that can expand the usage of polymer nanocomposites.

An accurate expiration for smart food packaging has been gained attention in food industry to reduce consumer's health risks from low-quality foods and food wastes disposal. Polylactic acid or PLA is a biodegradable and biocompatible polymer that can be used food packaging because of its easy processability, and commercially availability. PLA can be designed as highly porous films by adding calcium carbonate nanoparticles to increase porosity of the films resulting in high sensing element entrapment and offered high sensitivity to the fabricated food sensor. The porous structure offers high surface area to entrap sensing element and the film can be applied as on-packaging sensor.

Non-invasive wearable chemical sensors are attractive technology that facilitate remote health/in home-based monitoring, offer real-time information, and can be used without training. Biocompatible polymers, nanosized cellulose, are potentially materials for biomedical application since it has good mechanical properties due to its nano-sized fiber, and non-toxicity. Bacterial cellulose (BC) is a natural cellulose nanofiber hydrogel with good mechanical, high-water absorption and holding capability, however, BC lacks of re-swellability. Thus, tuning the properties of pristine BC, the developed BC was found to be a promising biocompatible substrate for enzymatic-based sensors since it has ability to preserve enzymes, and exhibits high biofluid absorption for a non-invasive diagnostic platform for sweat or other secretions.

Commercial contact lens was modified using cellulose nanofibrils to fabricate a theranostic contact lens for ocular infection. The polymer-based contact lens was chosen because it is wearable and made of 3D-network polymers providing biocompatibility and high-water absorption. These characteristics benefit ability to immobilized sensing elements and drug molecules. Cellulose nanofibrils was selected to enhance theranostic performance by increasing wettability, drug entrapment and acid-responsiveness due to its abundant functional groups. The theranostic contact lens was successfully designed for simultaneous tear pH measurement and releasing drug.

Moreover, this thesis also proposed chitosan-based thin film substrates for LDI-MS. Since chitosan is a cationic polymer with film-forming ability, chitosan is suitable for using as a carrier for the synthesized titanium dioxide/nitrogen-doped graphene nanocomposites. This chitosan-based thin film with laser-absorbing nanocomposites was able to be used for biomolecule determination using LDI-MS.

Herein, properties of pristine polymers were altered or improved by utilizing nanomaterials, i.e., graphene oxide, calcium carbonate nanoparticles, and cellulosic nanofibers, to be suitable for sensor, theranostic, and LDI-MS applications, for example, porous structure, laser-absorption ability, water absorption, and wettability.

In summary, this thesis focuses on designing biopolymer nanocomposite and utilizing nanomaterials to enhance performance of the chemical sensors for food quality control, health monitoring and biomedical applications.

1.2 Objectives

To design and prepare biopolymer nanocomposite-based chemical sensors for food safety and healthcare applications in 4 different platforms:

1. Dual on-package biogenic amine determination platform for quality control using colorimetric sensor and LDI-MS
2. Non-invasive wearable sensors for sweat pH and glucose based on bacterial cellulose
3. Theranostic contact lens for ocular bacterial infection based on cellulose nanofibrils
4. Titanium dioxide/N-doped graphene nanocomposite-chitosan film for LDI-MS detection of peptide biomarkers

1.3 Scope of research

This dissertation focuses on development of biocompatible polymeric nanocomposites for chemical/bio sensors and theranostic application. For food spoilage sensor, the sensor was developed to detect biogenic amines released from food decomposition by using graphene oxide and calcium carbonate nanoparticles for a quantitative and qualitative detection, respectively. For health monitoring wearable sensor, bacterial nanocellulose/carboxymethyl cellulose composite was created as a biocompatible hydrogel with high mechanical and re-swellability then, used for a sweat sensor due to its ability to absorb large amount of sweat sample. Cellulose nanofibrils/antibiotic drug nanocomposite was synthesized and applied for theranostic contact lens to indicate severity of eye infection and release proper dose of antibiotic drug depending on disease severity. Lastly, titanium dioxide/N-doped graphene nanocomposite-chitosan film was fabricated and used as an LDI-MS matrix for peptide biomarkers.
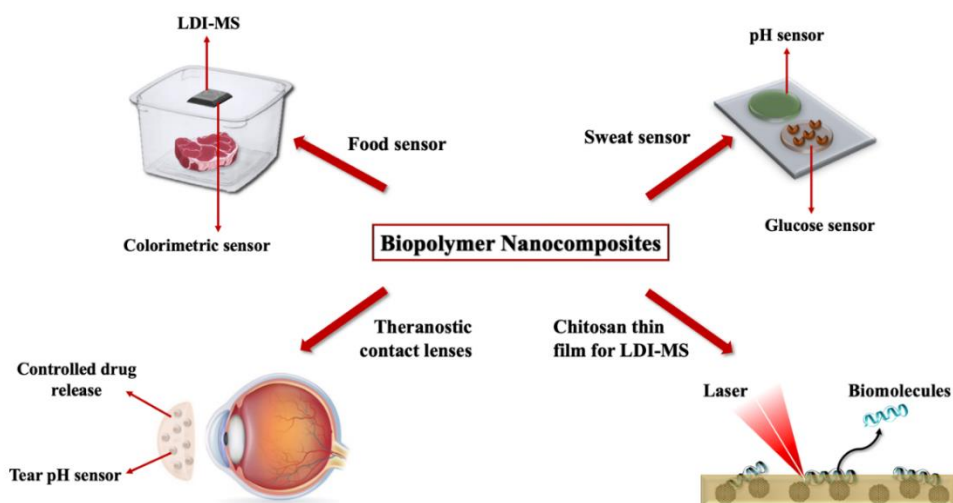
Figure 1.1 Schematic overview of the dissertation

CHAPTER II
THEORY AND LITERATURE REVIEW

2.1 Graphene and derivatives

2.1.1 Graphene

Graphene (G) is a monolayered carbon-based nanomaterial composed of sp^2-bonded in a honeycomb lattice. G possesses remarkably high electron mobility at room temperature and good mechanical properties which its approximate stiffness of 300–400 N/m, a breaking strength of 42 N/m, and Young's modulus 0.5–1.0 TPa, according to previous researches [6-8]. G can be reduced, oxidized, doped or functionalized to obtain different allotropes having different properties, suitable for different applications [9].

2.1.2 Graphene oxide

Graphene oxide (GO) is one of graphene derivatives derived by oxidation resulting in altered function apart from pristine graphene. GO has abundant active oxygen-containing functional groups (e.g., epoxide, carboxylic and hydroxyl), leading to higher hydrophilicity compared to G, and ability to be functionalized by small molecule or polymer intercalation [10, 11]. The functional group on GO sheets offer reaction sies for interaction with small molecules, polymers, biomacromolecules, and inorganic nanoparticles [12, 13]. The structures of G and GO prepared by oxidation were shown in **Figure 2.1**.
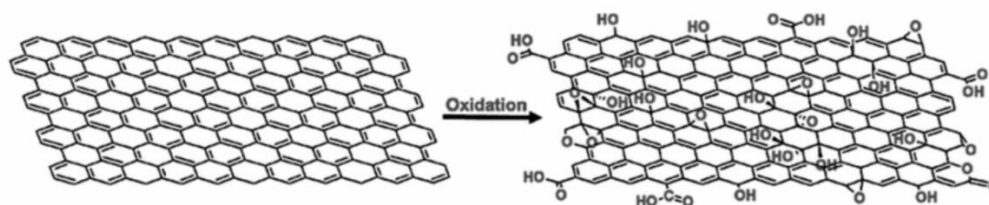
Figure 2.1 Graphene and graphene oxide synthesized from oxidation reaction [10].

2.1.3 Nitrogen-doped graphene

Nitrogen-doped graphene (NG) is graphene sheets with nitrogen (N) containing groups (i.e., quaternary N or graphitic N, pyridinic N and pyrrolic N), as shown in

Figure 2.2 [14, 15]. The NG presents different properties compared to graphene. For example, carbon charge distribution that are influenced by the nitrogen dopants inducing activation regions on the pristine graphene, and high positive atomic charge density [16].
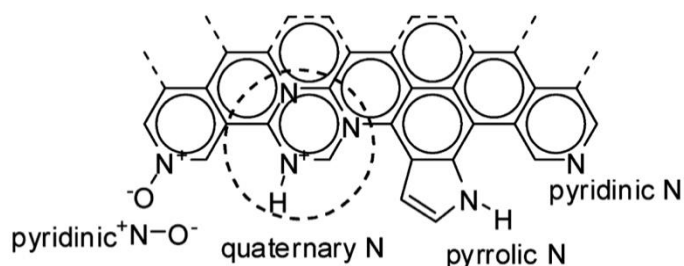
Figure 2.2 Schematic illustration of nitrogen-doped graphene [14].

2.2 Calcium carbonate

Calcium carbonate ($CaCO_3$) is the carbonic salt of calcium appearing as fine, white and odorless power. $CaCO_3$ existed in 3 polymorphic forms, calcite, aragonite and vaterite, which calcite is the most stable polymorph [17]. $CaCO_3$ is insoluble in water but found to be soluble in acid condition. Otherwise, $CaCO_3$ exhibits hygroscopicity, the ability of solids to adsorb moisture microscopically [18], which $CaCO_3$ exists as mono-, hexahydrate or anhydrous, depending on its polymorphic forms [19].
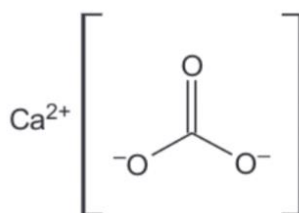
Figure 2.3 Chemical structure of calcium carbonate [19].

2.3 Nanocellulose

Cellulose is a renewable and sustainable material that can be obtained from plants, algae, tunicates, and cellulose-producing bacteria, for example acetobacter. It is composed of D-glucose units linked with β-1,4-glycosidic bonds. Nanocellulose

can be synthesized from native cellulose via pre-treatments of cellulose sources and acid hydrolysis, respectively (**Figure 2.4**). Nanocellulose can be divided into various forms, which are cellulose nanofibrils, cellulose nanocrystals, and bacterial cellulose, depending on cellulose origins, processing, and pre- or post-treatments [20].
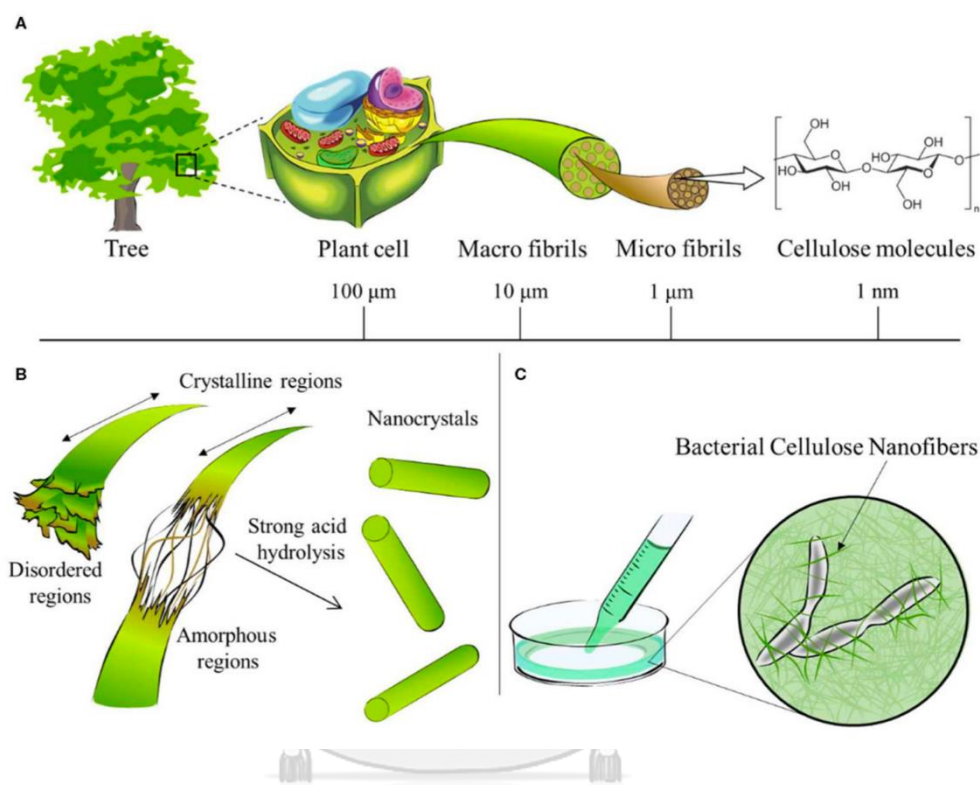
Figure 2.4 A) Various sizes of cellulose extracted from biomass, B) Schematic diagram of nanocellulose preparation, and C) Bacterial cellulose from cellulose-producing bacteria [21].

2.3.1 Bacterial cellulose

Bacterial cellulose (BC) is a three-dimensional structure of cellulose nanofibrils synthesized extracellularly by cellulose-producing bacteria. BC demonstrates high water-holding, capacity high crystallinity (84%–89%), high surface area with fiber diameter of 20–100 nm, and high tensile strength with Young's modulus of 15–18 GPa [22]. BC-based nanocomposites can be produced by using 2 approaches, disturbed BC network or undisturbed BC network. The disturbed BC network method requires BC disintegration before using it to form nanocomposites,

however, the undisturbed BC network method maintains the original BC network structure. The undisturbed network method is exploited to enhance properties of BC for the nanocomposite formation while maintaining the highly porous 3D-structure network of BC [23].

2.3.2 Cellulose nanofibrils

Cellulose nanofibrils (CNF) can be prepared from native cellulose using various methodologies, for instance, high pressure homogenization, ultrasonic treatment, milling, and etc. CNF exhibited excellent mechanical properties and good biocompatibility with large surface area and hydroxyl groups. Since CNF has abundance of hydroxyl groups, the CNF surface modification mainly rely on 2 modification methods: the surface adsorption modification and the chemical grafting [24].

2.4 Titanium dioxide

Titanium dioxide (TiO_2) is inorganic materials widely used as a n-type semiconductor and for photocatalytic application. TiO_2 occurs in 3 different polymorphs, which are rutile, anatase, and brookite. TiO_2 consists of TiO_6 octahedra with different distortion (**Figure 2.5**) where Ti–O bonds play significant roles the properties of different polymorphs, for example, structural and electronic properties (e.g., band gap) [25, 26]. Normally, rutile is stable but, in the solution, anatase structure is more favorable. This is related to surface energy, especially in nano-scale particles, which the surface energy of anatase is lower than rutile and brookite [27]. Nano-sized TiO_2 can be applied in various applications, for instance, photovoltaic cells, environmental, biomedical applications, biosensing, and drug delivery [28].
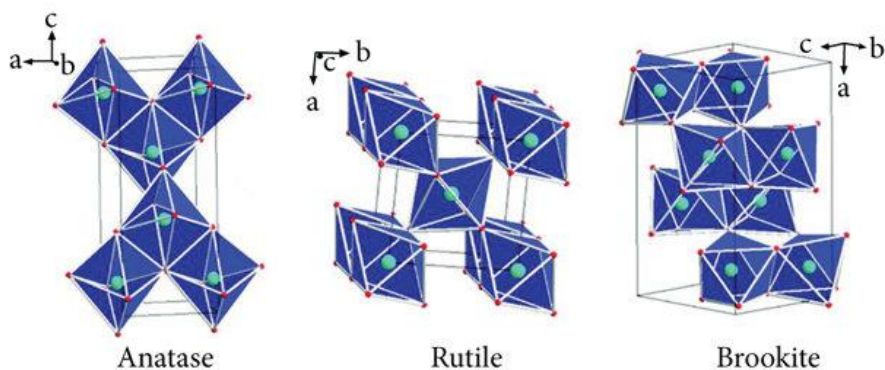
Figure 2.5 Common polymorphs of TiO_2 [29].

2.5 Laser Desorption/Ionization Mass Spectrometry

Mass spectrometry (MS) is an analytical tool applied for mass-to-charge ratio (m/z) measurement of analytes and presents the data output as spectrum. This technique is based on generating multiple ions from the sample using electron ionization to separate the ions derived from the specific mass-to-charge ratio (m/z) then, measure ion abundance of each ion species. Laser Desorption/Ionization Mass Spectrometry (LDI-MS) is a soft ionization mass spectrometry technique, commonly employed in MS-based analytical chemistry field because of its universal, sensitive, and quantitative uses [30]. Besides, LDI-MS have been considered as successful analytical method for small molecules [31]. As shown in **Figure 2.6**, the process of LDI-MS is that the laser shines on the sample and ionizes the sample and matrix. The matrix, used for radiation absorption which the analytes are not able to absorb, transfers the energy to the analyte and assists ionization and desorption of the sample [32].
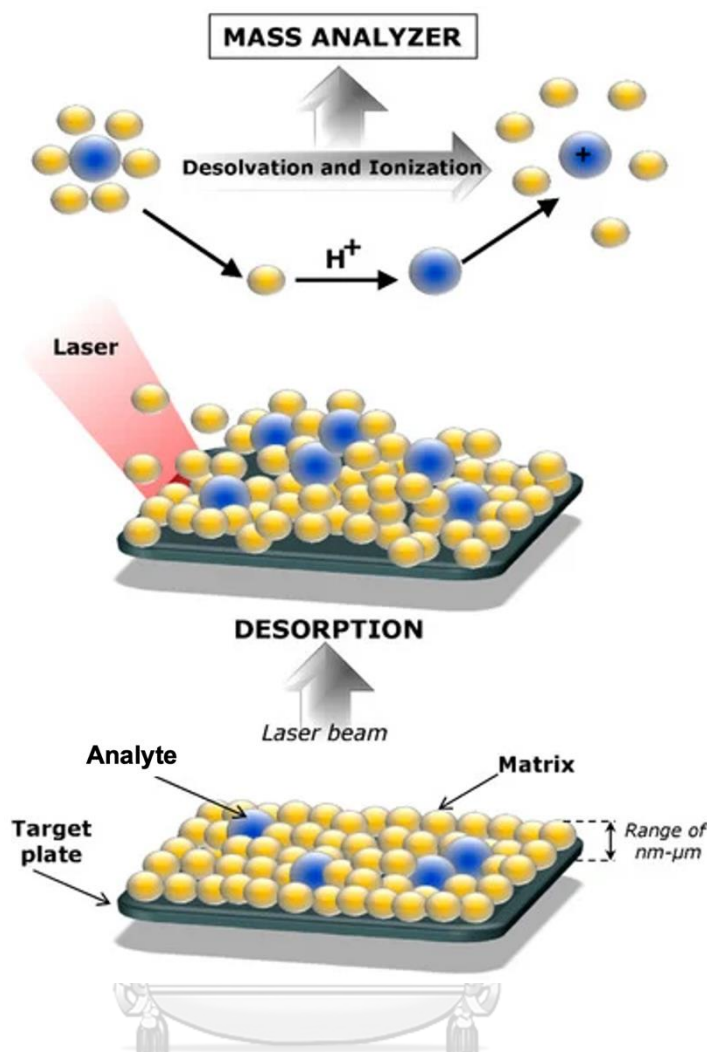
Figure 2.6 Ionization and desorption processes of laser desorption/ionization (adapted from [32]).

จุฬาลงกรณ์มหาวิทยาลัย

CHULALONGKORN UNIVERSITY

Conventional organic matrices commonly used in LDI-MS are α-Cyano-4-hydroxy-cinnamic acid (CHCA) and 2,5-dihydroxybenzoic acid (DHBA). The disadvantages of using organic matrices are that they produce matrix-related peaks in the low molecular-weight region limiting small molecules (m/z < 700 Da) determination [33]. Hence, inorganic nanomaterials have been developed to improve the detection performance of small molecules.

2.5.1 Graphene and derivatives as an alternative matrix for LDI-MS

Nanoparticle-assisted LDI-MS have gained more attention and considered as a promising technique because the using of nanomaterials as matrices/substrates for

LDI-MS gives low background noise in low m/z region and high reproducibility. Furthermore, this technique is able determine analytes in trace amounts that is resulted from efficient desorption/ionization and also high surface area of the nanomaterials that enrich the analytes [34].

Graphene and derivatives display many advantages over conventional organic matrices. For example, high surface area, simple sample preparation procedures, good reproducibility, high efficiency of desorption/ionization and ability to avoid the fragmentation of analytes [35].

2.6 Chemical sensors and biosensors

Chemical sensors are devices that convert chemical or physical properties of analytes into analytically measurable signals, that is normally to the analyte concentration [36]. The typical principle of a chemical or biochemical sensor was illustrated in **Figure 2.7**. The main functional units of the chemical sensors are recognition unit (chemical recognition phase with receptor elements) and transducer unit. The recognition unit is the part that interacts with or respond to analyte molecules then, the transducer translates the chemical interaction into signals, which a transduction element can be electrochemical, optical, and etc. [37, 38].
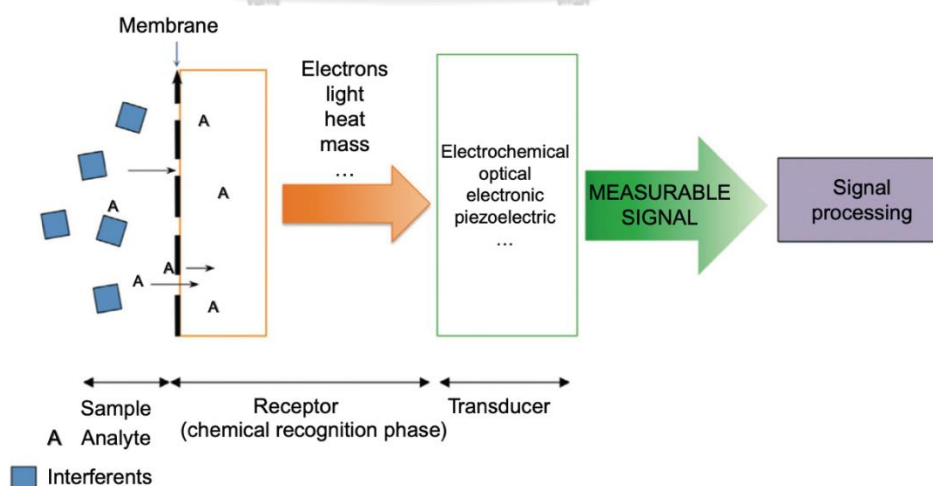
Figure 2.7 Schematic diagram of the working principle of a chemical or biochemical sensor [37].

2.6.1 Colorimetric sensors

Colorimetric sensors show potential toward the detection of biomolecules, ions, and other substances since they are easy to fabricate, exhibit high sensitivity and selectivity, rapid detection, and easy naked-eye sensing [39]. Typically, colorimetric sensors can be categorized depending on the interaction of analyte molecules: chemical and biomolecules. They are classified as chemical sensors and biosensors, respectively [40].
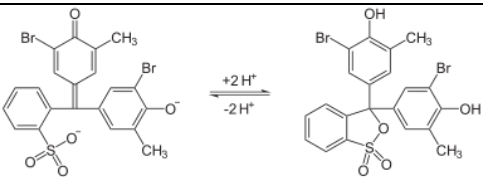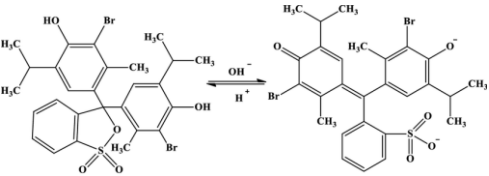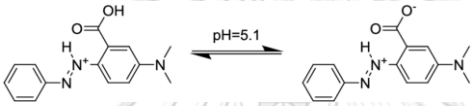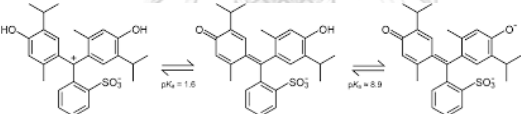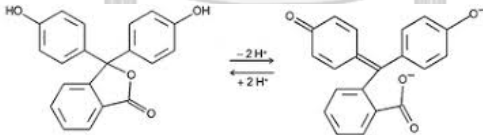
2.5.2 pH sensitive dyes

pH sensitive dyes or pH indicators are a moderately weak acids or bases exist as natural dyes using for indicate the H^+ concentration (or pH) by color changes since the ionic forms of the indicators show a color and constitution different from the neutral form. In aqueous solution, the following equilibrium represents the acid-base pair HI/I^-, where HI is an indicator acid and I represents indicator base form [41]:

$$HI + H_2O \rightarrow I^- + H_3O^+$$
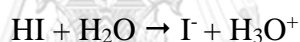
The examples of pH indicators were displayed in **Table 2.1**.

Table 2.1 pH indicators and their molecular structures

pH indicator	Molecular structure under pH changes	pH Transition	Ref.
Bromocresol purple		5.2 - 6.8	[42]
Bromothymol blue		6.0 - 7.6	[43]
Methyl red		4.4 - 6.2	[41, 44]
Thymol blue		1.2 -2.8 8.0 - 9.6	[41]
Phenolphthalein		8.0 -10.0	[41]

2.6.3 Cetyltrimethylammonium bromide

Cetyltrimethylammonium bromide (CTAB) is a cationic quaternary ammonium surfactant which its structure was shown in **Figure 2.8**. CTAB has been used to prevent dye leaching from textiles by forming micelles. Nadtinan *et. al.* (2019) introduced CTAB in the pH indicator mixture for color fading prevention and used as sweat sensor. The research reported that CTAB has ability to improve the interaction between its cations and anionic indicator dyes and results in the micellar structures formation that enhance durability of the color of the fabricated sensor [45].
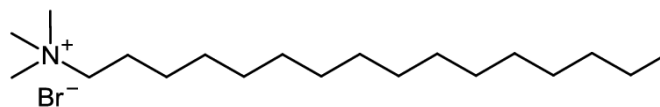
Figure 2.8 Chemical structure of CTAB [46].

2.6.2 Enzymatic glucose sensor

Glucose is a major energy source for cellular activity and commonly used a target analyte since diabetes mellitus, glucose-related metabolic disorders, is one of the most significant chronic diseases around the world. Thus, personal monitoring and also control of the blood glucose level are crucial for an effective medical care that leads to rapidly and continuously development of glucose sensors [47].

The system of the enzymatic glucose sensor applied in this thesis based on bienzymatic H_2O_2–induced potassium iodide (KI) color development. The oxidation reaction of glucose molecules is catalyzed by glucose oxidase (GOx) to produce hydrogen peroxide (H_2O_2) and gluconic acid while, horseradish peroxidase (HRP) catalyzes the hydrogen peroxide and KI reaction to produce iodine (I_2) displaying brown color. The cascade bienzymatic reaction of glucose was showed below [48, 49]:

$$Glucose + O_2 + H_2O + GOx \text{ (enzyme)} \rightarrow H_2O_2 + gluconic\ acid$$
$$H_2O_2 + KI + HRP \text{ (enzyme)} \rightarrow H_2O + I_2 \text{ (brown color)}$$
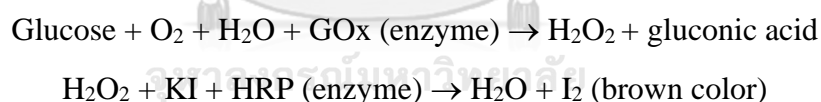
2.7 Non-invasive wearable sensors

Non-invasive wearable sensors have rapidly developed since they provide health/in home-based health monitoring and provide real-time health information, moreover, they can be used without special training.

2.7.1 Sweat

Recently, sweat has become a biofluid for non-invasive medical diagnostic for clinical identification of diseases since it contains minerals, and other biomarkers that are found in blood, for example, glucose. In addition, levels of several biomarkers in

sweat are well correlated with the values that found in blood, the conventional biofluids using for medical diagnostic [50].

2.7.2 Tear

Tear is an extracellular fluid covering the ocular surface [51]. Tear pH is one of physio-chemical properties that can be used to determine the health condition of eyes. According to previous report, normal tear pH is ranging from 6.5 to 7.6 [52], and the average value is approximately 7.4 [53]. The shifting of tear pH to acidic pH is related to various causes, for instance, conjunctival metabolism, and carbon dioxide level as well as the microbial infections [54].

2.6 Smart food packaging

Food packaging is normally utilized as a barrier for food protection, and according to specific requirements of specific type of food, superior quality packaging materials has been developed [55]. Smart food packaging is new technology that is newly developed by integrating sensors into the food packaging, such as, chemical sensor or biosensor to monitor food quality. The sensors can be designed to determine freshness, pathogens, leakage, carbon dioxide, oxygen, pH, or temperature. Thus, smart food packaging is highly needed to control food quality to prevent adverse effect to consumers and also to meet food regulations [56].

2.6.1 Polylactic acid

Polylactic acid (PLA) is a versatile, biodegradable polymer obtained from renewable resources that is considered as an alternative material to petrochemical-based plastics. PLA has been used in many applications, for instance, coating, fibers, films, and packaging [57]. The chemical structure of PLA can be seen in **Figure 2.9**.
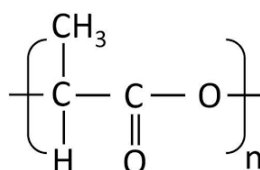
Figure 2.9 Chemical structure of polylactic acid (PLA) [58].

2.6.2 Porous structure film formation: Breath-figure self-assembly

Breath figure self-assembly method is a process of porous film formation that is widely used since it is simple, easy implementation with no complex setup and low-cost [59, 60]. The mechanism of porous structure formation via breath-figure self-assembly was shown in **Figure 2.10**. First, the surface of polymer solution dissolved in organic solvent offers the cold surface (step 1) since the endothermic evaporation of the solvent decreases the temperature of solution. Then, water droplets from high humidity environment contact with cold surface of the solution leading to water condensation on solution surface to form close-packed array (step 2-3). After that, the porous structure is formed (step 4). In order to obtained 3D array, the new water droplets deposit on the cold surface to form the array again (step 5-6). Lastly, after the organic solvent is completely evaporated, the 3D porous structure film is formed (step 7) [61].
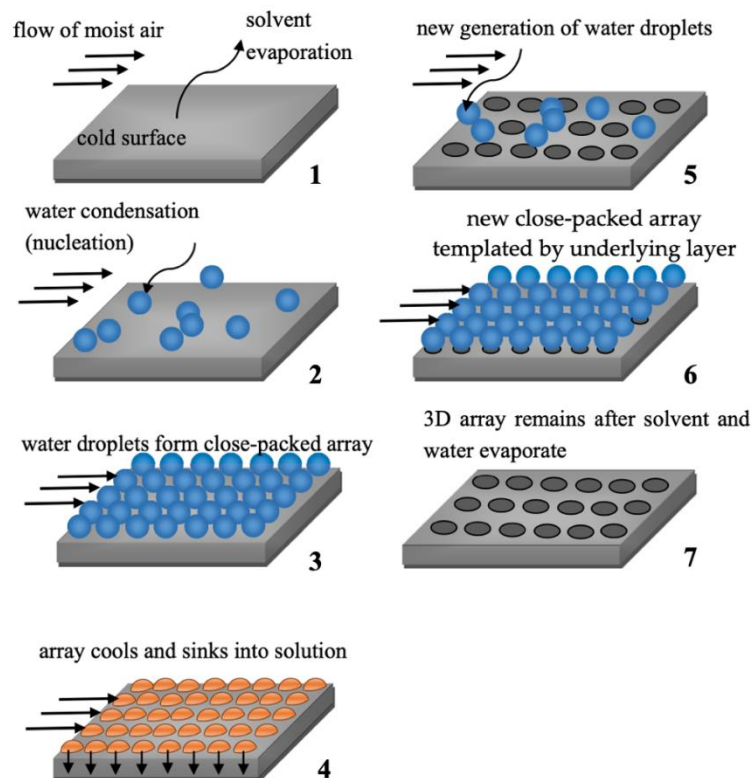
Figure 2.10 Mechanism of breath-figure self-assembly resulting in porous structures formation [62].

2.6.3 Biogenic amines

Biogenic amines are basic nitrogenous compounds produced by bacterial decarboxylation of amino acids in foods. As expected, all proteins containing foods or free amino acids can be raw materials to create the biogenic amines, for example, fish products, meat products, dairy products, including alcoholic beverages, vegetables, fruits, and nuts. Because of the generated biogenic amines concentration from foods is depended on hygienic of materials, microbial composition, fermentation condition and duration [63, 64]. Thus, biogenic amines can be used as indicator for food quality determination.

2.6.4 Putrescine and Cadaverine

Putrescine (butane-1,4-diamine, PUT) and cadaverine (pentane-1,5-diamine, CAD) is formed by the decarboxylation of ornithine and arginine, and lysine, respectively. In previous report, putrescine and cadaverine illustrated potential indirect toxic effects to human by potentiating the toxicity of other biogenic amines. Moreover, they have been considered as precursors of carcinogenic substances and also involved in the oncogenic process [65].
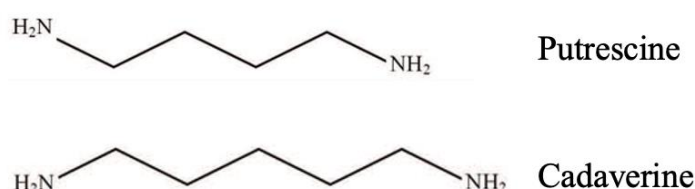
Figure 2.11 Chemical structure of putrescine and cadaverine [66].

2.7 Hydrogel

Hydrogels are water-insoluble three-dimensional polymer networks prepared from crosslinking water-soluble polymers. The major characteristic of hydrogels is that they are able to swell and hold large amount of fluids (for example, water) at least 20% and can reach values of 99% by weight, which the hydrogels that have ability to absorb water more than 95% by weight can be considered as superabsorbent.

Hydrogels can be divided into 2 types according to preparation process: physical crosslinking and chemical crosslinking [67, 68]. The equilibrium swelling ratio of hydrogels is used to illustrate the degree of swelling, commonly measured by gravimetric method. The swelling ratio measurement can be achieved by immersing a hydrogel sample in distilled water until the sample reaches equilibrium state, and get rid of the excess water that is not absorb by the sample. Then, the swollen hydrogel sample is weighted. The equilibrium swelling ratio (SR_{eq}) can be calculated using the following equation [69-71]:

$$SR_{eq} = W_s - W_d / W_d$$

where W_s is the weight of swollen hydrogel in equilibrium state

W_d is the initial dry weight of the hydrogel

Since the hydrogels can be respond to various stimuli, for instance, molecular species, ionic strength, pH, and solvent composition, they can be designed and adopted for numerous applications [72].

2.7.1 Carboxymethyl cellulose

Carboxymethyl cellulose (CMC) is a linear anionic cellulose derivative which its repeating units are linked by β-(1→4) glycosidic linkage. In the CMC molecular structure, anionic carboxymethyl groups (i.e., $-CH_2COOH$) replace some original hydroxyl groups on the pristine cellulose. There are many promising characteristics of CMC, such as, biocompatibility surface properties, tunable hydrophilicity, rheological properties, film forming ability, binding, thickening, stabilizing properties [73], as well as stimuli responsive properties [74]. Thus, CMC have been used in numerous industries and adopted for various applications, such as, biomedical, pharmaceutical, textile, construction, food, plastics, cosmetics, paper, and oil industries [73, 75].
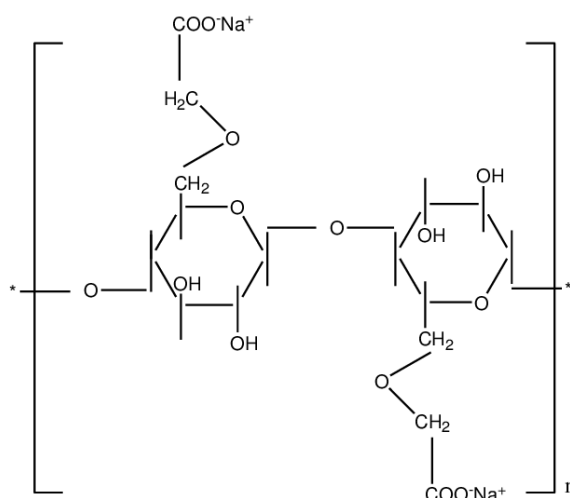
Figure 2.12 Chemical structure of carboxymethyl cellulose [76].

2.8 Contact lens

Contact lenses are ocular prosthetic devices used for vision correction, and cosmetic appearance. Contact lens materials significant affect to contact lens wearers thus, the selection of materials is crucial for maintain a regular corneal metabolism, and to preserve tear film stability in order to reduce adverse effects [77]. Materials that are commonly used for contact lenses fabrication were shown in Figure 2.14. Among various polymers-based hydrogels, the most common materials commercially available in world market are 67% for silicone-based hydrogels and 20% for hydrogels [78] because of their flexibility, and durability. Apart from the conventional purposes of using contact lenses, contact lenses have been developed as a minimally invasive platform for diagnostics and drug delivery [79].
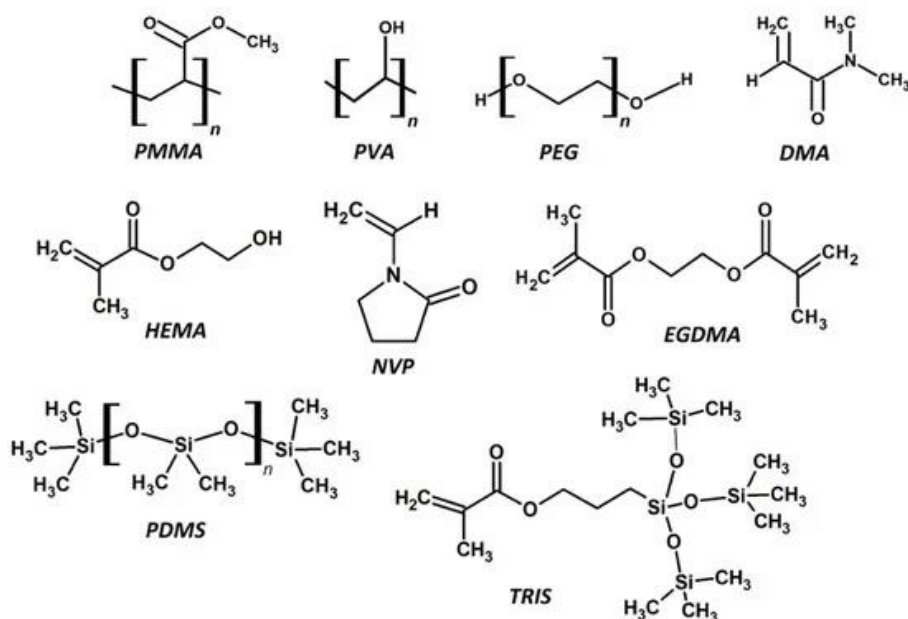
Figure 2.13 The chemical structures of common monomers and polymers utilized in contact lenses manufacturing [80].

2.8.1 Hilafilcon B

Hilafilcon B (molecular formula: $C_{29}H_{43}NO_{10}$) is a hydrogel-based material used for daily uses-soft contact lens production. The Hilafilcon B was developed, and its patent is owned by Bausch & Lomb, USA. The reported water content of Hilafilcon B-based contact lens is 59% [81].
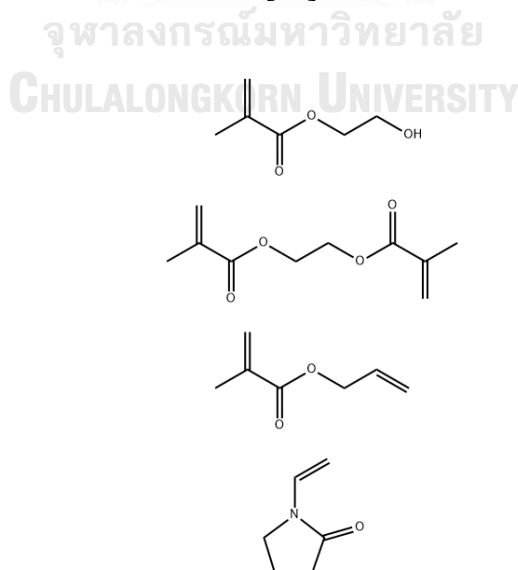
Figure 2.14 Hilafilcon B structure [82].

2.9 Theranostics

      Theranostics is the combination of therapeutics and diagnosis focusing on individual patients care [83]. This technology has been intensively developed since it provides personalized medicine instead of conventional medicine. This leads to appropriate and efficient pharmacotherapy by offering the right dose as part of personalized medicine without unnecessary treatment [84].

2.10 Levofloxacin

      Levofloxacin (LFX) is a fluoroquinolone antibacterial drug that is one of the most commonly used to treat a wide variety of bacterial infection [85]. LFX is considered as a zwitterionic substance since its carboxylic and piperazine amino functional groups in the structure can be charged in solution which depends on pH of the solvent [86].
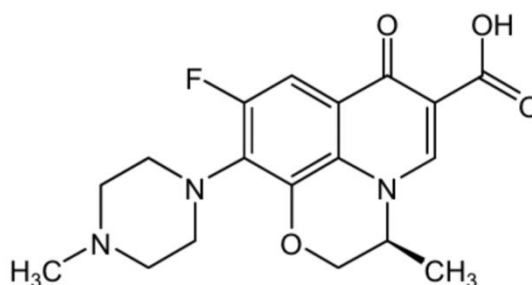
Figure 2.15 Chemical structure of levofloxacin [86].

2.11 Chitosan

      Chitosan (CH) is a cationic deacetylated derivative of chitin having linear polysaccharide of β-(1, 4)-linked N-acetylglucosamine, and contains nucleophilic functional groups: $C-NH_2$, and $C-OH$. CH is insoluble in neutral pH water and most organic solvents but can be dissolved in acidic solutions and considered as a weak polyamine with pKa of 6.5 imparting pH-responsiveness. The pH-sensitive property of CH is from a change in the intramolecular or intermolecular force of the polymer resulting from protonation of amino groups. CH offers good biocompatibility,

biodegradability, non- toxicity, and availability that can be used in numerous application [87-89].
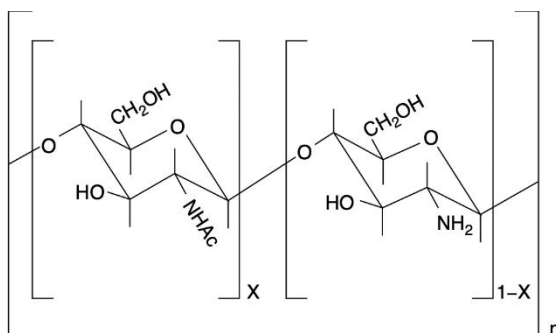
Figure 2.16 Chemical structure of chitosan, where X is degree of acetylation and n is number of units [90].
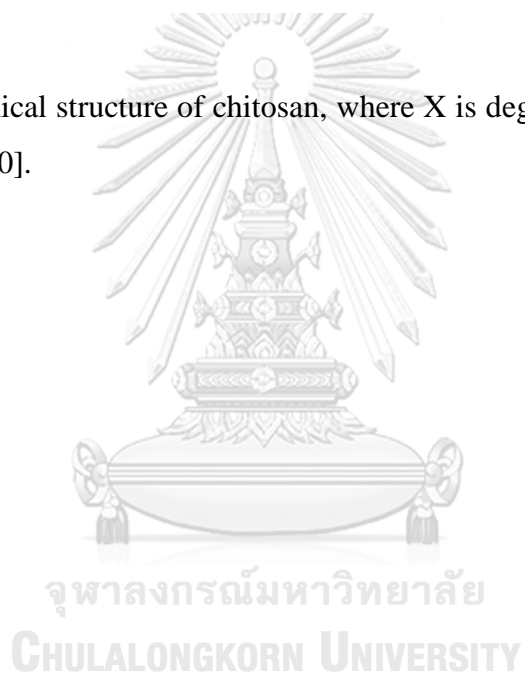
CHAPTER III

Colorimetric sensor and LDI-MS detection of biogenic amines in food spoilage based on porous PLA and graphene oxide

Tatiya Siripongpreda [a], Krisana Siralertmukul[b], Nadnudda Rodthongkum[b*]

[a] Nanoscience and Technology Interdisciplinary Program, Chulalongkorn University, Phayathai Road, Wangmai, Patumwan, Bangkok 10330, Thailand

b Metallurgy and Materials Science Research Institute, Chulalongkorn University, Phayathai Road, Wangmai, Patumwan, Bangkok 10330, Thailand

*Corresponding author e-mail: Nadnudda.R@chula.ac.th

Abstract

Biogenic amines are the important markers for food spoilage, thus, an on-package sensor for biogenic amine detection is crucial for food quality control. A dual detection platform including colorimetry and LDI-MS was developed for screening and quantitative determining of biogenic amines. Porous PLA film, was fabricated using calcium carbonate nanoparticles to enhance film porosity leading to increased surface area of colorimetric sensor. The color intensity significantly increases depending upon the enhanced analyte concentration with a linear range of 2.0–10.0 mg/mL for putrescine, and 0.1–6.0 mg/mL for cadaverine. On another layer, graphene oxide paper was applied as an LDI-MS substrate for sensitive quantification of biogenic amines. LOD values measured on graphene oxide coated side by LDI-MS were found to be 0.07 pM and 0.02 pM for putrescine and cadaverine, respectively. This platform was successfully applied for the detection of biogenic amines in pork samples with satisfactory results.

Keywords: Putrescine, Cadaverine, Food spoilage sensor, Calcium carbonate nanoparticles, Dual detection

Graphical abstract
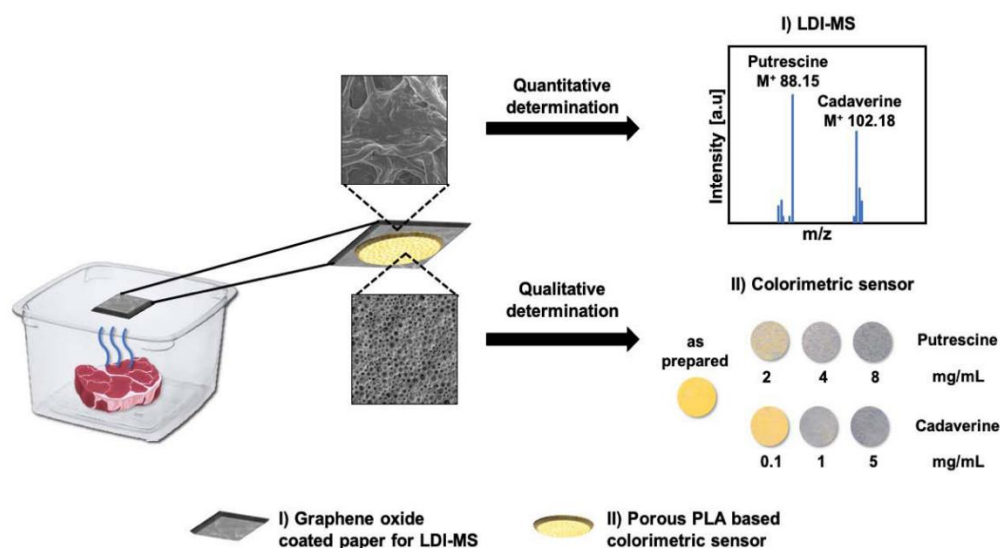
1. Introduction

"Best before" dating is a standard expiration information on food packaging that is mostly used nowadays to prevent consumer's health risks from consuming of low-quality foods. Nonetheless, this approach increases consumer disposal resulting in increased food wastes, which is an international ethical, economic, and environmental issues gained attention from the industrialized countries. Based on these problems, an intelligent packaging that can directly sense the food spoilage is one of the essential tools for controlling of food quality. During the spoilage of foods, biogenic amines are produced from bacterial decarboxylation of amino acids in the food products, in which histamine, tyramine, cadaverine, and putrescine are the most common substances found in meat, fish, dairy products. Since the biogenic amines are generated from spoilage and fermentation, an increasing of such compounds can be used as a quality indicator to indicate the food spoilage [91-94]. Consuming the high content of biogenic amines causes the adverse effects on human health, such as, allergic and carcinogenic effects. The total volatile basic amine (TVBN) level is ≤ 20 mg of generated amines/100 g of meat, considered as acceptable value [95, 96]. Nowadays, putrescine and cadaverine, the amines of concern, is becoming interesting biogenic amines because they are able to promote the toxicological effects of histamine [97]. For raw pork meat, various studies show significant increasing of

cadaverine and putrescine levels during storage [98]. A suggested reasonable biogenic amine index (BAI) is the sum of putrescine and cadaverine content which raw pork meat with BAI >15 mg/1 kg of pork is considered as a spoiled meat [99].

Porous poly(lactic) acid (PLA) film is an interesting solid matrix due to its ability to entrap the sensing elements, inexpensive and simple fabrication, which can be applied for the development of food packaging sensors. PLA is a biodegradable polymer, which has a potential to be used as biomaterial for food packaging due to its easy processability and non-toxicity [100]. The porous PLA films can be easily fabricated by using a breath figure method [101]. Furthermore, the addition of calcium carbonate nanoparticles as a porogen significantly increases the porosity of the PLA film providing higher surface area, which allows the sensing element to be entrapped onto the surface of this sensor. Recently, many research groups have developed the colorimetric sensor using pH-sensitive dyes-based indicator for real-time monitoring of food quality as [95, 102-104]. An optoelectronic nose for squid shelf-life assessment was designed to measure CO_2 and O_2 by depositing dyes onto aluminium oxide and silica gel supports [105]. A colorimetric sensor array for fish spoilage monitoring was constructed by applying pH indicator solutions on silica gel Kieselgel 60F254 plates. The sensor color changed when facing typical volatile spoilage biogenic amines used to evaluate the fish spoilage [106]. A safe colorimetric pH sensor using *Clitoria* sp and *Brassica* sp extracted dyes was fabricated and used for determination of shrimp and durian freshness [107]. The polyvinyl alcohol/cellulose-based pH sensor was fabricated for food safety monitoring, which it changes the color from yellow to brown after exposing to the spoiled shrimp [108]. Although the pH-sensitive dyes-based sensor is a simple way to monitor food quality, which can be observed by naked eyes; however, it provides only semi-quantitative information and relatively low sensitivity.

To accurately and sensitively detect the toxic substances, laser desorption-ionization mass spectrometry (LDI-MS) was chosen along with the colorimetric sensor. LDI-MS is a soft ionization mass spectrometry, widely used in MS-based analytical chemistry owing to its universal, sensitive, qualitative and quantitative uses. This technique is also selective to organic molecules since the signals are obtained from relative molecular mass [109]. To design the LDI-MS substrate, graphene oxide

(GO), 1-dimentional carbon-based nanomaterial consisting of a one-atom thick planar sheet of sp^2-bonded carbon atoms with oxygen containing functionalities, has become an interesting substance for analyte trapping. Furthermore, GO exhibits strong adsorption capacity which can adsorb and desorb a variety of organic molecules in LDI-MS [110]. Recently, GO nanosheet-modified N^+-nylon membrane has been prepared and used as a substrate for MS detection of malachite green, a carcinogenic substance used to prevent protozoal infections in aquaculture industry owing to the high surface area and high electrostatic interaction with analyte [111]. GO aggregate was applied as the matrix for plasma triacylglycerol detection which the use of GO provides rapid, selective and sensitive signals [112]. Based on the unique properties of GO, it is a promising matrix for LDI-MS substrate [113].

Herein, a highly porous PLA film was prepared as a colorimetric sensor to detect the biogenic amines (e.g., putrescine and cadaverine) released from the food spoilage. For another layer, GO-coated filter paper was fabricated and used as a LDI-MS substrate for sensitive detection of such compounds. The colorimetric responses were measured by using a spectrophotometer. Furthermore, LDI-MS was used to sensitively detect the biogenic amines to identify the food spoilage. Eventually, this platform was successfully applied for monitoring of putrescine and cadaverine produced from pork spoilage.

2. Materials and methods

2.1 Materials and reagents

Biogenic amines (e.g., putrescine and cadaverine) were purchased from Sigma-Aldrich (St. Louis, MO). Phosphate buffer was prepared by using disodium hydrogen phosphate (Na_2HPO_4) from Carlo Erba Reagents S. A. S (Val de Reuil, France), and adjusted to pH 8 by using hydrochloric acid (HCl) and sodium hydroxide (NaOH) obtained from QReC (New Zealand) and Merck (Darmstadt, Germany). Porous PLA films were fabricated by using poly-lactic acid in pellet form, grade 2002D, purchased from NatureWorks, and calcium carbonate nanoparticles (NCC) were prepared by a precipitation technique. Dichloromethane (CH_2Cl_2) used as a solvent was purchased from Fisher Scientific (Loughborough, UK) and RCI Labscan (Bangkok, Thailand), respectively. Bromocresol purple ($C_{21}H_{16}Br_2O_5S$), pH-sensitive

dye with pH range 5.2 - 6.8, used as sensing elements was obtained from Tokyo Chemical Industry (Tokyo, Japan). Absolute ethanol was purchased from Carlo Erba Reagents S. A. S (Val de Reuil, France). For GO-coated filter paper preparation, GO dispersion (Ultra HC-Graphene oxide, aqueous solution, concentration of 6.2 g/L) and filter paper grade no.1 were purchased from Graphene Supermarket (USA) and Whatman, respectively. The fresh pork meat samples were purchased from local supermarket for spoilage trial study.

2.2   Fabrication of porous PLA-based colorimetric sensor

To prepare substrate of the sensor, porous PLA film was fabricated using a breath figure method [114]. First, three grams of PLA pellet were dissolved in 100 mL of dichloromethane and 1.0 % (w/w) of NCC was dispersed in the solution using magnetic stirrer. After that, PLA-NCC mixture was sonicated using ultrasonication (20 kHz, 750 W) for 1 min. The mixture was poured onto 17x13 cm glass mold and left to dry at 99% of relative humidity then, porous PLA film was obtained. Bromocresol purple was immobilized on the porous PLA substrate by using adsorption method. The procedure was carried out by soaking the porous PLA film in 0.1 % (w/v) bromocresol purple dissolved in absolute ethanol for 24 hrs, and dried at room temperature before washing with deionized water until the water was clear in order to remove the excess pH indicator. Then, the film was left to dry at room temperature overnight.

2.3   Preparation of GO-coated filter paper for LDI-MS

Preparation of GO-coated filter paper was obtained and adapted from previous research [110]. Filter paper no.1 was washed with acetone and distilled water and, dried at 60 °C. GO dispersion was diluted using distilled water to obtain concentration of 2.0 g/L, and sonicated by ultrasonication bath (60 Hz) for 30 min. The clean filter paper was immersed in the diluted GO dispersion under bath sonication for 20 min and dried at 120 °C for 20 min. The coating process was repeated for 3 times before washing the coated filter paper with deionized water to remove an excess GO and the GO-coated filter paper was dried at 100 °C overnight.

To assembly a dual detection platform, the GO-coated filter paper was immersed in dichloromethane and attached to the non-porous side of the porous PLA substrate. Finally, the dual detection platform was obtained (**Figure S2.1**).

2.4   Material characterization

The morphologies of the colorimetric sensor and the GO-coated filter paper were observed by scanning electron microscope (JEOL Model IT 500 HR). Energy dispersive X-rays spectroscopy (EDX) (JSM-6400; Japan Electron Optics Laboratory Co., Ltd., Japan) and X-ray photoelectron spectroscope (XPS) (Kratos Model Axis ultra DLD) were applied for the chemical analysis. The specific surface area of the porous PLA substrate was measured by Brunauer–Emmett–Teller (BET) analyzer (Micromeritics ASAP® 2420 Accelerated surface area and porosimetry system).

2.5   Cytotoxicity testing

MTT cytotoxicity assay was used to investigate the cellular response with PLA-based colorimetric sensor. Firstly, the PLA-based colorimetric sensor was extracted by cutting the sensor into 1.5×1.5 cm, adding MEM medium, and incubating at 37°C for 24 hrs. L929, mouse fibroblast cells, were incubated at 37°C for 24 hrs in MEM medium prior to testing to obtain monolayer of cells in a well-plate. Then, the MEM was replaced with the extract of the prepared colorimetric sensor then incubated at 37°C for 24 hrs. After incubation, the viable cells were stained with MTT and incubated at 37°C for 2 hrs. MTT was removed and DMSO was added to each well. The absorbance was measure using a microplate reader (EASYS, UVM340 S/N ASY54180) at 570 nm. Thermanox coverslip was used as a negative control and polyurethane film containing 0.1% zinc diethyldithiocarbamate was used as a positive control. The viability was calculated as a following equation:

$$\text{Viability} = 100 \text{ OD}_{570a}/\text{OD}_{570b}$$

Where OD_{570a} = optical density of 100% extracts of test sample

OD_{570b} = optical density of 100% extracts of the blank

2.6   Color change of PLA-based sensor toward biogenic amines

The biogenic amine vapors were collected by a static headspace sampling method. Firstly, the stock solutions of putrescine and cadaverine were prepared by dissolving of 10.0 mg/mL in deionized water. The stock solutions of biogenic amines were diluted to various concentrations from 0.1 to 8.0 mg/mL. After that, 1.0 mL of the prepared solutions were added to 30 mL plastic container with the colorimetric sensor attached on the container lid. The added solution was left to vaporize at 30 °C for 30 min, 1, 2, 4, 8, 24, and 48 hrs. The color change responses of the colorimetric sensors were measured by using a portable spectrophotometer (Datacolor CHECK3, Datacolor, USA). The color changes were given in hue angle (h°) referring to the dominant wavelength was calculated and used for the analysis.

2.7   LDI-MS detection of biogenic amines on GO-coated filter paper

For LDI-MS detection, each GO-coated filter paper was attached onto a stainless steel MALDI target by using a conductive carbon tape. Then, 10 µL of each biogenic amine solution was deposited on to each GO-coated filter paper substrate and dried at a room temperature 25±5 °C prior to inserting into a MALDI mass spectrometer for the analysis. All LDI-MS experiments were performed on a Bruker Autoflex III MALDI-TOF mass spectrometer with 30% N_2 laser (337 nM) intensities and 30 laser shots.

2.8   Pork spoilage trial

The fresh ground pork was purchased from the local supermarket. Ten grams of the ground pork meat sample was immediately placed and enclosed in 30 mL plastic container with the dual detection platform attached on the container lid. The pork meat samples were stored in the refrigerator (4 °C) for 5 and 3 days before

measurement of the colorimetric response of the sensor and LDI-MS detection, respectively.

3. Results and discussion

3.1 Material Characterization

The photographs (**Figure 3.1**) show the appearances of a dual detection platform having 2 layers, the porous PLA based colorimetric sensor (**Figure 3.1a-3.1c**) and GO-coated filter paper for LDI-MS detection (**Figure 3.1d- 3.1e**). The porous PLA film used as a sensor substrate shows white color, opaque and rough surface indicating its porosity (**Figure 3.1a**). After soaking the porous PLA film in bromocresol purple solution, the colorimetric sensor was obtained. The original sensor exhibits yellow color and suddenly changes to purple color upon exposing to the basic compounds, as shown in **Figure 3.1b** and **Figure 3.1c**, respectively. For the bottom layer of the dual detection platform, **Figure 3.1d** displays the uncoated filter paper in white color and it turns to dark grey color after coating with GO solution (**Figure 3.1e**).
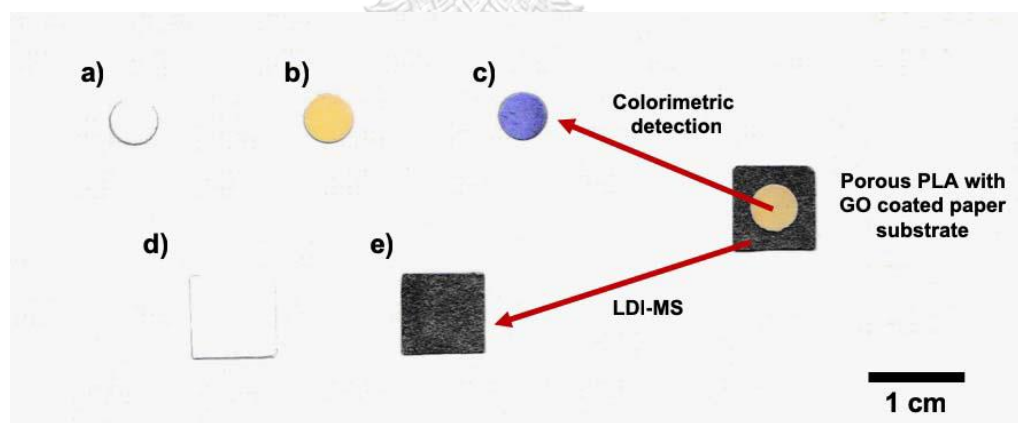
Figure 3.1 Photographs of the dual detection platform, a) porous poly(lactic) acid film, b) poly(lactic) acid-based colorimetric sensor before exposing to amines, c) poly(lactic) acid-based colorimetric sensor after exposure, d) uncoated paper, and e) graphene oxide-coated filter paper.

The surface morphology of the porous PLA based colorimetric sensor and GO-coated filter paper was characterized by scanning electron microscope (SEM). **Figure 3.2a** shows the microporous structure of PLA film prepared without using NCC. The non-uniform pore size was observed with an approximate diameter ranging from 6 to 82 μm. In contrast, the porous PLA film with adding NCC shows the higher porosity with uniform three-dimensional structure as shown in **Figure 3.2b**. The pore size of the film was decreased to 0.6 - 9 μm leading to increased specific surface area. BET was used to determine the specific surface area of the porous PLA film and PLA film prepared with adding NCC shows 10 times higher surface area, 89 m^2/g, than PLA film without adding NCC, 9 m^2/g. The porous structured film offers high sensing element entrapment. Therefore, it was considered as a suitable substrate for colorimetric sensor with enhanced sensitivity.

From SEM-EDX spectrum as shown in **Figure 3.2c**, the high intensity of C and O with low intensity of Ca verifies that there are some of calcium carbonate successfully embedded in PLA film containing mostly C and O. On another side of the substrate, **Figure 3.2d** displays the fibrous structure of cellulose filter paper without any modification, and **Figure 3.2e** shows the thin layer of GO covering on the cellulose filter paper surface which clearly differs from an original fibrous cellulose structure. In addition, XPS spectrum of C1S of GO coated paper (**Figure 3.2f**) showed the 2 dominant peaks at 284.6 eV of C-C, and 286.2 of C-O. The presence of peaks around 287.1 - 288.4 eV was corresponded to C=O [115, 116]. This verifies that GO is successfully coated on the cellulose filter paper surface.
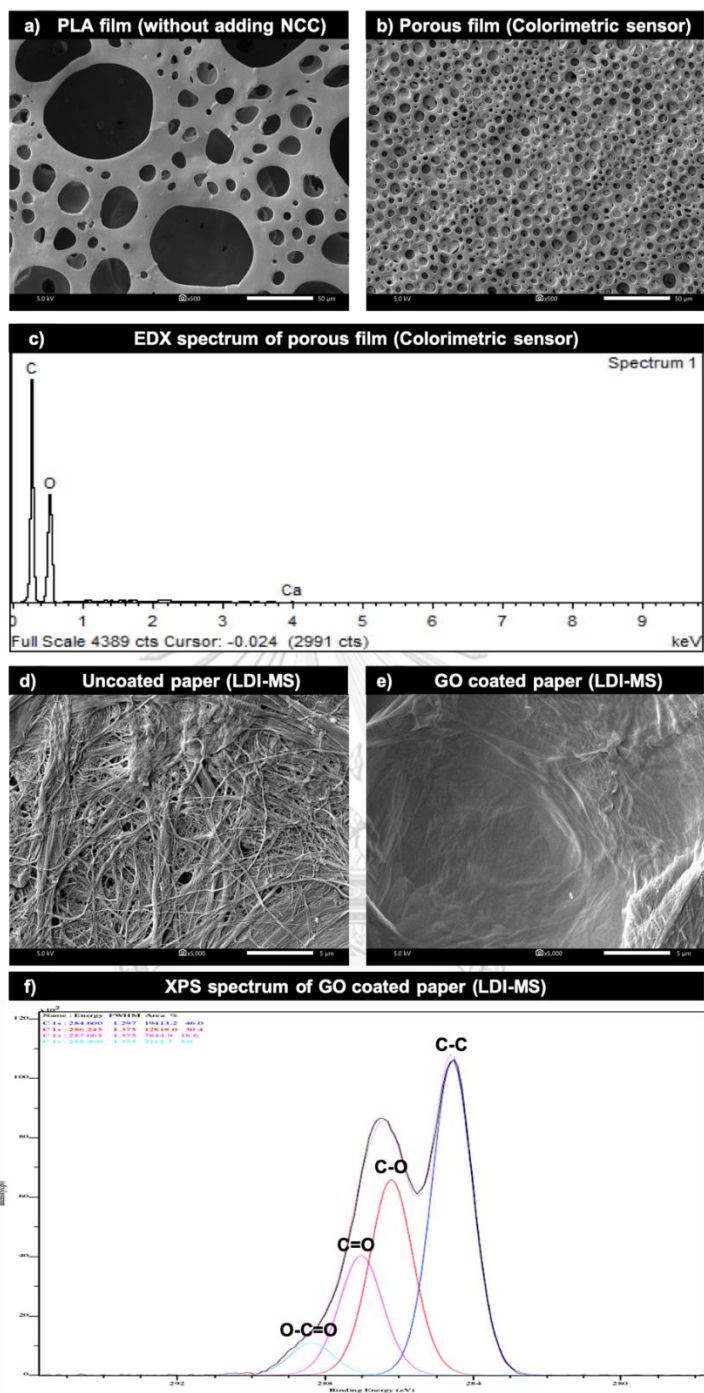
Figure 3.2 SEM images of a) poly(lactic) acid film without calcium carbonate nanoparticles, b) porous poly(lactic) acid film with calcium carbonate nanoparticles, c) EDX spectrum of porous poly(lactic) acid film, d) uncoated filter paper, e) graphene oxide-coated filter paper, and f) XPS spectrum of graphene oxide coated paper.

3.2   Cytotoxicity testing

To confirm the compatibility and safety for using this material substrate as food packaging sensor, the colorimetric sensor was subjected to MTT cytotoxicity assay based on ISO 10993-5 [117] to evaluate the cellular response of the colorimetric sensor extract by calculating viability of the viable cells. If viability is less than 70% of the blank, it indicated that the specimen has a cytotoxic potential [118]. For the developed colorimetric sensor, the percent of viability of the sample was 100% compared to negative controls which do not produce a cytotoxic response to the cultured L929 of mouse fibroblast cells (**Table S3.1**). Thus, it can be concluded that our developed colorimetric sensor is safe and it has a potential to be used in real food spoilage sensor applications.

3.3   Colorimetric responses toward biogenic amine exposure

The prepared colorimetric sensor was exposed to vapor from 1 mL of 5.0 mg/mL of putrescine and cadaverine at different time interval, to investigate the degree of colorimetric response of the sensor. The color changes of the sensor were measured in Δ h° value. As a result, the colorimetric sensor exposed to cadaverine changed its color at 30 mins, whereas the sensor started to change its color at 8 hrs towards putrescine. The sensor color changes increased over time since the amine solutions vaporize leading to increase of pH in the headspace. After the amine vapors contact to the sensor, bromocresol purple changes its color from yellow to purple, which is a changing from acidic form to basic form of pH indicator. The Δ h° values of putrescine and cadaverine steadily increased and almost reached a plateau after 24 hrs of exposure indicating the sensor saturation (shown in **Figure S3.2**). Therefore, 24 hrs of exposure time was applied for all further experiments.

To investigate an effect of analyte concentration on the sensor color, the sensor was exposed to amine vapors from 0.1 to 10.0 mg/mL for 24 hrs before measurement. The color of the sensor started to change when exposing to 1.0 mg/mL and 0.1 mg/mL for putrescine and cadaverine. After that, the Δ h° values tend to increase with the increase of biogenic amines. As shown in the **Figure 3.3a** and **Figure 3.3b**, Δ h° values of the sensor increased linearly with putrescine concentration in a range of 2.0

– 10.0 mg/mL and with cadaverine concentration in a range of 0.1 - 6.0 mg/mL. The linearity of Δ h° value versus the amine concentrations with the coefficient of determination (R^2) of 0.9920 and 0.9912 were obtained for putrescine and cadaverine, respectively.
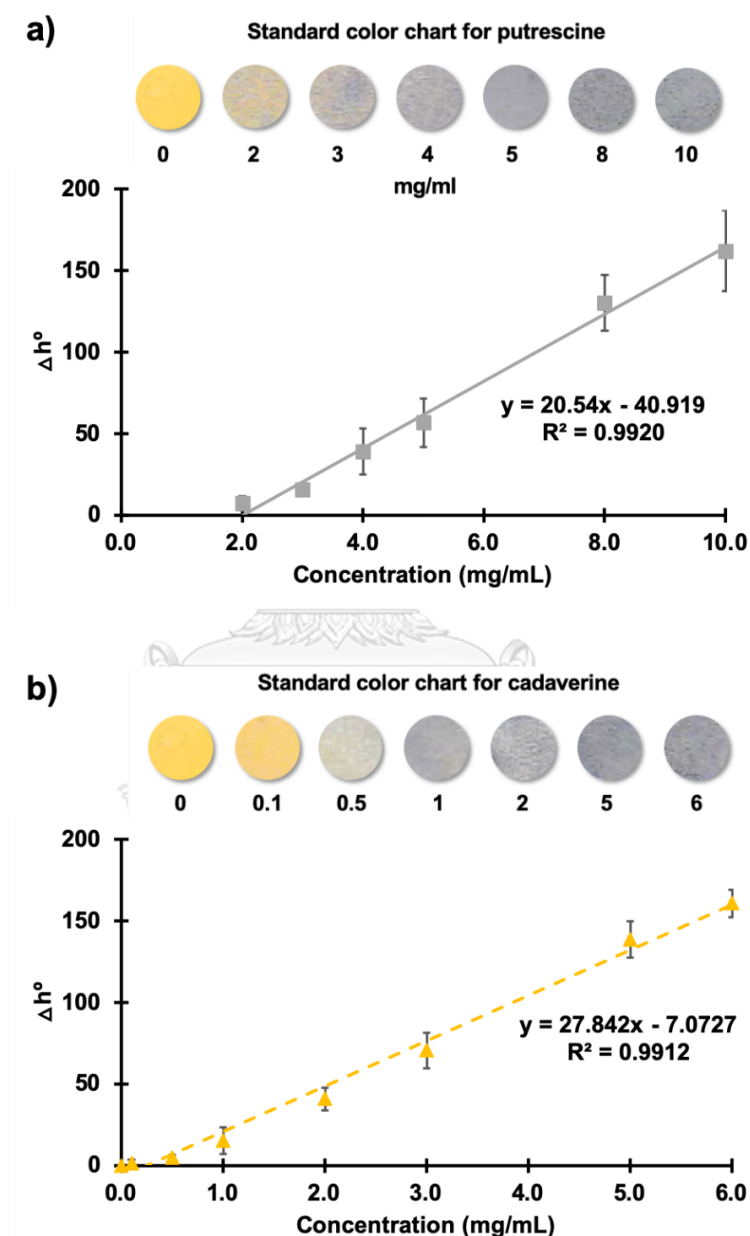
Figure 3.3 The standard color charts and plots of biogenic amine concentration versus the Δ h° values for a) putrescine and b) cadaverine.

3.4   LDI-MS detection of putrescine and cadaverine

LDI-MS was used for specific identification, and sensitive detection of putrescine and cadaverine on GO-coated filter paper attached on another layer of the porous PLA film. Previously, it was reported that graphene and its derivatives have been used as the matrices that can promote the ionization and detection of small molecules by LDI-MS [119-121]. Herein, GO was selected to adsorb and pre-concentrated putrescine and cadaverine due to its high surface area and active surface functionality. The biogenic amines with different concentrations ranging from 0.01 to 0.1 pM were directly dropped and adsorbed on GO-coated filter paper for LDI-MS detection with 30% N_2 laser intensities and 30 of N_2 laser shots. Linear ranges were 0.05 - 100 pM, and 0.01 - 100 pM for putrescine and cadaverine, respectively (shown in **Figure S3.3**). Limit of detection (LOD) values (S/N $\geq$ 3) of putrescine and cadaverine with the molecular ion (M^+) of 88.15 and 102.18 were found to be 0.07 pM and 0.02 pM, respectively on GO-coated filter paper substrate as shown in **Figure 3.4**.
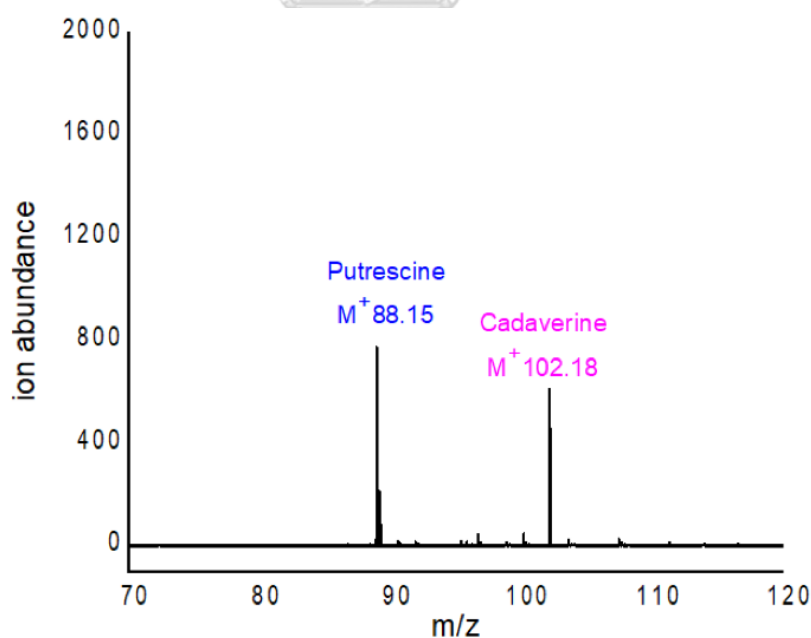
Figure 3.4 LDI-MS spectra of 0.07 pM of putrescine and 0.02 pM of cadaverine measured on graphene oxide-coated filter paper.

3.5   Pork spoilage trial

The potential application of this developed dual detection platform were placed in the sealed containers with ground pork samples at 4°C for 5 days for exposing to biogenic amines generated by the pork spoilage. The responses of the colorimetric sensor were given in $\Delta h°$ values as shown in **Figure 3.5**. The color gradually changed for the first 2 days of exposure. Afterward, the drastic change of the color has been observed, especially between day 2 and 3, which the color obviously changed from yellow to purple and it became darker purple at day 4. The color change of the sensor dropped and became lighter purple on day 5. This can be related to CO_2 releasing from food spoilage which affects to the change in color of the colorimetric sensor by decreasing in pH in the headspace [105, 106]. However, this colorimetric sensor offers non-selectively responses on the total amount of amines, rather than selectively response to specific amines. These results verify that our colorimetric sensor can be successfully applied in real matrices of pork samples as the food spoilage indicator in the food container.
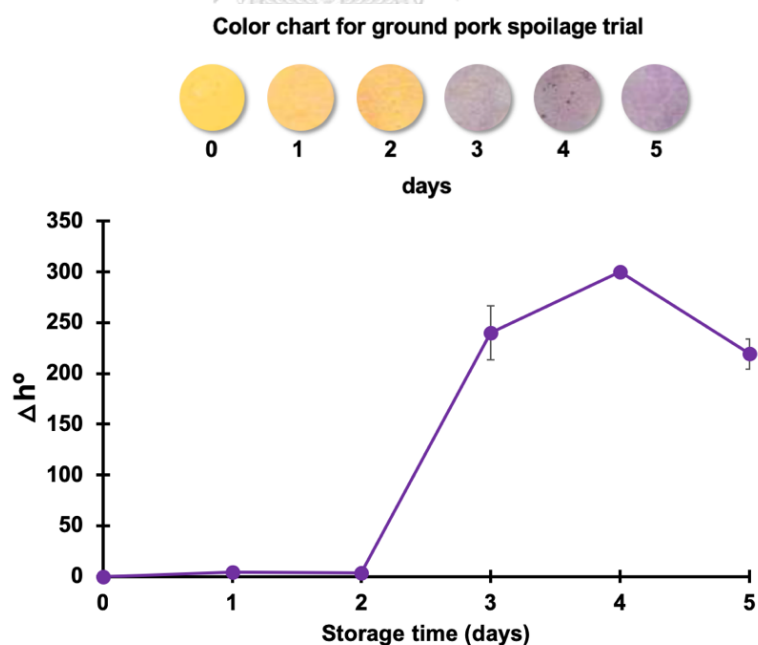
Figure 3.5 Color changes of the colorimetric sensor from yellow to purple upon the exposure to the ground pork samples stored at 4°C.

As for LDI-MS analysis of the real pork samples, there are several unknown interferent ion peaks adsorbed on the GO-coated filter paper as shown in the **Figure 3.6**. However, 0.1 pM of putrescine and cadaverine spiked into the real matrices of pork are clearly observed on our detection platform as shown in the asterisks of **Figure 3.6**. Additionally, the ground pork samples were spiked with 0.1 pM of putrescine and cadaverine and stored at 4°C for 3 days to get spoiled prior to LDI-MS detection. The putrescine and cadaverine found in the samples at day 3 were 5.46 and 5.30 pM, respectively. The putrescine and cadaverine found in the samples at day 3 were 5.46 and 5.30 pM, respectively. The LDI-MS spectra of the amines in real sample were illustrated in **Figure S3.4**.

The LDI-MS detection of these two biogenic amines spiked in real sample verified the powerful of this approach, which two putrescine and cadaverine adsorbed on the GO coated paper on the porous PLA film can be sensitively detected and specifically identified at the trace level in real pork and pork spoilage samples.
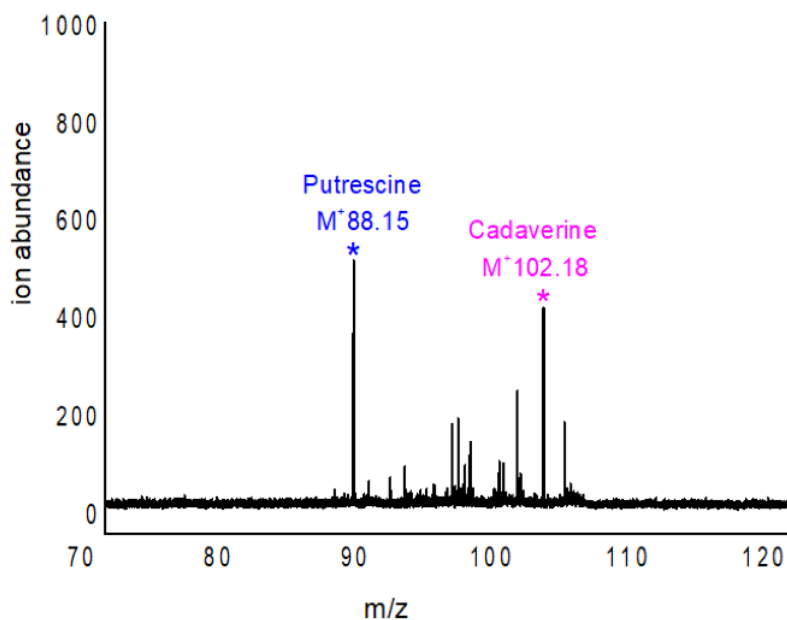
Figure 3.6 LDI-MS spectra of 0.1 pM of putrescine and cadaverine spiked into the ground pork samples measured on graphene oxide-coated filter paper.

Hence this porous PLA and graphene oxide substrate used in a dual detection platform developed in this study might be very useful tool for the screening as well as the specific identification of the biogenic amines and other food toxins in the smart packaging application.

Conclusions

This work successfully created a novel porous PLA and graphene oxide substrate used in a dual detection platform to monitor the food quality by detection of putrescine and cadaverine released from the pork spoilage samples. The colorimetric sensor provides easy-to-use and safe smart food packaging for costumers due to its inexpensive, simple, portable size, while the GO coated paper for LDI-MS provides specific and highly sensitive determination of such compounds with LOD values of 0.07 pM and 0.02 pM for putrescine and cadaverine which can be used for quality controlling in food industry, respectively. The response of the colorimetric sensor showed the linear relationship with putrescine and cadaverine concentrations and capable to use in real pork samples. This substrate along with a dual-detection technique might be useful for screening of food expiration date in the smart packaging and it will be applied for the sensitive detection of other trace level toxins and biomarkers in various applications in the future.

Acknowledgements

Supporting Information
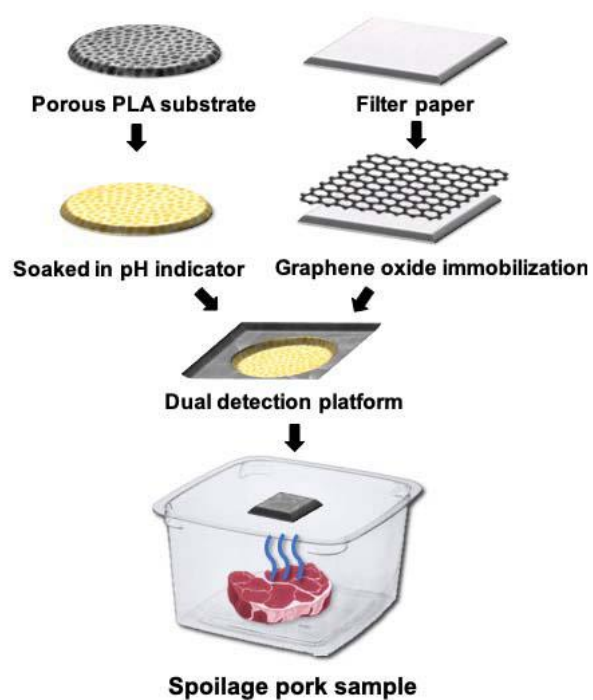
Figure S3.1 Schematic diagram of dual detection platform preparation.

Table S3.2 Percentage of cell viability using MTT cytotoxicity assay testing.

Sample	The average of	
	OD 570 nm	%Viability
Blank	0.663	100
Negative control	0.657	99
Positive control	0.000	0
PLA-based Colorimetric sensor	0.668	100
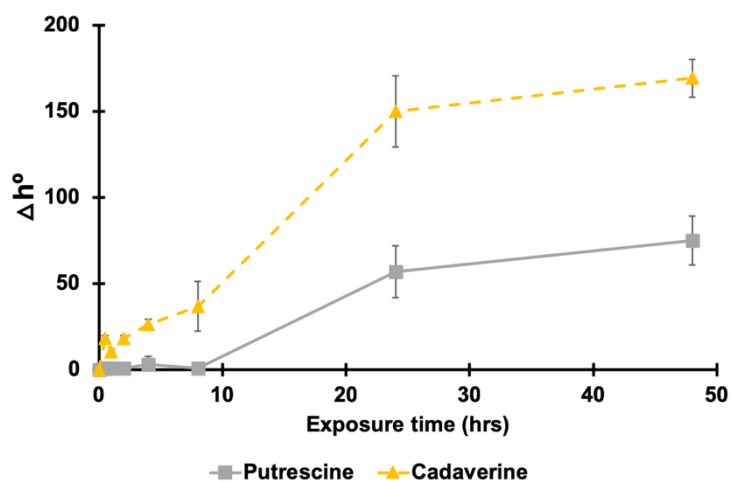
Figure S3.2 The rate of colorimetric sensor response upon exposing to putrescine and cadaverine vapors vaporized from 5.0 mg biogenic amines at 30 °C at different time length.
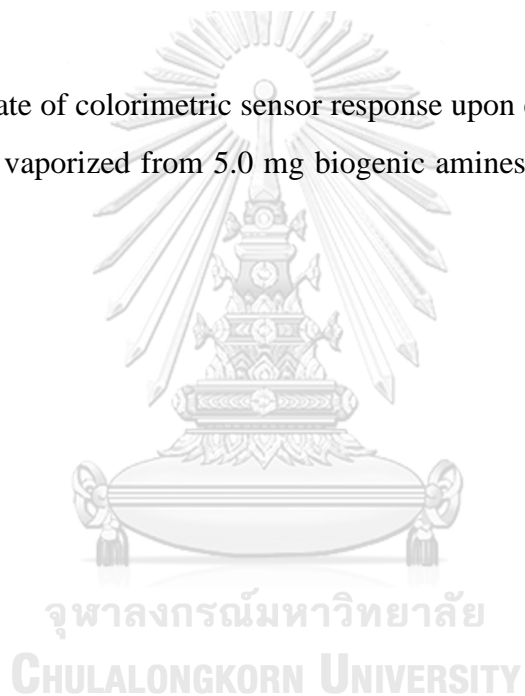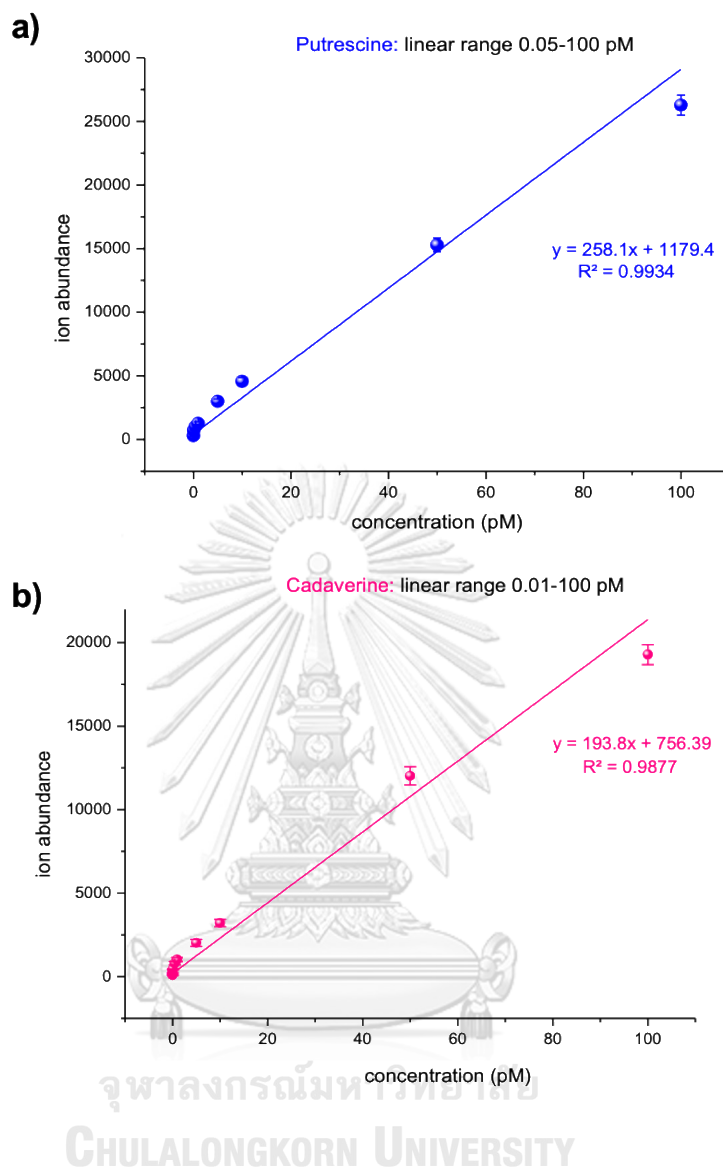
Figure S3.3 Calibration plots of a) putrescine and b) cadaverine analyzed by LDI-MS.
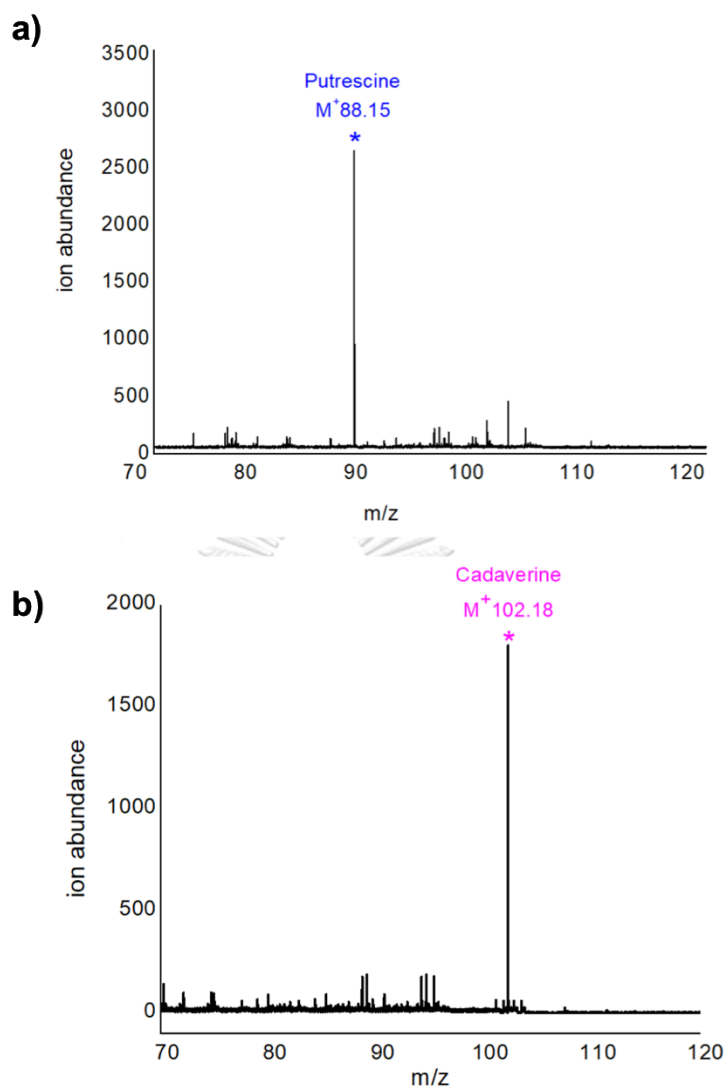
Figure S3.4 LDI-MS spectra of ground pork with spiking 0.1 pM of a) putrescine, and b) cadaverine after stored at 4°C for 3 days.

CHAPTER IV

Bacterial cellulose-based re-swellable hydrogel: Facile preparation and its potential application as colorimetric sensor of sweat pH and glucose

Tatiya Siripongpreda[1], Benjawan Somchob[2], Nadnudda Rodthongkum[3,4*], Voravee P. Hoven[4,5,6*]

[1]Nanoscience and Technology Interdisciplinary Program, Chulalongkorn University, Phayathai Road, Wangmai, Pathumwan, Bangkok 10330, Thailand

[2]Program in Petrochemistry and Polymer Science, Faculty of Science, Chulalongkorn University, Phayathai Road, Wangmai, Pathumwan, Bangkok 10330, Thailand

[3]Metallurgy and Materials Science Research Institute, Chulalongkorn University, Phayathai Road, Wangmai, Pathumwan, Bangkok 10330, Thailand

[4]Nanotec-CU Center of Excellence on Food and Agriculture, Department of Chemistry, Faculty of Science, Chulalongkorn University, Bangkok 10330, Thailand

[5]Department of Chemistry, Faculty of Science, Chulalongkorn University, Phayathai Road, Wangmai, Pathumwan, Bangkok 10330, Thailand

[6]Center of Excellence in Materials and Biointerfaces, Chulalongkorn University, Phayathai Road, Wangmai, Pathumwan, Bangkok 10330, Thailand

*Corresponding author e-mail: Nadnudda.R@chula.ac.th, Vipavee.P@chula.ac.th

Abstract

Direct deposition of the negatively charged polyelectrolyte, carboxymethyl cellulose (CMC), into a bacterial cellulose (BC) matrix was used as a simple route to fabricate a re-swellable and biocompatible cellulose-based hydrogel. As a result of this non-destructive approach, the physical and mechanical property of the original BC were well-preserved within the resulting BC/CMC hydrogel. As a BC/CMC-based colorimetric pH sensor, it exhibited a rapid response with an easy color differentiation between each pH by the naked eye, and wide linear range of pH 4.0–9.0 with good linearity. For the detection of glucose in sweat, the BC/CMC-based colorimetric glucose sensor provided a low limit of detection (25 µM) with a wide linear detection range (0.0–0.5 mM) and high accuracy. These BC/CMC based sensors could potentially be applied as non-invasive semi-quantitative sensors for on-skin health monitoring.

Keywords: Biocompatible hydrogel, Carboxymethyl cellulose, Semi-double network, Non-invasive sensor

Graphical abstract

Bacterial cellulose/Carboxymethyl cellulose hydrogel · Non-invasive sweat sensor
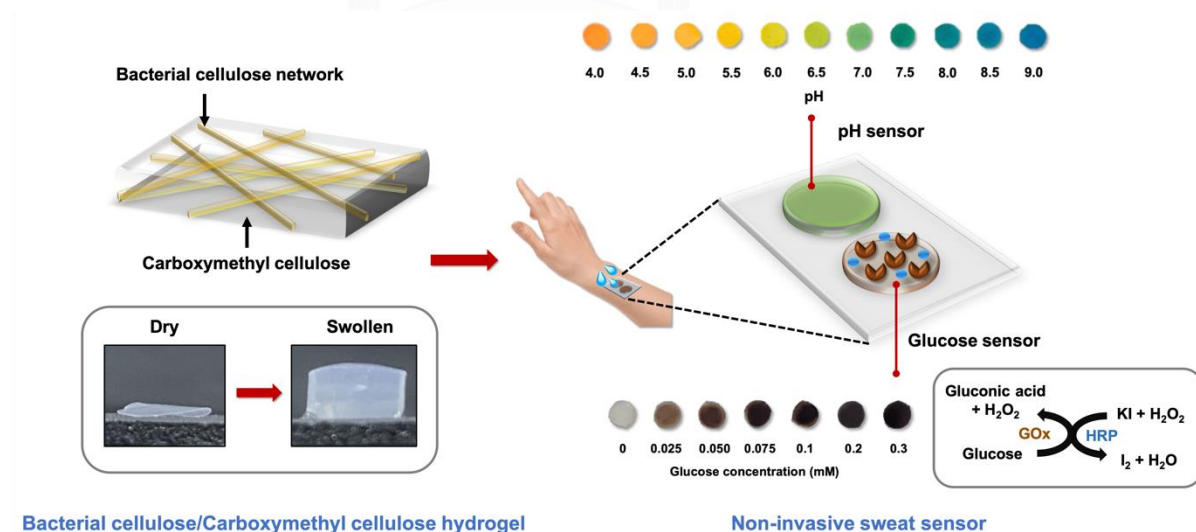
1. Introduction

Non-invasive diagnostics is an analytical approach for health monitoring, disease screening, and athletic performance evaluation with minimal incision to the body. It provides less trauma to the skin, nerves, muscles, and tissues, and reduces bleeding, pain, and infection risk after the sampling. Sweat is one of the interstitial biofluids containing minerals and clinical biomarkers, found in blood. Since sweat sampling can be done non-invasively and the levels of several biomarkers in sweat are well correlated with those in the blood [50], it is an interesting alternative biofluid for medical diagnostics. Glucose is one of the biomarkers found in all interstitial fluids that can be used for the diagnostics of various diseases. A concentration of 0.3 mM glucose in sweat corresponds to 300 mg dL^{-1} glucose in blood. As a result, glucose analysis in sweat is a promising approach for the diagnosis of hyper-/hypo-glycaemia and diabetes mellitus [122].

To fabricate a highly specific and sensitive glucose sensor, enzymatic reactions have been commonly utilized. Nevertheless, enzyme-based sensors still have some limitations due to the loss of enzymatic activity upon storage that potentially affects the sensor's performance [123]. The use of a biocompatible hydrogel for enzyme entrapment was found to protect the enzyme from denaturation and to retain the activity [124]. Furthermore, the pH of sweat is another interesting indicator that can reflect the physical conditions of the person, such as dehydration, sweat rate, muscle fatigue, faint [45, 125], and skin-related diseases [122]. The normal sweat pH lies in the range of 4.0–7.0 whereas an abnormal pH can reach up to 9.0 [50, 126-128]. Various forms of cellulose, namely textile, thread, and filter paper can be used to collect sweat samples for the development of non-invasive sweat sensors [45, 125, 129]. Nonetheless, the small sample volume and rapid evaporation of sweat limits the sensitivity and reliability of the sensors. Therefore, a suitable substrate for sweat sensors should be able to effectively collect and store the small amount of excreted sweat [130].

Cellulose is the *most abundant natural polymer*, and can be synthesized by a large number of living organisms ranging from bacteria to plants [131]. Recently, we have explored cellulose-based materials in sensors including a cotton textile-based non-invasive sensor for sweat pH and lactate [45], a cellulose paper-based sensor for

creatinine detection [132], and a kenaf cellulose-based three-dimensional printed device for a Ni(II) sensor [133].

Bacterial cellulose (BC) is another potential carbohydrate-based material synthesized extracellularly by bacteria. The production is found to be most effective in *Gluconacetobacter*, such as *G. xylinum*, *G. hansenii*, and *G. pasteurianus*, [23]. Currently, BC has been used for various biomedical applications owing to its biocompatibility, non-toxicity, low immunogenicity, high mechanical property, and low cost [23, 134, 135]. Despite its favorable characteristics, the fibrous structure of BC tends to collapse upon drying in ambient conditions resulting in a lack of ability to re-swell due to strong hydrogen bonding among the BC nanofibers [136]. For this reason, BC is often fabricated in the form of composites.

There are two general approaches for preparing BC composites, namely the disturbed and undisturbed methods [23]. For the disturbed approach, the original BC structure is modified by disintegration, being extracted as whiskers, crosslinking, or derivatization. On the other hand, the original BC matrix structure is maintained in the case of the undisturbed approach. The second matrix is introduced to the existing BC network by incorporation during BC production or after via *in situ* polymerization, crosslinking to form a double network, or matrix deposition by direct BC matrix immersion in the designated matrix.

To overcome the problem of the BC network collapsing and being unable to rehydrate upon drying, carboxymethyl cellulose (CMC), a negatively charged biocompatible polyelectrolyte, was *in situ* incorporated by addition into the culture media used for BC production [137, 138]. The added CMC generated small microfibrils which could then interfere with the BC crystallization by preventing the packing of microfibrils or cellulose ribbons during bacterial growth [139]. The negative charges along the CMC backbone introduced repulsion that loosened the BC network packing. The steric hindrance imposed by CMC also blocks the H-bonding among microfibrils. This *in situ* modification yielded a BC/CMC hydrogel with a satisfactory reswelling property, but with an unavoidable decrease in mechanical strength and crystallinity [137].

Herein, the BC/CMC hydrogel was prepared to generate a reswellable hydrogel using a simpler protocol based on matrix deposition, one of the undisturbed methods.

Generally, the BC membrane was directly immersed in a CMC solution, allowing CMC to diffuse in-between the BC network. This proposed method is safe, of low cost, and easy, and does not require special tools, chemicals, or prior BC modification. In other words, the BC/CMC hydrogel can be obtained from any commercially available BC and CMC, regardless of their origins. Culturing method that strictly requires hygienic condition for microorganism handling is not certainly required. This definitely reduces the process time and complication. The fabrication process therefore becomes more practical than the *in situ* BC incorporation from commercial point of view.

The swelling behavior of the BC/CMC hydrogel as a function of the soaking time and CMC concentration was systematically evaluated. Physical, mechanical, and cytocompatibility of the BC/CMC hydrogel was also determined. The developed hydrogel was then incorporated with a universal pH indicator or glucose oxidase enzyme (GOx) and applied as colorimetric pH or glucose sensor, respectively. The color differentiation performance of the pH sensor was determined over a pH range of 4.0–9.0 and the enzymatic glucose sensor was tested with glucose-spiked artificial sweat to confirm its sensing performance.

2. Experimental

2.1 Materials and reagents

The BC produced by *Acetobacter xylinum* was obtained from Thai-nanocellulose Co. Ltd. (Phatthalung, Thailand), while CMC, as the sodium salt with a typical $\overline{M}_w$ of 250,000 g mol^{-1} and degree of substitution of 1.20, cetyltrimethyl ammonium bromide (CTAB), methyl red, thymol blue, bromothymol blue, phenolphthalein, GOx from *Aspergillus niger* [Type II, $\geq$ 15,000 units (U) g^{-1} solid], horseradish peroxidase (HRP), phosphate buffer saline (PBS) tablet, potassium iodide (KI), and Starch Assay Kit (based on amylase/amyloglucosidase method) were purchased from Sigma-Aldrich, USA. Absolute ethanol, sodium hydroxide (NaOH), and hydrochloric acid were purchased from Merck, Germany. D (+)-Glucose anhydrous was from Carlo Erba Reagents S.A.S., and simulated sweat was obtained from Moulage Sciences & Training, LLC (*USA*). The 3-(4,5-dimethylthiazol-2-yl)-5-(3-carboxymethoxyphenyl)-2-(4-sulfophenyl)-2H-tetrazolium (MTS) assay reagent

was obtained from Promega (USA). All chemicals were used as received without additional purification.

2.2 Preparation of BC/CMC hydrogel

Firstly, the BC sheet (2 x 2 cm) was soaked in deionized (DI) water for 1 h with constant stirring before immersing in CMC solution (0.1–1.0% $w.v^{-1}$) for the desired period of time (0.5–48 h). The obtained BC/CMC hydrogel was dried at room temperature (RT; 25 ± 2 °C). The dried hydrogel was rinsed with DI water to get rid of excess CMC and dried at RT to give the BC/CMC hydrogel.

2.3 Characterization of BC/CMC hydrogels

2.3.1 Swelling behavior

The prepared dry BC/CMC hydrogel was weighed (W_d) and then put into a tea bag (10.0 × 8.0 cm) before being immersed in DI water or artificial sweat for 1, 3, or 24 h. After that, the tea bag carrying the swollen hydrogel was hung for 10 min to remove excess water. The swollen hydrogel was removed from the tea bag and then weighed (W_w). The swelling ratio of the hydrogel was calculated according to Eq. (1),

$$Swelling\ ratio\ (\%) = (W_w - W_d)/W_d \times 100 \qquad (1)$$

2.3.2 Physical properties

The pristine BC and the BC/CMC hydrogels were immersed in DI water for 3 h to reach an equilibrium swelling. The swollen hydrogels were then dried using a critical point dryer (Leica EM CPD300, Leica Microsystems, Germany). The surface of the samples was sputter-coated with gold. The morphology of the hydrogels was characterized using field emission scanning electron microscopy (FESEM; JEOL JSM-7610F, Oxford X-Max 20, Japan). The crystallinity of the hydrogels was determined after being air-dried by X-ray diffraction (XRD) (Rigaku, SmartLab 30 kV/PC X-ray diffractometer, Japan), operated at 40 kV and 30 mA. The range of diffraction angle (Two-Theta) was set at 5–80° with a scanning speed of 10° min-1. The percentage of crystalline was calculated from Eq. (2);

$$\text{Crystallinity (\%)} = (\text{Area}_{crystalline})/(\text{Area}_{all\ peaks}) \times 100 \qquad (2)$$

where Area$_{crystalline}$ is the area of the crystalline peak and Area$_{all\ peaks}$ is area of all the peaks (crystalline + amorphous).

Thermogravimetric analysis (TGA) of all samples was performed using a Pyris 1 TGA thermal analyzer (Perkin Elmer, USA) with a heating rate of 20 °C min-1 over a range of 50–700 °C under a flowing nitrogen atmosphere.

2.3.3 Mechanical properties

The tensile test was performed using the LLOYD Universal Testing Machine (UTM LS1). The air-dried pristine BC and BC/CMC hydrogels were cut into 1×5 cm rectangles. The measurements were performed in triplicate at RT at a strain rate of 0.01 mm.min^{-1} to a maximum strain of 0.7 (%).

2.3.5 Cytocompatibility

The cytotoxicity of any leaching substances from pristine BC and BC/CMC hydrogels was tested against L929 cells using the MTS assay. In brief, the hydrogels were immersed in complete medium [CM: minimum essential medium (Gibco) supplemented with 10% v.v^{-1} fetal bovine serum (Bio West) and 1.0% v.v^{-1} antibiotic-antimycotic (Gibco)] at 37 °C under 5% v.v^{-1} carbon dioxide (CO_2) for 24 h. Then, 100 µL of the CM incubated with the designated hydrogel was removed and added into a 96-well plate containing the precultured L929 cells (5000 cells.well-1.100 µL-1 CM) at 37 °C under 5% v.v^{-1} CO_2 for 24 h. After 20 h incubation, 10 µL of MTS solution was added and continuously incubated for 4 h. The absorbance of each well was detected at 492 nm (A492) using a microplate reader (Multiskan FC, Thermoscientific, USA). The relative cell viability (%) was calculated from Eq. (3);

$$\text{Relative cell viability (\%)} = \left(A_{492} \text{ of sample}\right) \times \left(A_{492} \text{ of control}\right)^{-1} \times 100 \qquad (3)$$

where A_{492} of sample is the absorbance of cells treated with the designated hydrogel and A_{492} of control is the absorbance of untreated cells.

2.3.6 Determination of starch in BC

The starch content of BC was determined by destructive analysis and consisted of washing the BC in ethanol to remove residual glucose, followed by a two-step enzymatic digestion of the starch, and subsequent glucose assay. The procedure was modified from a previously published procedure [140], and is detailed in the Supporting Information.

2.4 Fabrication of the BC/CMC-based colorimetric pH sensor

The pH indicator solution was prepared by a method modified from a previous published procedure [141] by dissolving four pH indicators, methyl red (0.625% w.v^{-1}), thymol blue (0.25% w.v^{-1}), bromothymol blue (3.0% w.v^{-1}), and phenolphthalein (5.0% w.v^{-1}) in 50% v.v^{-1} ethanol/H_2O, and neutralized with NaOH. After that, CTAB was added to the solution which was then vortexed until the CTAB was completely dissolved. The final CTAB concentration in the solution was 0.1% w.v^{-1}. To fabricate a colorimetric pH sensor, the BC/CMC hydrogel was immersed in the above prepared pH indicator solution for 15 min, rinsed with DI water to remove excess pH indicator, and then air-dried at RT.

The performance of the fabricated pH sensor was determined by adding various known pH buffers on the sensor, and the color change of the sensor was measured in terms of the hue angle value by a portable spectrophotometer (Datacolor CHECK3, Datacolor, USA).

2.5 Fabrication of BC/CMC-based colorimetric glucose sensor

The colorimetric glucose sensor was based on the color development of KI by hydrogen peroxide (H_2O_2) from enzymatic reaction of GOx. The enzyme mixture was prepared by combining GOx and HRP solutions dissolved in PBS at a ratio of 120:30

U.mL^{-1}. Briefly, 10.0 μL of 0.5 M KI was dropped onto the BC/CMC hydrogel, followed by 2.5 μL of the enzyme mixture to generate the BC/CMC-based glucose sensor.

To investigate the color intensity development with different glucose concentrations, D-glucose was dissolved in PBS in a concentration range of 0.00–0.50 mM. Then 10.0 μL of the specific glucose solution was dropped onto the BC/CMC-based glucose sensor and incubated at RT for 10 min before measuring the color in K/S's value, which expresses the color strength, using a portable spectrophotometer. Moreover, the accuracy of the fabricated BC/CMC-based glucose sensor was also evaluated by measuring glucose levels in the artificial sweat that was spiked with known standard concentrations (0.05, 0.10, and 0.20 mM) of glucose.

3. Results and discussion

3.1 Preparation and characterization of the BC/CMC hydrogel

Herein, CMC was incorporated into the BC network by a simple approach based on matrix deposition. The soaking time and CMC concentration used for the BC/CMC hydrogel preparation were found to have a strong impact on the swelling behavior of the resulting BC/CMC hydrogel. As shown in **Figure 4.1a**, a longer period of time used for soaking the BC network in 1.0% w.v^{-1} solution provided a BC/CMC hydrogel with a higher swelling ratio, and this dramatically increased within the first 3 h and then insignificantly increased upon prolonged soaking for up to 48 h. As shown in **Figure 4b**, By elevating the CMC concentration from 0.1 to 0.5 and to 1.0 w.v^{-1}, the swelling ratio of the obtained BC/CMC hydrogel proportionally increased, implying that more CMC can be incorporated as a function of the CMC concentration. This observation follows the same trend as that previously reported based on the *in situ* incorporation of CMC during BC production [137]. However, the BC/CMC hydrogel prepared from CMC concentrations higher than 1.00% w.v^{-1}, exhibited a swelling ratio with an exceedingly large standard deviation. Consequently, a soaking time of 24 h and a CMC concentration of 1.00% w.v^{-1} was selected as the optimal condition for preparing the BC/CMC hydrogel for further characterization and development of the colorimetric pH and glucose sensors.

The content of incorporated CMC in the BC/CMC hydrogel was also evaluated by gravimetric analysis. The results shown in **Figure S4.1 (Supporting Information)** suggests that the content of CMC incorporated into the hydrogel proportionally increases with the CMC concentration used in the preparation. At the optimal CMC concentration of 1.0 % w.v^{-1}, the incorporated CMC was found to be 54.1 ± 3.2% w.w^{-1}.
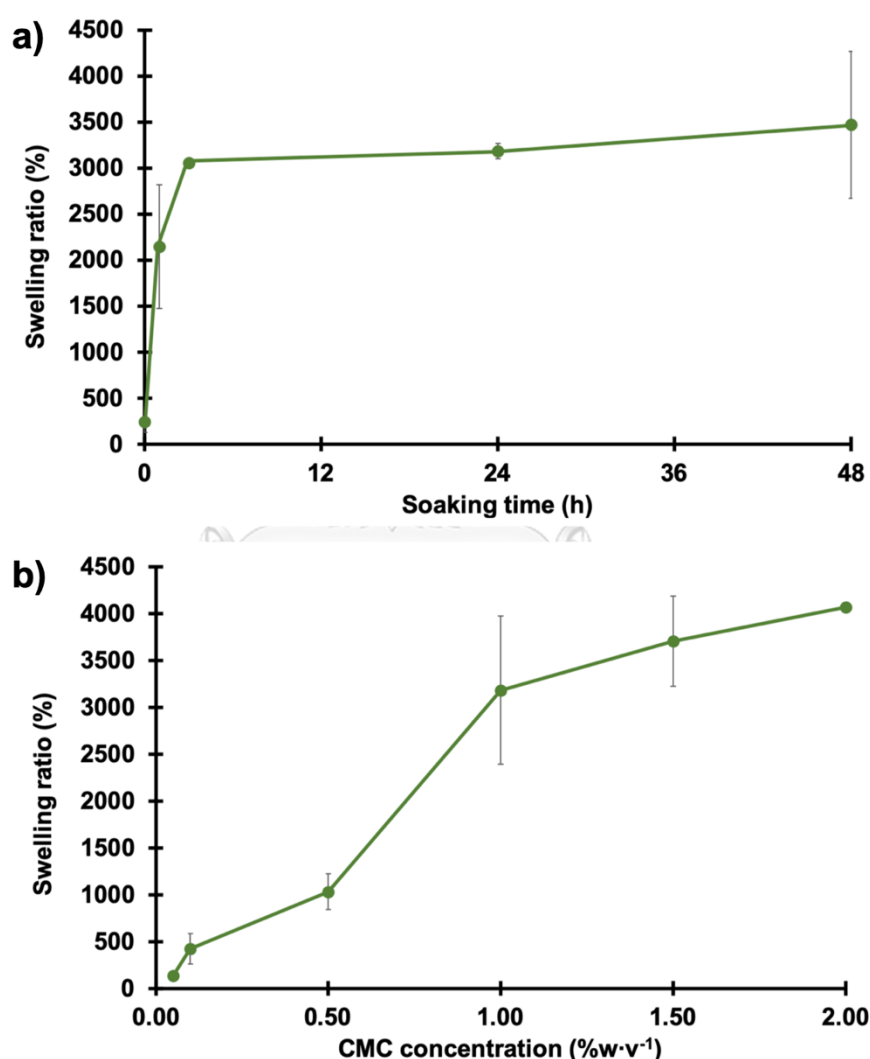
Figure 4.1 Swelling ratios of the BC/CMC hydrogels prepared by using (a) 1.0% w.v^{-1} CMC solution with different soaking times, and (b) varied CMC concentrations with a 24 h soaking time.

The differences in the re-swellability of the pristine BC and the BC/CMC hydrogel are shown in **Figure 4.2**. The pristine BC (**Figure 4.2a**) apparently collapsed into a flat film upon air-drying (**Figure 4.2b**) and was unable re-absorb water, and so remained as a white thin film (**Figure 4.2c**). In contrast, the thickness of the freshly prepared (**Figure 4.2d**) and re-swollen BC/CMC hydrogel after drying (**Figure 4.2f**) were quite similar (~ 4.0 mm), indicating that the developed hydrogel BC/CMC was re-swellable and that the incorporation of hydrophilic CMC helped prevent the collapse of the BC fibrous structure upon drying.

Morphological structures of both the pristine BC and BC/CMC hydrogels in fresh, air-dried, and re-swollen stages were evaluated by FE-SEM. Incorporating CMC into the BC seemed to alter the packing density of the BC fibrous network. The fibrous network of the BC/CMC hydrogel (**Figure 4.2D**) was more loosely packed than that of the pristine BC (**Figure 4.2A**). It should be noted that the fiber diameters of the BC remained almost unchanged upon CMC incorporation (51.52 ± 10.53 and 50.91 ± 11.17 nm for BC and BC/CMC hydrogels, respectively). Once air-dried, both the pristine BC (**Figure 4.2B**) and BC/CMC (**Figure 4.2E**) hydrogels showed a similar collapsed fibrous network, as anticipated. A CMC film was also prepared as a control. As shown in **Figure S4.2 (Supporting Information)**, the dried CMC film showed smooth surface. After re-swelling, the surface of the CMC film became rougher with some shallow pores distributed evenly throughout the whole surface. This result emphasizes that the fibrous morphology observed on the BC/CMC hydrogel originates from the BC alone, not from the CMC.

Nevertheless, the air-dried pristine BC lacked the ability to re-swell, where the collapsed fibrous network was still observed after hydration (**Figure 4.2C**). This may be explained as a result of H-bond formation among the BC fibers [142]. On the other hand, the BC/CMC hydrogel could re-swell once soaked in water and had a morphology of a loosely packed BC network (**Figure 4.2F**) similar to that of the freshly prepared BC/CMC hydrogel before air drying (**Figure 4.2D**). This morphological analysis is consistent with the physical appearances of the gels displayed in **Figure 4.2a-f**. The negative charges along CMC that covered the BC fibers would introduce repulsion and so loosen the packing of dry BC fibers, as well as increasing the hydrophilicity of the pristine BC [143]. This implied that the

developed hydrogel was re-swellable and able to adsorb large amounts of aqueous-based solutions, such as sweat and other aqueous-based biofluids, and should be very useful for wearable sensing applications. Moreover, incorporating BC by soaking directly into the CMC solution prevented packing of BC fibers but did not alter the fibrous structure of the pristine BC.
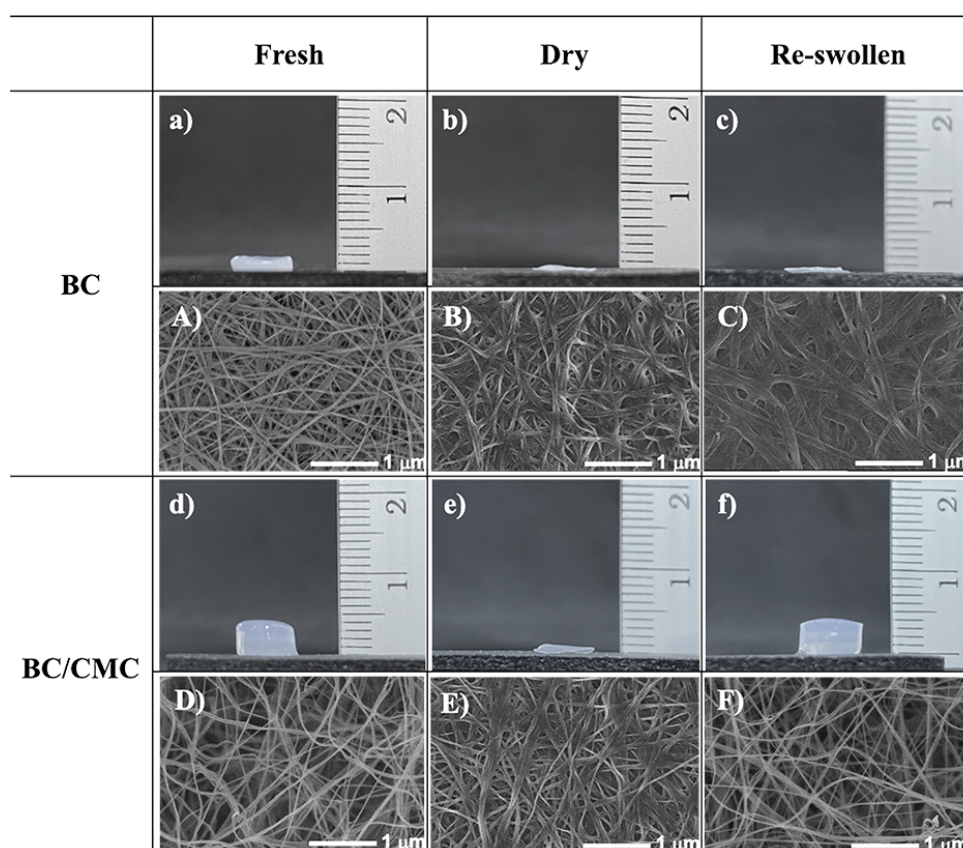
Figure 4.2 Representative (a–f) photographs and (A–F) FE-SEM micrographs (20,000x of magnification) of pristine BC and BC/CMC hydrogels in (a, A, d, D) fresh, (b, B, e, E) dry, and (c, C, f, F) re-swollen stages. The scale bar in micrographs is 1 μm.

X-ray diffraction analysis was performed to investigate the crystalline structure of the BC, BC/CMC and CMC (**Figure 4.3a**). XRD pattern of the pure CMC powder displayed a broad peak at $2\theta = 20.72°$ corresponding to the amorphous nature of the

pure CMC. The BC and BC/CMC hydrogel exhibited three main characteristic diffraction peaks at 15.5°, 17.4°, and 23.7°, which were assigned to the (1$\bar{1}$0), (110), and (200) reflection planes of the cellulose type I of BC [144]. This implies that the incorporation of CMC did not change the crystalline nature of pristine BC. With the XRD patterns of the two hydrogels being almost superimposable, the degree of crystallinity of the BC/CMC hydrogel (72.57 %) was found to be only slightly lower than that of the pristine BC (73.56%), implying that the CMC incorporation had no significant effect on the crystallinity of BC. This outcome was in good agreement with the morphological information, as evaluated by FE-SEM, in which the nanofibrous structure and fiber size of BC/CMC was unchanged in comparison with BC.

As shown in **Figure 4.3b**, both the BC and BC/CMC hydrogels showed a similar slope in the linear range of stress-strain curves, suggesting their equivalent Young's modulus (1.89 ± 0.06 and 1.84 ± 0.10 GPa for the BC and BC/CMC hydrogels, respectively). Yield stress was slightly elevated from 115.08 MPa of BC hydrogel to 121.77 MPa of BC/CMC hydrogel. This indicated that the incorporation of CMC into the fibrous network of BC did not significantly affect the mechanical strength of BC. This outcome is in contrast with that previously reported in a BC/CMC composite prepared by the CMC incorporation in the media used for culturing bacteria during BC formation [145]. This *in situ* incorporation should provide an intimate contact and additional interactions between CMC and the fibrous network of BC, and the H-bonding among the fibrous network of BC should be weakened [146]. Nevertheless, an increase in the elongation at break was observed for the BC/CMC hydrogel (6.7%) compared with the pristine BC (5.3%).

TGA and derivatized thermogravimetric (DTG) curves are demonstrated in **Figure 4.3c** and **4.3d**, respectively. Pure CMC exhibited a weight loss of 48% in a temperature range of 260-350 °C. The pristine BC showed a major weight loss of 80% at a temperature ranging from 280 to 410 °C. This result could be contributed to the degradation of the main cellulose skeleton. In the case of BC/CMC, the degradation profile was observed in a broader range of 255-410 °C (65% weight loss) that covers decomposition of both BC and CMC. The BC was completely decomposed at 563 °C. A 100% weight loss of BC/CMC hydrogel was noticed at a higher temperature (633

^{o}C) suggesting that the thermal stability was improved in the presence of CMC. [147-149] .
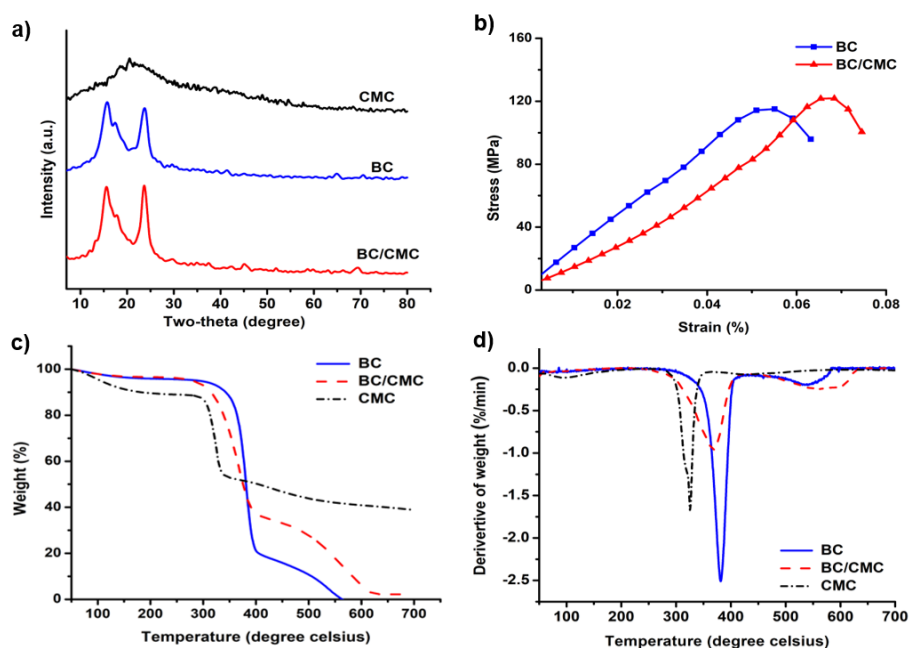
Figure 4.3 (a) XRD patterns, (b) stress-strain curves, (c) TGA curves, (d) and DTG curves of the CMC, BC and BC/CMC hydrogels.

To evaluate the cytotoxicity, L929 cells were incubated for 24 h in CM treated with BC and BC/CMC hydrogels. As determined using the MTS assay in comparison with untreated cells (set to 100% cell viability), the relative cell viability (%) of both BC and BC/CMC hydrogels was higher than 80%, indicating a relatively good biocompatibility. The fact that there was no significant statistical difference between the relative cell viability of the BC hydrogel and that of BC/CMC hydrogel verified that having CMC inside BC did not alter the cytocompatibility of the original BC.

3.2 BC/CMC-based colorimetric pH sensor

Previously, BC membranes have been developed into a paper-based sticker sensor by introducing methyl red as indicator to assess the freshness of cut chicken meat

[150], curcumin to detect volatile amines released during fish spoilage [151], bromophenol blue to assess the freshness of guava fruit [152], and anthocyanin extracted from *Brassica oleracea* as pH indicator in a pH range of 2–10 [153]. Although the success of employing BC membranes as pH sensing platforms have been demonstrated, all these applications used BC membranes in a paper-like format to monitor the target analytes in the gas phase or in enclosed systems in which high water absorptivity is not critically required. Unlike the above-mentioned studies, this research aimed to develop a BC/CMC hydrogel for a sweat pH sensor, in which high water adsorption capacity is crucial to the efficiency to collect the sample and prevent it from evaporation, and also to preserve the immobilized enzyme activity.

To determine whether the pH indicator remained stable inside the BC/CMC hydrogel, the prepared BC/CMC-based pH sensors prepared with/without CTAB were immersed in artificial sweat for 2 h. As shown in **Figure 4.4a**, the artificial sweat turned yellow once soaked with the BC/CMC-based pH sensors prepared without the surfactant (CTAB), indicating that there was leaching of the pH indicator. The color of the BC/CMC-based pH sensor also faded away. In contrast, the color of the artificial sweat soaked with the BC/CMC-based pH sensor prepared with CTAB remained clear. This result emphasized the necessity of using CTAB to effectively stabilize the pH indicator, which was accomplished via the electrostatic interactions between the positively charged CTAB and the negatively charged indicator dyes [45, 154].

Furthermore, the CTAB addition together with the pH indicator solution also enhanced the differentiation ability of the color change of the colorimetric sensor as a function of the pH (**Figure 4.4b**). On the other hand, the color of BC/CMC-based pH sensor prepared without CTAB showed no difference in color for pH 4.0–6.0, which is in the crucial pH range of human sweat [126, 127]. According to previous studies, CTAB shifts the pKa of free anionic pH indicators to a more acidic pH value, which alters the color change behavior and color transition range of pH indicators [155, 156].
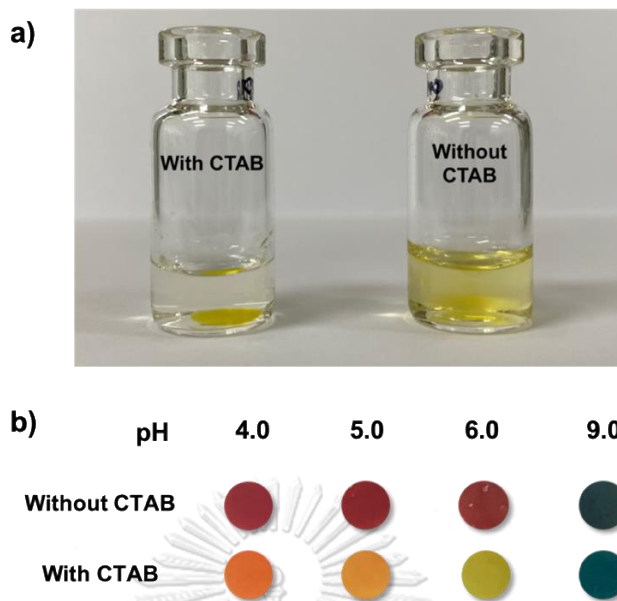
Figure 4.4 (a) The appearance of artificial sweat after soaking with a BC/CMC-based pH sensor prepared (Left) with and (Right) without CTAB, and (b) color changes of BC/CMC-based pH sensor prepared without and with CTAB after being tested with different pH buffers.

The fabricated BC/CMC-based pH sensor exhibited a fast response, with the color change occurring immediately after the pH buffer solutions was added, and the color change could be readily differentiated by naked eyes between each integer pH value. At a low pH (pH 4.0), the sensor appeared orange, then turned to yellow and green when the pH was increased to 5.0 and 6.0, respectively, and started to turn blue at pH 8.0–9.0. As illustrated in **Figure 4.5**, the hue angle of the calibration plot displayed a good correlation coefficient of determination ($R^2 = 0.9617$). Furthermore, the BC/CMC-based pH sensor showed its versatility towards various types of biological fluids, for example, pH 4.0–9.0 for sweat [126], 4.5–9.0 for urine [157, 158], 5.0–8.5 for tears [159], and 5.5–7.5 for saliva [160, 161], due to its wide linear detection range with a vivid color change.
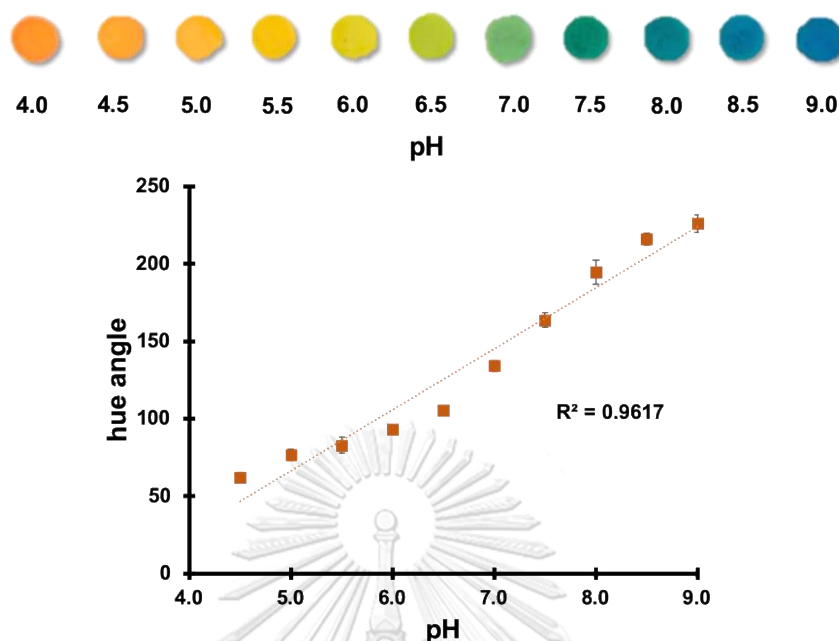
Figure 4.5 Standard color chart and a calibration plot of the BC/CMC-based pH sensor over a pH range of 4.0–9.0. Data are shown as the mean ± 1 SD (n = 5).

In addition, it should also emphasized that the BC/CMC-based pH sensor requires much less amount of sample (10 μL) than the textile-based pH sensor (50 μL) previously reported by Promphet *et al*. [45]. The former is also more sensitive in detecting pH variation of 0.5 as opposed to 1.0 of the latter.

To demonstrate that the BC/CMC hydrogel is a superior substrate to the BC hydrogel as pH sensor, the BC-based pH sensors were prepared by soaking both dry and wet BC films in the pH indicator mixture overnight, dried at room temperature and then washed with DI water. As shown in **Figure S4.3 (Supporting Information)**, the BC/CMC-based pH sensor gave the highest intensity of response towards pH 4.0 buffer solution as compared with the BC-based pH sensors (prepared from both dry and wet BC). The BC/CMC hydrogel can effectively absorb large amount of sensing element (pH indicators) and allowed the fluid sample (pH buffer) to penetrate through the fibrous network of BC and interact with the indicators. On the contrary, the dry BC could not absorb pH indicators right from the beginning resulting in the lowest color intensity. Although the wet BC was able to absorb sensing element (pH

indicators) while the network of BC was swollen in the wet state, the pH 4.0 buffer solution could not penetrate into the collapsed BC network of the dried BC-based pH sensor.

The comparison was also done with CMC hydrogels, prepared by crosslinking CMC with $AlCl_3 \cdot 6H_2O$ and citric acid and designated as $CMC/AlCl_3$ and CMC/CA hydrogels, respectively. Both $CMC/AlCl_3$ and CMC/CAs hydrogels in dry stage were hard and brittle unlike the BC/CMC hydrogel which is soft and flexible. After soaking both CMC hydrogels in the pH-responsive dye mixture and washing the excess dyes with deionized water, the as-prepared $CMC/AlCl_3$ and CMC/CA hydrogels exhibited orange-red color caused by acidic crosslinking agent, whereas the proposed BC/CMC hydrogel displayed yellow-green color indicating its relatively neutral pH as shown in **Figure S4.4 (Supporting Information)**. It should be emphasized that CMC film completely dissolved in the aqueous dye mixture so that the pH sensor cannot be fabricated from CMC alone without undergoing crosslinking.

To investigate the color sensing performance, different pH buffer solutions (pH 5.00, 7.40 (PBS), and 8.00) were dropped onto the as-prepared pH sensors. It was found that only BC/CMC-based pH sensor changed its color in response to pH variation as shown **Figure S4.5 (Supporting Information)**. Due to the residual acidic crosslinking agent remained in the as-prepared hydrogels, the pH sensors based on $CMC/AlCl_3$ and CMC/CA hydrogels could not sense the pH in a range of 5.00 - 8.00. Therefore, the CMC hydrogel is not suitable substrate for pH sensor.

3.3 BC/CMC-based colorimetric glucose sensor

Normally, colorimetric glucose sensing based on KI oxidation by H_2O_2 from the GOx enzymatic reaction changes the color from colorless to yellow-brown. In this case, the reaction between the residual starch components within the BC obtained from the bacterial cultivation process (3.65 ± 0.42 % $w.w^{-1}$ starch found in pristine BC) and iodine results in a purple color [48, 162]. Inherently having starch inside BC truly enhances the sensitivity of glucose detection in which the colorimetric assay relies on iodine oxidation and the formation of starch-iodine complex.

As shown in **Figure 4.6**, the color intensity of the BC/CMC-based glucose sensor increased linearly with the glucose concentration ($R^2 = 0.9930$). The glucose sensor exhibited a low limit of detection (LOD) of 25 µM and a wide linear detection range of 0.0–0.5 mM, which covers the glucose levels observed in human sweat, saliva, and ocular fluids [163].

For comparison, the BC-based glucose sensors were also prepared by dropping KI and the mixture of enzymes (GOx and HRP) onto dry and wet BC films. After that, the glucose solution was dropped onto the BC-based glucose sensors and incubated for 10 min before measuring the color responses in K/S's value. It was found that none of the KI and enzyme solution was absorbed by the dry BC so that the enzymatic reaction and color development cannot take place on the BC-based glucose sensor prepared from the dry BC due to its poor water absorptivity. The wet BC can absorb some of KI and the mixture of enzymes, however, its BC-based glucose sensor exhibited only 73.8% of color intensity as compared with the BC/CMC-based glucose sensor. Both CMC/AlCl$_3$ and CMC/CA hydrogels were also fabricated into glucose sensors using the same approach. Upon testing against 0.3 mM glucose in artificial sweat, no color change was observed on both CMC/AlCl$_3$ and CMC/CA-based glucose sensors (**Figure S4.6, Supporting Information**). This may be explained as a result of enzymatic denaturation caused by highly acidic chemicals used as crosslinking agents for CMC/AlCl$_3$ and CMC/CA hydrogels. Such problem does not exist in the BC/CMC hydrogel which can be prepared without crosslinking agent. It is biocompatible and has neutral pH so that incorporated enzyme can maintain its function and reactivity. Unlike the BC/CMC hydrogel which can well maintain its shape and texture as flat, soft and flexible film, both CMC/AlCl$_3$ and CMC/CA hydrogels lost their original shape and are hard so that they are definitely not suitable substrates for on-skin colorimetric sensor of sweat pH and glucose.

As compared with previous studies that used other types of sensing substrates, this developed glucose sensor exhibited a relatively wider linear detection range with a lower LOD. A comparison of the sensor performance is given in **Table S4.1 (Supporting Information)**. For instance, the sensor based on cotton thread combined with paper had a LOD for glucose of approximately 35 µM with a linear detection range from 50–250 µM [129], which was a higher LOD and narrower linear detection

range than the BC/CMC hydrogel-based sensor developed in this study. We have also investigated the stability of the developed glucose sensor. The results displayed in **Figure S4.7 (Supporting Information)** indicated that the BC/CMC-based glucose sensor retained up to 86% of its initial response (expressed in term of %K/S's) after storage period of 7 days when tested against 0.01 mM glucose. This outcome suggests that the developed BC/CMC hydrogel can act as a versatile platform that can reasonably maintain enzymatic activity of both GOx and HRP.
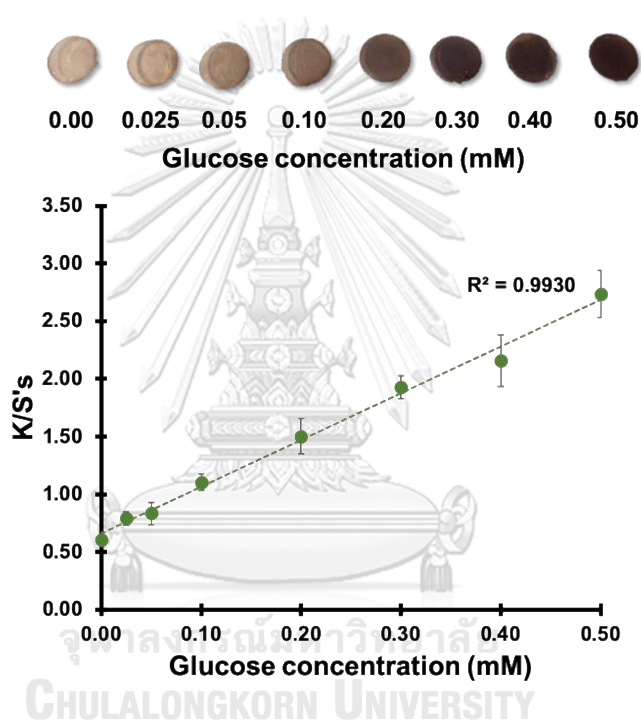
Figure 4.6 Standard color chart and a calibration plot of BC/CMC-based glucose sensor in a concentration range of 0.00–0.50 mM glucose. The color intensity of the sensor was measured in K/s's value. Data are shown as the mean ± 1SD (n = 5).

The developed BC/CMC based glucose sensor was also used to determine the glucose level of glucose-spiked artificial sweat. Sweat was selected as a biofluid sample model since sweat contains various biomarkers of diseases and the sampling is non-invasive. The K/S's values found in the artificial sweat samples with spiked glucose were comparable to the K/S's values from the calibration plot with a %

recovery in the acceptable range [164] (**Table 4.1**). For this reason, the proposed sensing platform can be used as a semi-quantitative glucose sensor for medical diagnosis in various designs, such as an on-body wearable sensor, wrist band sensor, and smart belt sensor.

Table 4.1 Recovery (%) of artificial sweat samples with spiked glucose (n = 3).

Spiked glucose level (mM)	Found glucose concentration (mM)	% Recovery
0.05	0.06 ± 0.01	105.4 ± 10.8
0.10	0.11 ± 0.02	100.6 ± 11.1
0.20	0.21 ± 0.00	100.0 ± 2.2

Conclusion

This research demonstrated that a reswellable BC/CMC hydrogel can be fabricated by a facile approach based on matrix deposition of water soluble and biocompatible CMC into the BC network without the requirement for special physical or chemical treatment. The crystallinity, thermal degradation, tensile property, and cytocompatibility of the resulting BC/CMC hydrogel closely resembled those of the pristine BC, supporting that the preparative method was truly non-destructive. The high-water absorption capacity, a favorable characteristic for effective biofluid sample collection, renders the developed BC/CMC hydrogel a potential platform for non-invasive sensors for sweat pH and glucose, providing a high analytical performance, including a wide linear detection range and a low LOD with low sample volume requirement. The wide linear detection range of the pH and glucose sensors will also be of benefit for application in various medical applications, such as it can be adapted for glucose monitoring in diabetes patients, pH of the urine for urinary tract diseases, and others.

Acknowledgements

Supporting Information

Determination of starch in BC

The starch content of BC was determined using a stepwise procedure as follows.

Step 1: Sample preparation

Firstly, 100 mg of air-dried BC was soaked in 5.0 mL of 80% $v.v^{-1}$ ethanol in a centrifuge tube and incubated at 80° C for 5 min. An additional 5.0 mL of 80% $v.v^{-1}$ ethanol was then added to the incubated mixture followed by centrifugation at 4,500 rpm for 10 min at room temperature (25 ± 2° C). Then, the supernatant was then discarded. Finally, the BC was subjected to digestion in the next step.

Step 2: Starch digestion

The starch digestion was used to convert starch in BC into glucose. Firstly, a mixture of 0.2 mL of 80% $v.v^{-1}$ ethanol and 3.0 mL of DI water was added to the BC obtained from step 1. After that, 0.02 mL of α-amylase was added into the solution mixture and incubated for 5 min in a boiling water bath, then cooled down to room temperature. The volume of the solution mixture was adjusted to 10.0 mL with DI water. Next, 1.0 mL of the solution mixture was mixed with 1.0 mL of amyloglucosidase and incubated in a water bath at 60 °C for 15 min. After cooling the incubated sample down to room temperature, the solution was diluted to 10.0 mL with DI water in a centrifuge tube and used for glucose determination (step 3). The same digestion was also performed on standard corn starch (10 mg).

Step 3: Glucose assay

After the digestion (step 2), the amount of glucose was analyzed using an enzymatic glucose assay. To start the reaction, 2.0 mL of the glucose assay reagent containing the o-dianisidine reagent and the glucose oxidase/peroxidase reagent was added to 1.0 mL of the digested solution mixture obtained from step 2, the reagent blank (the solution mixture used for starch digestion), standard blank (DI water), and glucose standard. Each mixture was mixed thoroughly and incubated at 37 $^{\circ}$C for 30 min. Sulfuric acid (12 N, 2.0 mL) was added to stop the reaction, and the absorbance of each sample was then measured at 540 nm. The percentage of starch was calculated using Eqs. (S1)–(S3):

$$\Delta A_{standard} = A_{standard} - A_{standard\ blank} \qquad (S1),$$

$$\Delta A_{test} = A_{test} - A_{reagent\ blank} \qquad (S2),$$

$$\% Starch = (\Delta A_{TEST} \times DF \times MWF \times 100)/(\Delta A_{STANDARD} \times Sample\ weight) \quad (S3),$$

where $A_{standard}$ is the absorbance of the standard glucose reagent, A_{test} is the absorbance of the sample solution, DF is a dilution factor, and MWF is thea molecular weight of the starch monomer divided by that of glucose.
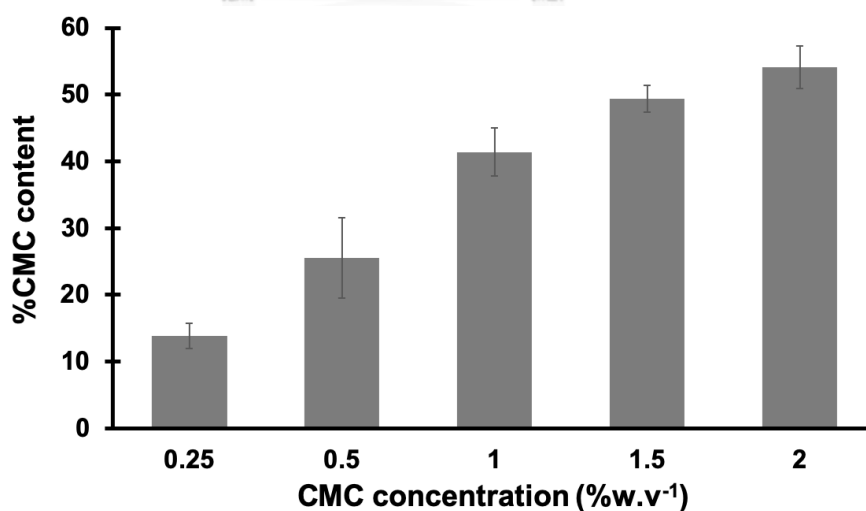
Figure S4.1 CMC content in the BC/CMC hydrogel prepared using different CMC concentration (n = 3).
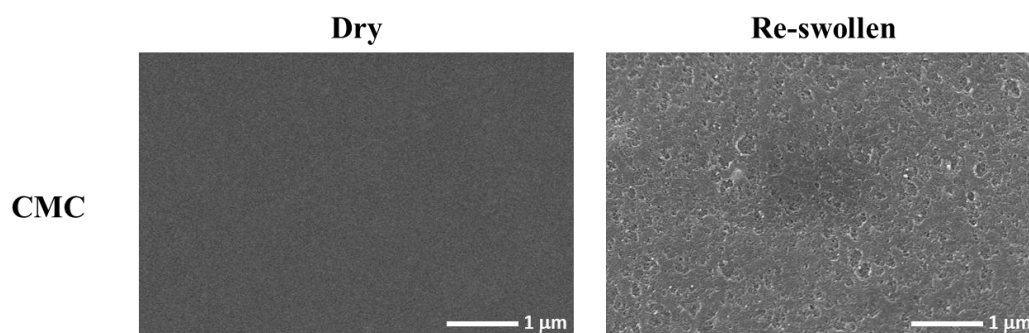
	Dry	Re-swollen

Figure S4.2 FE-SEM micrographs of dry (left) and re-swollen (right) CMC films.
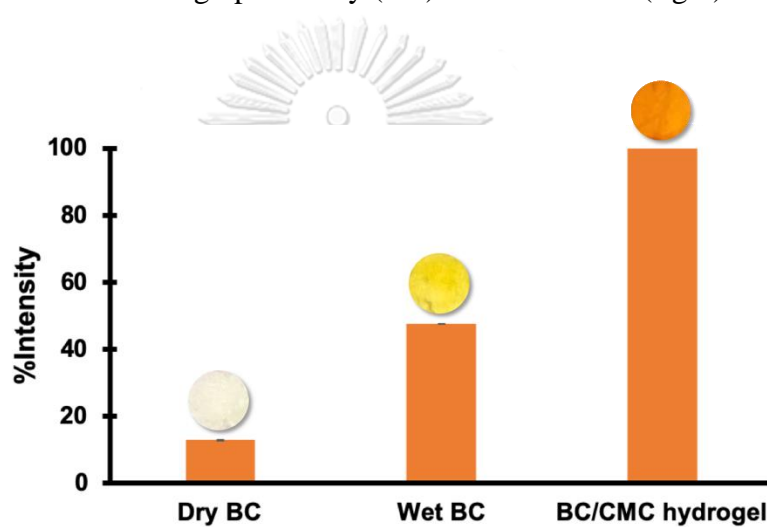
Figure S4.3 Intensity percentage calculated from K/S's value (n = 3) of the BC- and BC/CMC-based pH sensors when tested against a pH 4.0 buffer solution.
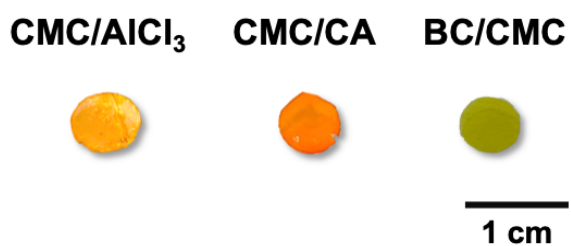
Figure S4.4 Appearance of the as-prepared CMC- and BC/CMC-based pH sensors.
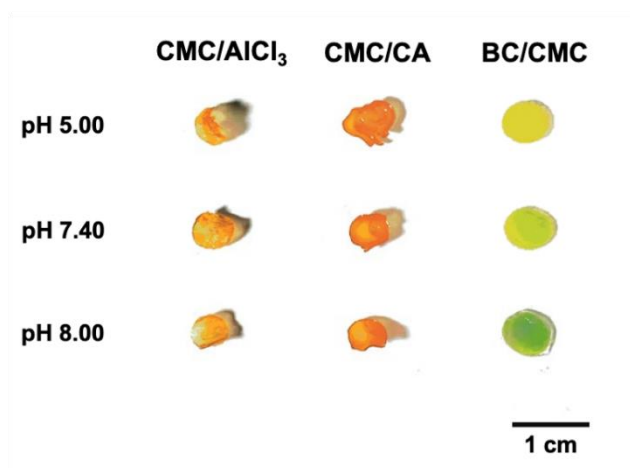
Figure S4.5 Color responses of the CMC and BC/CMC-based pH sensors.
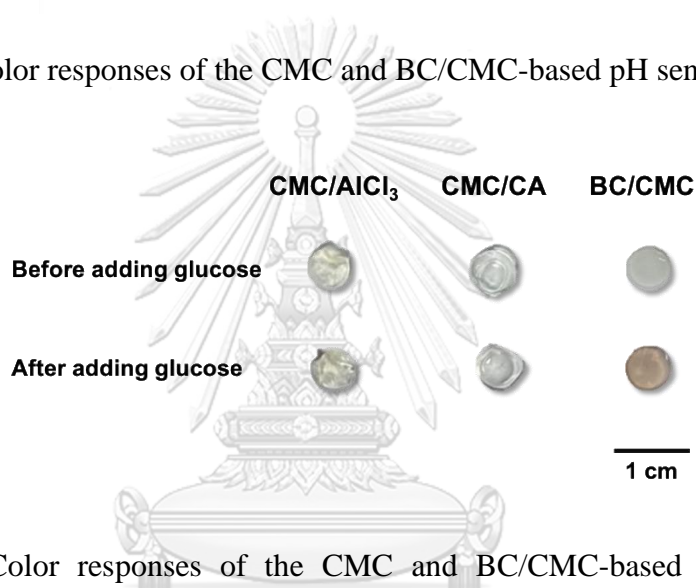
Figure S4.6 Color responses of the CMC and BC/CMC-based glucose sensors towards 0.3 mM glucose in commercial artificial sweat.
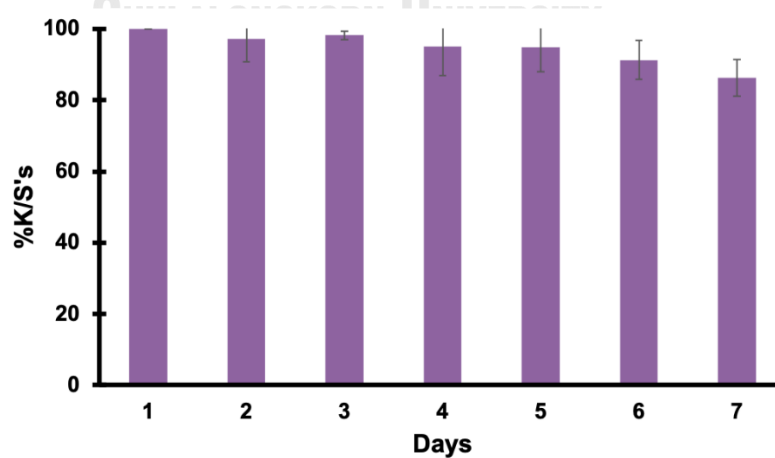
Figure S4.7 %K/s's of BC/CMC-based glucose sensor upon detecting 0.01 mM glucose (n=5) as a function of storage time for up to 7 days.

Table S4.1 Comparison of the developed BC/CMC based glucose sensor to other previously reported sensors based on different substrates.

Sensor substrate	Glucose sensor performance		Ref.
	LOD (mM)	Linear range (mM)	
Filter paper	0.2	N/A	[165]
Filter paper	0.1	0.5 - 5.0	[166]
Filter paper, cotton thread	0.035	0.05 - 0.25	[129]
Paper	0.4	0.5 – 10.0	[167]
Nanocellulose cryogels	0.1	N/A	[168]
BC/CMC hydrogel	0.025	0.00 - 0.50	This work

จุฬาลงกรณ์มหาวิทยาลัย

CHULALONGKORN UNIVERSITY
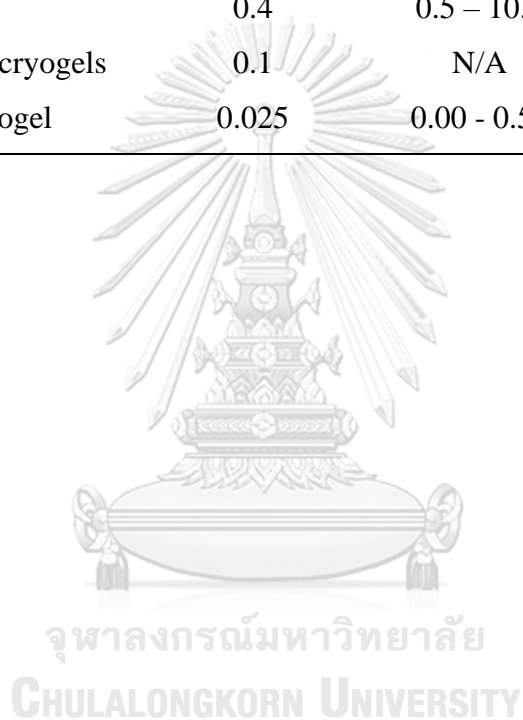
CHAPTER V

Theranostic contact lens based on cellulose nanofibrils/levofloxacin nanocomposite for ocular bacterial infection

Tatiya Siripongpreda [a], Pear Pongsachareonnont [b], Nadnudda Rodthongkum [c,d*]

[a] Nanoscience and Technology Interdisciplinary Program, Chulalongkorn University, Phayathai Road, Wangmai, Patumwan, Bangkok 10330, Thailand

[b] Vitreoretinal Research Unit, Department of Ophthalmology, Faculty of Medicine, Chulalongkorn University and King Chulalongkorn Memorial Hospital, Rama4 rd., Patumwan, Bangkok,10330, Thailand

[c] Metallurgy and Materials Science Research Institute, Chulalongkorn University, Phayathai Road, Wangmai, Patumwan, Bangkok 10330, Thailand

[d] Center of Excellence in Responsive Wearable Materials, Chulalongkorn University, Soi Chula 12, Phayathai Road, Pathumwan, Bangkok, 10330, Thailand

*Corresponding author e-mail: Nadnudda.R@chula.ac.th

Abstract

Ocular bacterial infection is one of the causes of tear pH decrease; nonetheless, common topical drugs give low bioavailability. For simultaneous diagnosis and treatment, theranostic contact lens integrated with cellulose nanofibril/levofloxacin nanocomposite is developed. Cellulose nanofibrils is selected to increase surface area with hydroxyl groups which improves drug binding efficiency without significant lens surface roughness alteration, and also increase hydrophilicity of the contact lens. The as prepared contact lens exhibits the satisfied results of both diagnosis and drug releasing. The sensing function of the lens shows sensitive responses towards tear with R^2 of 0.9601, and also illustrates vivid color change when tear pH decreases indicating the infection severity. At healthy eye condition, the lens displays vibrant green color while turns orange-red color at infections condition. Theranostic contact

lens offers pH-responsive releasing behavior with high content of levofloxacin (up to 106.49 ± 0.77 μg over 24 h) resulted from drug-CNF interaction that releases in acid condition of infection state, yet the drug content substantially decreases when pH increases. Furthermore, the cellulose nanofibrils-based theranostic lens offers non-cytotoxicity confirmed by MTT. This platform might assist both ophthalmologists and patients by offering diagnosis and treatment without invasive procedure.

Keywords: Cellulose nanofibrils, Levofloxacin, Theranostics, Ocular bacterial infection, Colorimetric sensor

Graphical Abstract
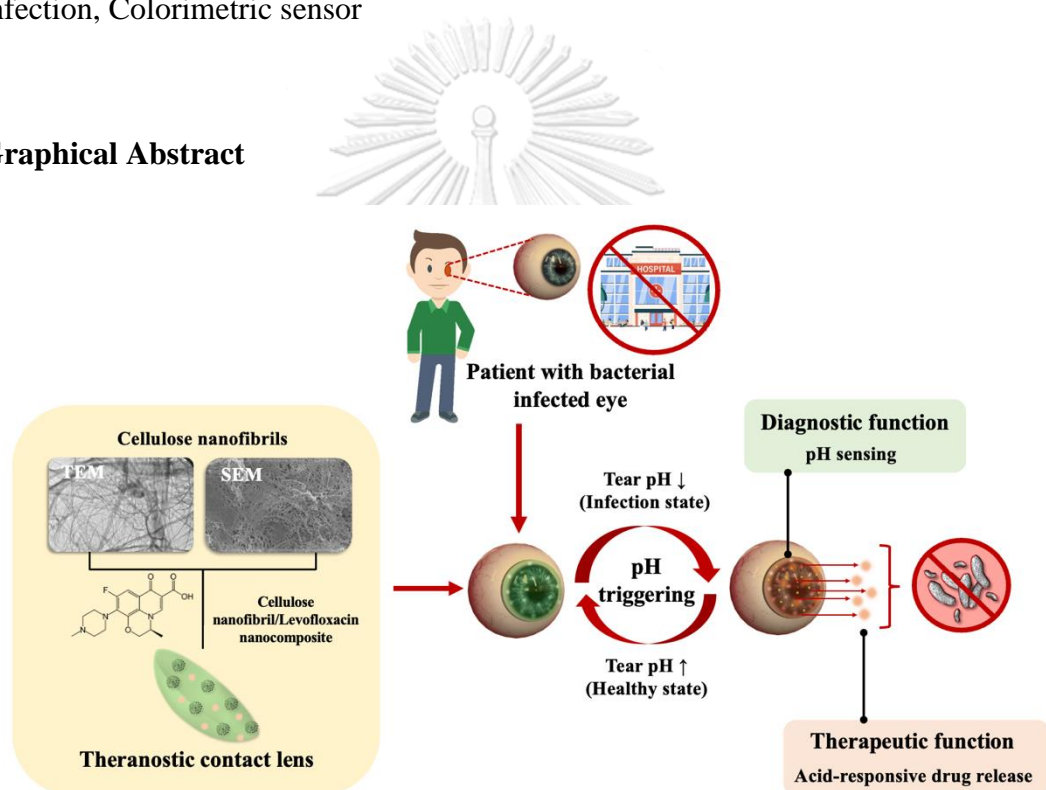
1. Introduction

Tear pH is one of the most important physio-chemical properties of tear film that can indicate the physiological condition of eyes. Healthy tear pH values range from 6.0 to 7.6 [52, 169], which an average is approximately 7.4 [170, 171]. The alteration of tear pH is related to mucin secreted by the conjunctival goblet cells, Meibomian glands secretion, transudation, conjunctival metabolism and carbon dioxide level including the infectious condition of eyes, which the neutral tear pH shifts to acidic pH [171-173]. Ocular bacterial infection is the most common cause of infectious keratitis and related to various types of ocular infections [174]. The infectious pathogens can potentially cause serious intraocular infections leading to visual impairments and blindness [175]. Utilization of antibiotics is commonly treated in form of topical installations (e. g. eye drop, ointment) as it is the most convenient and non-invasive route of drug administration [176]. Furthermore, the antibiotics have been prescribed for treatment and prevent of post-surgical infection from eye surgeries. The common operation performed to treat visual disturbance ocular disease is cataract surgery. Although, antibiotic may cause ocular surface adverse effect to the patients and promote antibiotic resistance [177]. Generally, most ocular diseases for the eye rely on the topical installations, which levofloxacin (e.g. 5 mg/mL^{-1} QUIXIN®) is an antibiotic drug that is frequently used [178]. According to previous report, the conventional topical medication is inefficient with low bioavailability (~5%) since the applied drug is quickly reduced leading to low drug residence time [179]. To increase bioavailability, high frequency of the drug administration is required causing the risk of side effects because of drug overdose and toxicity, and interferes with patient daily activities due to frequent instillation [178, 180].

Recently, wearable technologies integrated with sensors have been growing drastically with higher number of publications [181, 182]. Soft contact lenses have become a high-potential alternative platform for ophthalmic drug delivery due to comfortability to wearers and biological tissue compatibility. Moreover, the drug bioavailability offered by contact lenses under ideal conditions (~50%) is dramatically higher than bioavailability offered by eye drops [183]. The use contact lenses in ophthalmic drug delivery has been investigated [184], nonetheless, there is main obstacle of drug loading using soaking method, which is the rapid drug

diffusion. In the past, contact lens for delivering ophthalmic drug have been developed resulting much longer drug residence time compared to topical delivery [178, 180]. Moreover, the contact lens attaching to the eye surface offers continuous monitoring of eyes physiological condition with minimal invasiveness [79]. For the detection, colorimetry is easy to be monitor without the specific equipment for interpretation which is beneficial to both doctors and home users. Consequently, to simultaneously diagnose and customized therapy, the contact lens was a promising wearable platform for theranostic of ocular bacterial infection. Theranostic integrating diagnoses and therapeutics in a single platform [185], has gained tremendous attention because there is inter-individual variation in drug responses [186], thus efficiently deliver the right amount of drug is crucial for personalized treatment [187].

Cellulose-based nanomaterials have attracted much interest in biomedical application [188, 189], for example, using as hydrogels or substrates for electrochemical [190, 191] and colorimetric sensors [192-194] for increasing sensing sensitivity, water absorbency or mechanical property [195], since it offers abundance of functional group and high specific surface area. Cellulose nanofibrils (CNF) demonstrate notable tendency to form entangling networks facilitating the hydrogel formation [196]. The promising characteristics of the cellulose-based nanomaterials in drug delivery are due to its biocompatibility, and high surface area to volume ratio [197, 198] including stimuli-responsiveness, for example, pH, and ionic strength [198, 199]. CNF also possesses large specific surface area for positive drug-CNF interaction [200] (e.g., levofloxacin) causing high level of drug binding capacity [201]. From the previous reports, the nanocellulose-based composites have been used to control drug release [202, 203]. Hence, CNF is selected for tuning drug release performance and it has been exploited to sustain drug release, such as, anti-inflammatory [204] and anti-cancer drugs. However, the reported works need to modify or grafting the nanosized-cellulose with polymers or drugs to achieve the desired properties, which requires complicated procedures and chemicals [205-207].

Herein, we demonstrated a proof-of-concept for theranostic contact lens, which is the combination of diagnosis and therapy, using commercial contact lens modified with cellulose nanofibrils/levofloxacin nanocomposite for pH-responsive with dual-function including continuous diagnosis and treatment for oscular bacterial

infection. This approach was facile, yet, provided desired stimuli-responsiveness. Furthermore, MTT assay was conducted for biocompatibility verification. This platform might become a novel wearable theranostic approach facilitating the patients, and ophthalmologists to follow-up and treat the disease.

2. Experimental

2.1 Materials and chemicals

Softlens with aspheric optics (-1.00) daily disposable contact lens was bought Bausch + Lomb Incorporated, USA (Made in Ireland). Levofloxacin, LFX ($\geq$98.0%, HPLC), phosphate buffer saline tablet (PBS), cetrimonium bromide (CTAB), methyl red, thymol blue, bromothymol blue, and phenolphthalein were purchased from Sigma-Aldrich. Sodium hydroxide (NaOH), hydrochloric acid (HCl) and acetic acid (CH_3COOH) were obtained from Merck, Germany. Sodium chloride (NaCl) was from CARLO ERBA reagent, Italy. Cellulose nanofibrils (CNF) prepared by supermass colloider was purchased from Cellulose Lab, Canada. Commercial eye drop was from Alcon Laboratories Inc., USA.

2.2 Preparation of pH-responsive dye-micelle embedded contact lens

The commercial contact lenses were washed with deionized water to remove salts and dried at room temperature before further use. The mixture of pH-responsive dyes was composed of 0.0125% w v^{-1} methyl red, 0.0050 % w v^{-1} thymol blue, 0.0600% w v^{-1} bromothymol blue, 0.1000% w v^{-1} phenolphthalein, and 0.1% w v^{-1} of CTAB were dissolved and vortexed in 50% v v^{-1} ethanol/water with NaOH to form micelles. The contact lens was immersed in the dye-micelle mixture for 24 h and washed with deionized water to get rid of the unentrapped dyes. Then, the pH-responsive dye-micelle embedded contact lens (pH sensor-based contact lens) was dried at room temperature.

2.3 Fabrication of a therapeutic contact lens

The as-prepared pH sensor-based contact lens was used as a substrate for drug immobilization, which was carried out by soaking method. First, an LFX loaded

contact lens was prepared by soaking method, which the contact lens was immersed in 1.0 mg mL^{-1} LFX solution for 7 days before blotting and drying at room temperature. For CNF-drug loaded contact lens, the CNF slurry was diluted and dispersed in DI water before adding LFX and using ultrasonication to homogenous dispersion of CNF/LFX nanocomposite. The final concentration of CNF and LFX in the prepared nanocomposite were 0.1% w v^{-1} and 1.0 mg mL^{-1}, respectively. The as-prepared pH sensor-based contact lens was immersed in the nanocomposite dispersion for 7 days then, the contact lens was blotted and dried at room temperature. The preparation process of the theranostic was illustrated in **Figure 4.1**.
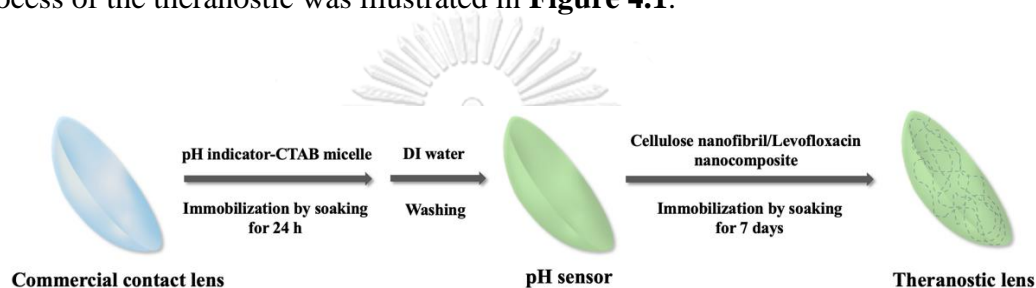
Figure 5.1 Preparation process of the pH-responsive theranostic in ocular bacterial infection based on cellulose nanofibrils/levofloxacin nanocomposite.

2.4 Material characterization

The appearance of the theranostic contact lens was observed and the morphology of the fabricated theranostic contact lens was investigated using scanning electron microscope or SEM (SU3500, Hitachi, Japan). The samples were sputter-coated with gold before the SEM observation. A Hitachi/s-4800 transmission electron microscope (TEM) was used for CNF characterization. The chemical characteristic of materials and composite was studied by using Fourier-transform infrared spectroscopy (FTIR) (Nicolet iZ10, ThermoFisher Scientific). Atomic force microscopy, AFM, (Bruker Icon AFM) was performed to determine the roughness of the contact lens surfaces. Water contact angle measurement was conducted (3 replicates) using a contact angle goniometer (ramé-hart, model 200-F1) using 20 μL drop of water.

2.5 Solid-state UV-visible spectroscopy

The color response towards different pH of the pH-responsive dyes embedded contact lens was evaluated by using a portable spectrophotometer (Datacolor` CHECK3, Datacolor, USA), which the response was measured in CIE h (hue) value.

2.6 Levofloxacin release experiment

For in-vitro drug release profiling, all prepared contact lens was placed in the well plate then, 3.0 mL of 0.01 M buffer solutions with controlled ionic strength (pH 5.0, 7.4 and 8.0) were added into each well, and 1.0 mL of sample solution was collected from the medium at different time intervals. After each collection, the 1.0 mL of fresh buffer was replaced to the well. The released drug concentration was determined by a UV–Visible spectrophotometer (Agilent CrossLab 8453), which standard absorbance curve for LFX was plotted using λ_{max}.

2.7 MTT cytotoxicity assay

The experiment was carried out using method in ISO 0993-5, which L929 mouse fibroblast cells were incubated at 37°C for 24 h in MEM medium, which the medium was replaced with the extract of the samples and incubated at 37°C for 24 h. Next, the viable cells were stained with MTT and incubated at 37°C for 2 h. The MTT was replaced with DMSO in each well. The absorbance at 570 nm was measured using a microplate reader (EASYS, UVM340 S/N ASY54180). Thermanox coverslip was used as a negative control and polyurethane film containing 0.1% zinc diethyldithiocarbamate was used as a positive control. The %viability was calculated from the following equation:

$$\%\text{viability} = (OD_{570a}/OD_{570b}) \times 100$$

Where OD_{570a} is the optical density of 100% extracts of the sample, and OD_{570b} is the optical density of 100% extracts of blank.

3. Results and discussion

3.1 Appearance and roughness of theranostic contact lens

Initially, the morphology of cellulose nanofibrils (CNF) used to fabricate CNF/LFX nanocomposite was characterized by transmission electron microscopy to ensure the nano-size with well dispersion as shown in **Figure 5.2a**. Appearance and roughness of the contact lenses was observed using AFM since the CNF/LFX nanocomposites attachment might cause an alteration of surface roughness of the lens. Commercial contact lens was washed with DI water to remove salts and dried at a room temperature prior to surface modification. The clean unmodified contact lens was displayed in **Figure 5.2b**, it was clear and slightly blue in color. The average Ra of the unmodified contact lens was found to be 31.66 ± 3.97 nm (**Figure 5.2c**). After soaking in a mixture of pH-indicator/CTAB, the contact lens became clear and green, as presented in **Figure 5.2d**. The intensity of color at the edges of the lens was greater than middle area because of the higher thickness of the substrate. To fabricate the theranostic contact lens, the as prepared pH-indicator/CTAB loaded contact lens was immersed in the CNF/LFX nanocomposite, which the slightly change in color was found, and the nanocomposite agglomerates were not observed on the lens surface as shown in **Figure 5.2e.** It was found that no significant change in Ra was found in presence of 0.10% CNF/LFX nanocomposite which the average Ra of the 0.10% CNF/LFX loaded contact lens was found to be 33.91 ± 5.55 nm, respectively. This might be corresponded with the thin coating of LFX/nano-sized polymer on the unmodified lens surface and slightly increased Ra of the unmodified lens. Accordingly, this suggested that the drug-nanocomposite loaded contact lens can provide the comfort wear to the user.
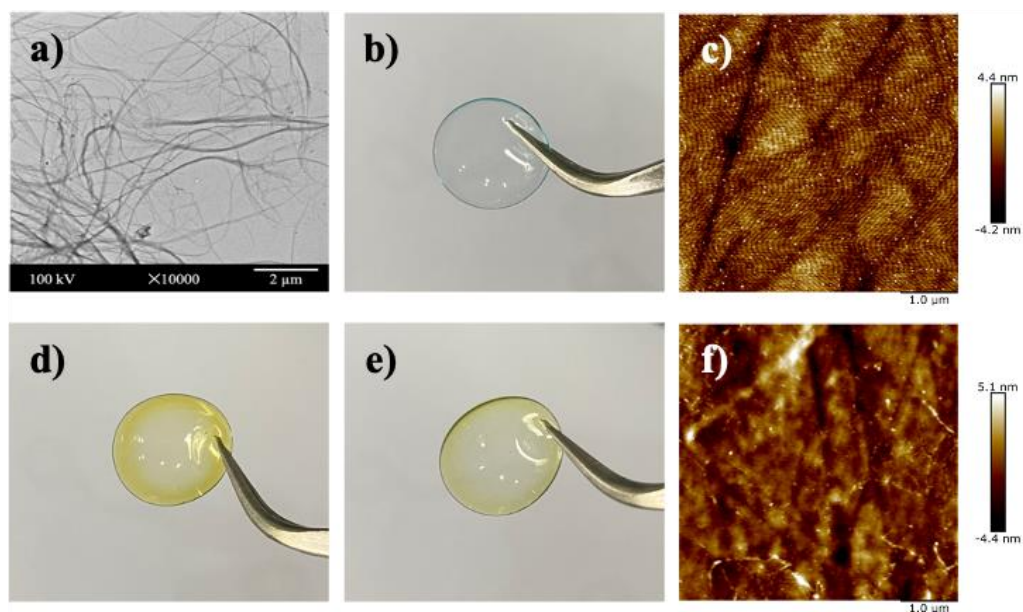
Figure 5.2 TEM micrograph of a) cellulose nanofibrils, and photograph of b) unmodified contact lens and c) AFM image of the unmodified contact lens, photographs d) pH-indicator/CTAB loaded contact lens, e) theranostic contact lens and f) AFM image of the theranostic contact lens.

3.2 Optimization of cellulose nanofibrils concentration in CNF/LFX nanocomposites

As illustrated in **Figure 5.3**, the CNF/LFX nanocomposite prepared using 0.10% w v^{-1} CNF that was loaded onto contact lens exhibited pH-sensitive drug release ability, which the accumulative amount of released LFX at pH 5.0 was higher than pH 7.4 and 8.0, respectively. Although, the CNF/LFX nanocomposite contact lenses prepared from 0.01% w v^{-1} and 0.05% w v^{-1} CNF did not show significant pH-responsiveness or acid-triggered drug release characteristic. Accordingly, the CNF concentration of 0.10% w v^{-1} was used for preparation of the further CNF/LFX nanocomposite, and fabrication of theranostic contact lens.
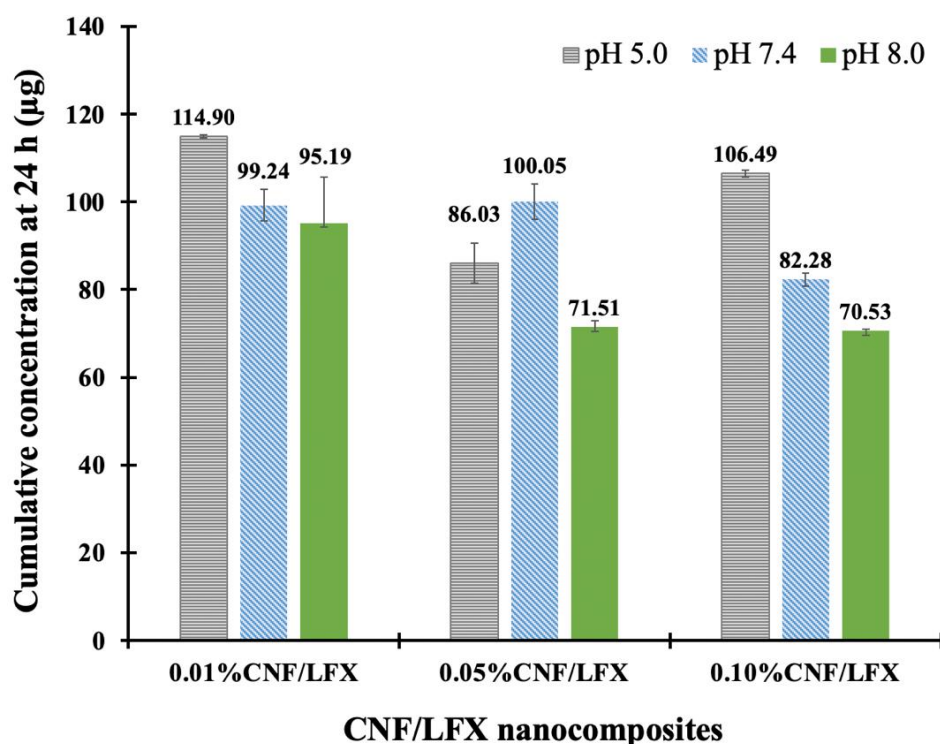
Figure 5.3 Total cumulative release (µg) of LFX released from CNF/LFX loaded contact lenses prepared from 0.01%, 0.05% and 0.10% w v^{-1} cellulose nanofibrils at 24 h (n = 3).

3.3 Surface characterization of theranostic contact lens

SEM micrographs demonstrated the different surface morphologies between before and after the modification from the pristine contact lens to the theranostic contact lens. The unmodified contact lens showed the smooth surface (**Figure 5.4a**). After loading the pH-indicator/CTAB micelles, the small particles of pH-indicator/CTAB agglomerates were found to be attached to the lens surface (**Figure 5.4b**). The surface of the theranostic contact lens displayed wrinkled layer of the nanofibers from the CNF/LFX nanocomposites covered on the surface (**Figure 5.4c**). The micrographs confirmed that CNF/LFX nanocomposite was successfully attached onto the contact lens surface throughout the preparation including blotting process. In swollen state, the unmodified and the theranostic contact lens were subjected to freeze-drying prior to the observation. As presented in **Figure 5.4d,** the freeze-dried

commercial contact lens showed the smooth surface with porous structure, which the average pore size was approximately 8.85 μm. For the theranostic contact lens, the 3D fibrous structure of the CNF was observed showing interconnected 3D network nanostructure, and the size CNF fiber was approximately 37 nm in width, as shown in **Figure 5.4e**.
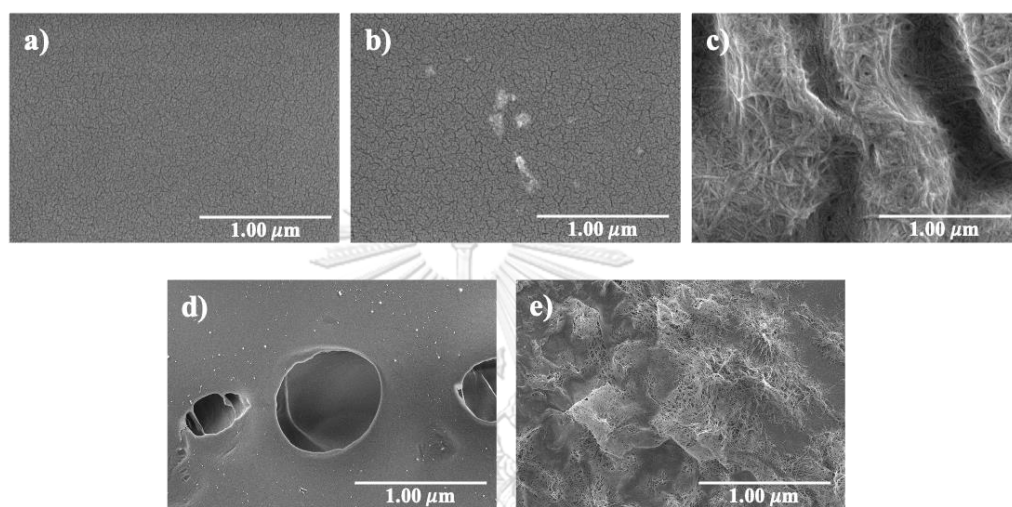
Figure 5.4 SEM micrographs of a) the unmodified contact lens, b) pH-indicator/CTAB loaded contact lens, c) the theranostic contact lens, d) the freeze-dried unmodified contact lens, and e) the freeze-dried theranostic contact lens with magnification of 50,000.

Water contact angles of the contact lenses were carried out to study hydrophilicity of the lens surfaced after modifying the pristine contact lens with CNF/LFX nanocomposite. It was found that water contact angle of the unmodified contact lens approximately 75.2° and the CNF/LFX modified contact lens was 52.4°, as displayed in **Figure 5.5**. This indicated that the CNF increased hydrophilicity and wettability of the pristine contact lens. This result suggested that the modification can increase the ability to entrap the drug molecules and the water absorbency, which led to higher sensitivity in pH sensing response.
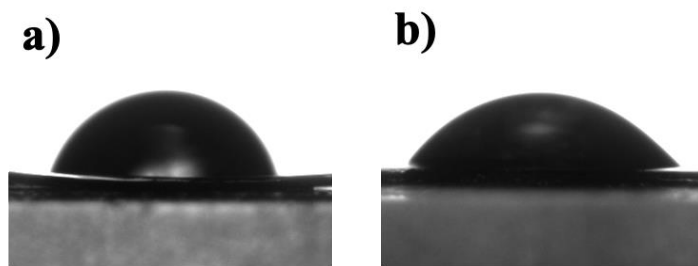
Figure 5.5 Water contact angle photographs of a) the unmodified contact lens, and b) the CNF/LFX loaded contact lenses.

3.3 FTIR of the CNF/LFX nanocomposite and the nanocomposite-loaded contact lens

FTIR spectra of CNF, LFX, an CNF/LFX nanocomposite were demonstrated in **Figure 5.6a**. The significant peaks obtained from cellulose-containing substances were the −OH stretching is located at wavenumber between 3600 - 3200 cm^{-1} and the C−H stretching vibration approximately at 2909 - 2846 cm^{-1}, which can be seen in the spectra of CNF and CNF/LFX nanocomposite [208, 209]. The peak at 2949 cm^{-1} was corresponded to the C−H stretching vibration of cellulose which is polysaccharide [209]. In the spectrum of LFX, 3247 cm^{-1}, and 1720 cm^{-1} represented the aromatic ring, and C=O stretching in −COOH functional group in the drug structure, respectively [210-212].

The shifts and intensity of the spectrum of CNF/LFX nanocomposite was correlated to the intermolecular interaction between drug and polysaccharide (CNF), such as, hydrogen bonding and electrostatic interaction. For example, −OH stretching of CNF of cellulose from 3517 cm^{-1} to 3528 cm^{-1} and, and −OH stretching of LFX from 3247 cm^{-1} to 3272 cm^{-1}, and C=O stretching in −COOH from 1720 cm^{-1} to 1709 cm^{-1} of the nanocomposite spectra.

For the unmodified contact lens, LFX loaded contact lens, and CNF/LFX loaded contact lens, FTIR spectra were illustrated in **Figure 5.6b**. Since the Hilafilcon B (the unmodified contact lens) is commercial silicone, the structure of Hilafilcon B

was predicted using the FTIR spectrum. All the spectra showed -OH stretching is located at wavenumber between 3600 - 3200 cm^{-1}, however, the 3535 cm^{-1} of the unmodified contact lens spectrum indicated the O-H stretching, which shifted to 3518 cm^{-1} in the LFX loaded contact lens. At wavenumber 3100 - 2800 cm^{-1}, and 1719 - 1620 cm^{-1} represent the aliphatic carbon (-CH_2, -CH_3) and C=O, C=C stretching, respectively, which presented in all spectra. Moreover, at wavenumber between 1230 - 1020 cm^{-1} is dominated by C-N stretching that presented in all spectra but the wavenumber and peak intensity changes was found in the CNF/LFX loaded contact lens [213, 214]. The shifting of the peak and changes in intensities in the spectra of the CNF/LFX loaded contact lens might be correlated to interaction between the lens and the CNF/LFX.
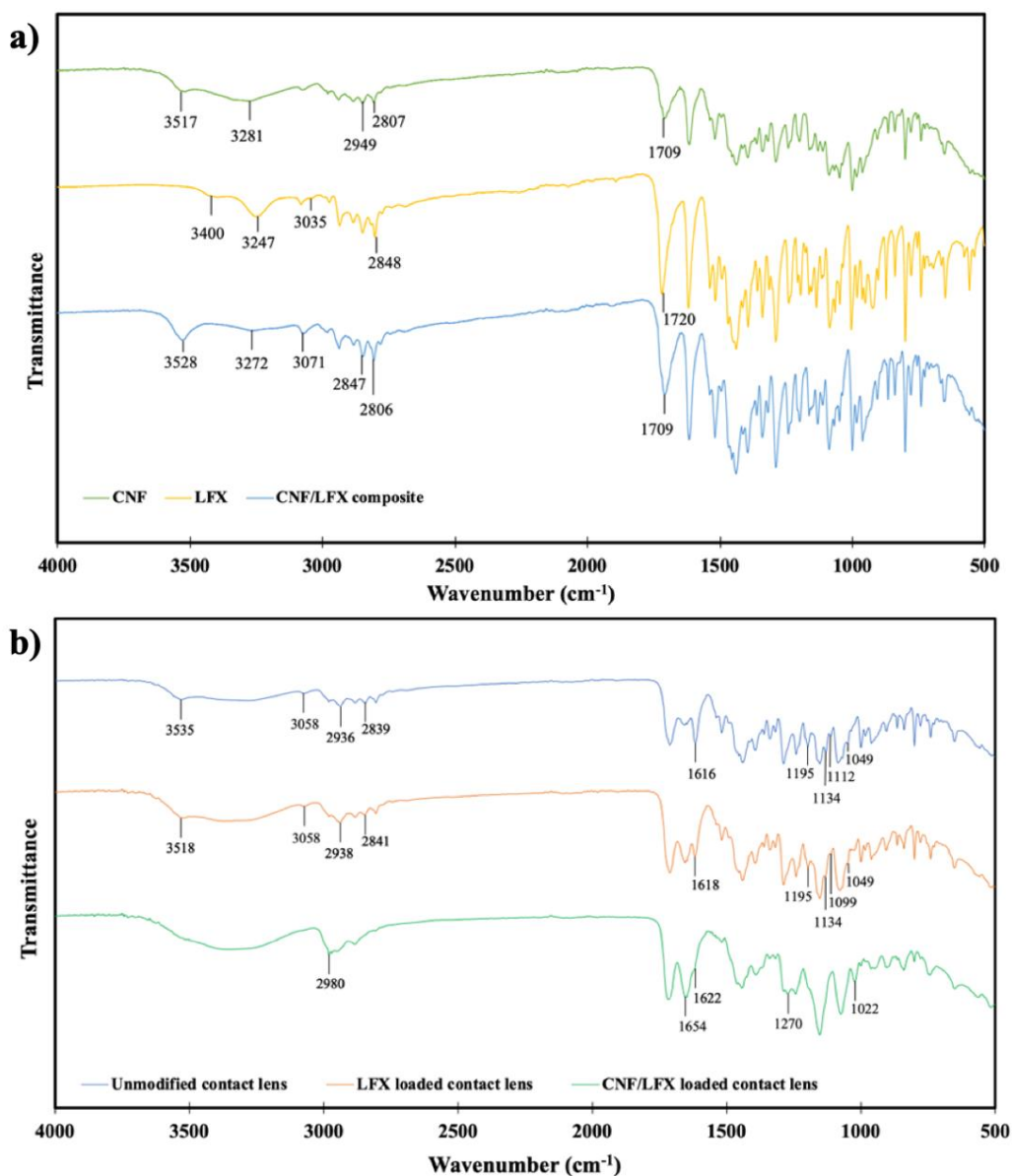
Figure 5.6 a) FTIR spectra of cellulose nanofibrils (CNF), levofloxacin (LFX), and CNF/LFX nanocomposite, and b) FTIR spectra of unmodified contact lens, levofloxacin (LFX)-loaded contact lens, and CNF/LFX nanocomposite-loaded contact lens.

3.4 Visible colorimetric response towards different pH

The performance contact lens-based pH sensor was investigated by immersing the theranostic contact lens in the buffer solutions with different pH e. g.

5.0, 7.4, and 8.0 and measured the color using solid-state UV-Visible spectroscopy technique. The incorporating of CTAB in pH-indicator mixtures helps preventing leakage of pH-responsive dyes that can cause harmful effects, as reported previously [45] and also alter pKa of the dyes giving highly sensitive color changes towards pH [215]. In effect, the dyes embedded contact lens demonstrated a distinctive color changed from orange to green when pH was varied from 5.0 to 8.0, which is the range of tear pH [216], as shown in **Figure 5.7**. The color of the contact lens was measured in hue value. It was found that the calibration plot of the obtained value showed a good correlation coefficient (R^2) of 0.9601, which will assist the precisely follow-up and diagnostic procedure by observing highly sensitive color change towards pHs.

As for the infectious condition, the acidic shift in tear pH from approximately 7.2 - 7.4 was reported [170, 171, 173, 217]. Thus, the contact lens should change from green to yellow-red when the eye is infected, which the color can screen the infection and track the disease severity.
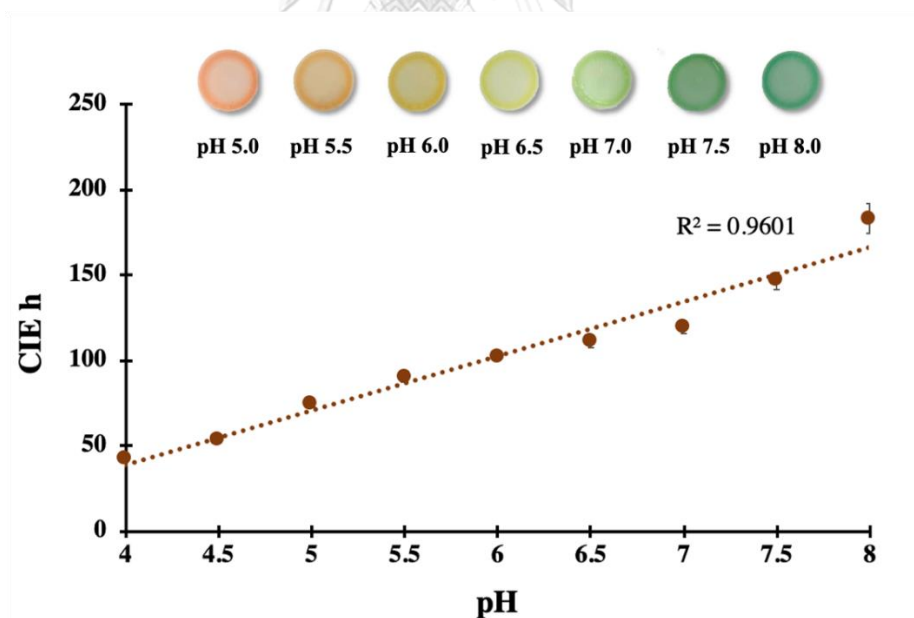
Figure 5.7 Color response and calibration plot of contact lens-based pH sensor (n = 5).

3.6 Levofloxacin releasing profiles

The *in-vitro* drug release profiling of LFX-loaded and theranostic contact lens was performed in acetate and PBS buffer solutions (pH 5.0, 7.4, and 8.0) with controlled ionic strength and determined the LFX concentration in media using UV-visible spectrophotometer. The rapid release of the LFX loaded contact lens was found within 30 min, after that, the slightly increasing of LFX until 1 h was observed. The significant increasing of LFX concentration was not found after 1 h, as illustrated in **Figure 5.8a**. Likewise, the 0.10% CNF/LFX loaded contact lens exhibited the rapid release of the LFX displayed 30 min, however, the increasing of cumulative LFX until 6 h of releasing time was observed with low SD. Moreover, the amount of released LFX was higher than the LFX loaded lens. Upon the increasing of pH to 7.4, which is the physiological pH of healthy eyes as shown in **Figure 5.8b**, LFX from of LFX loaded lens showed the similar trend as the releasing at pH 5.0 but the amount of LFX was relatively higher than LFX amount released from the 0.10% CNF/LFX loaded contact lens. At pH 8.0, the drug releasing behavior the LFX loaded lens was the same as that of 0.10% CNF/LFX loaded lens (**Figure 5.8c**). Compared with the drug release at different pH, the pH 8.0 demonstrated the lowest amount of drug releasing for both prepared drug-loaded lenses. This relatively low cumulative release behavior of LFX at pH 8.0 from both lenses was related to the lower solubility of levofloxacin under basic condition [205].
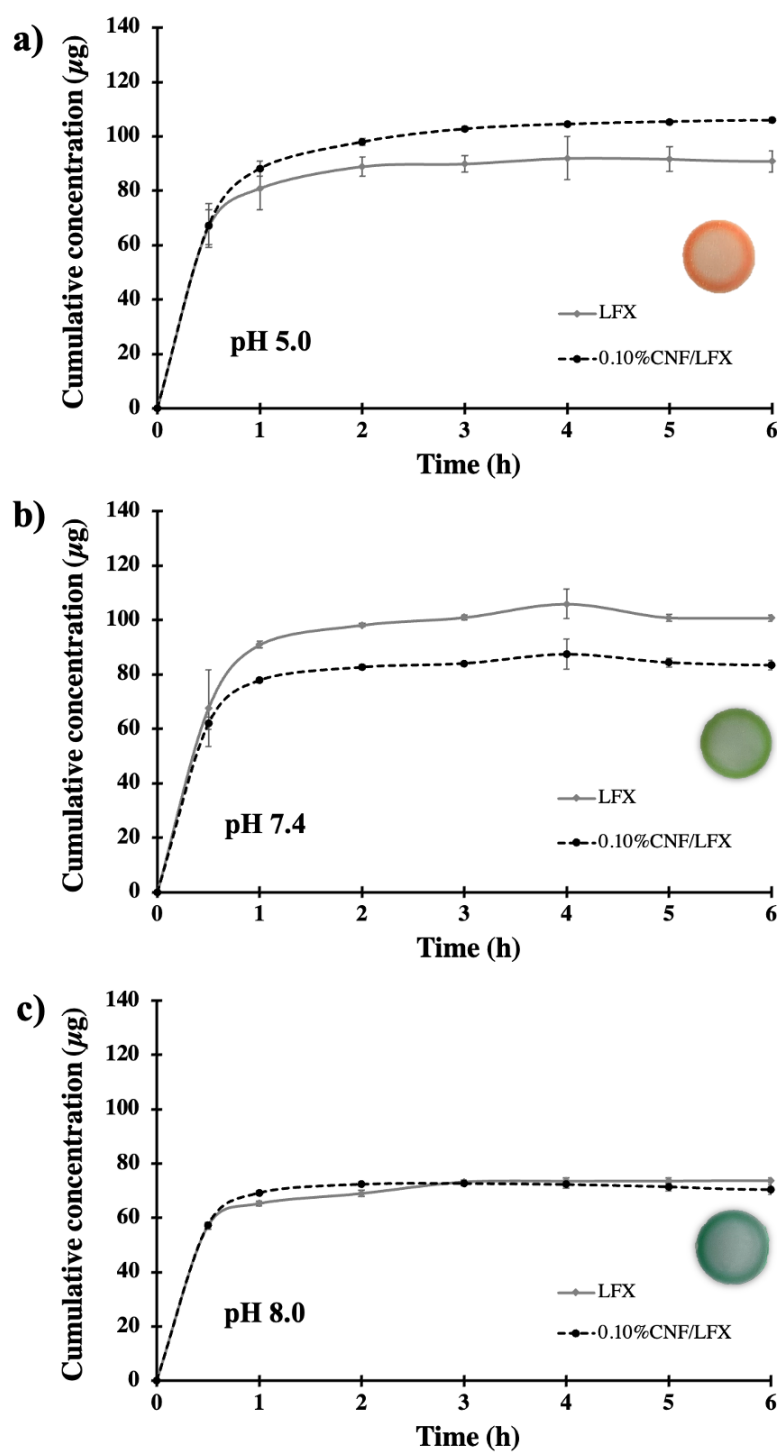
Figure 5.8 Cumulative drug releasing (μg) at (a) pH 5.0, (b) 7.4 and (c) 8.0 from LFX-loaded and theranostic contact lens including the changing of color toward different pH (n = 3).

As shown in **Figure 5.9a** and **Figure 5.9b**, the absorbance value of the released LFX reduced over the time for both LFX-loaded and theranostic contact lens at all pH. The value of the absorbance is proportional to LFX concentration, as described by Beer-Lambert Law [218]. In **Figure 5.9a**, the absorbance at pH 7.4 was relatively high than pH 5.0 and 8.0, while the theranostic contact lens composed of CNF/LFX nanocomposite exhibited higher absorbance at pH 5.0 than high pH values (**Figure 5.9b**). These spectrums displayed good correlation with the accumulative concentration. The total cumulative release (μg) of LFX loaded contact lens prepared by soaking method was presented in **Figure 5.9c**. In 24 h of releasing time, the cumulative concentration of LFX towards pH buffers were found to be 89.4 ± 4.99, 100.6 ± 1.15, and 73.81 ± 0.89 μg for pH 5.0, 7.4 and 8.0, respectively. On the contrary, 0.10% CNF/LFX loaded contact lens presented acid-responsive characteristic of drug release, which the maximum cumulative drug concentrations over 24 h took place at pH 5.0, 7.4 and 8.0 were 106.49 ± 0.77, 82.28 ± 1.56, and 70.53 ± 0.39 μg, respectively.
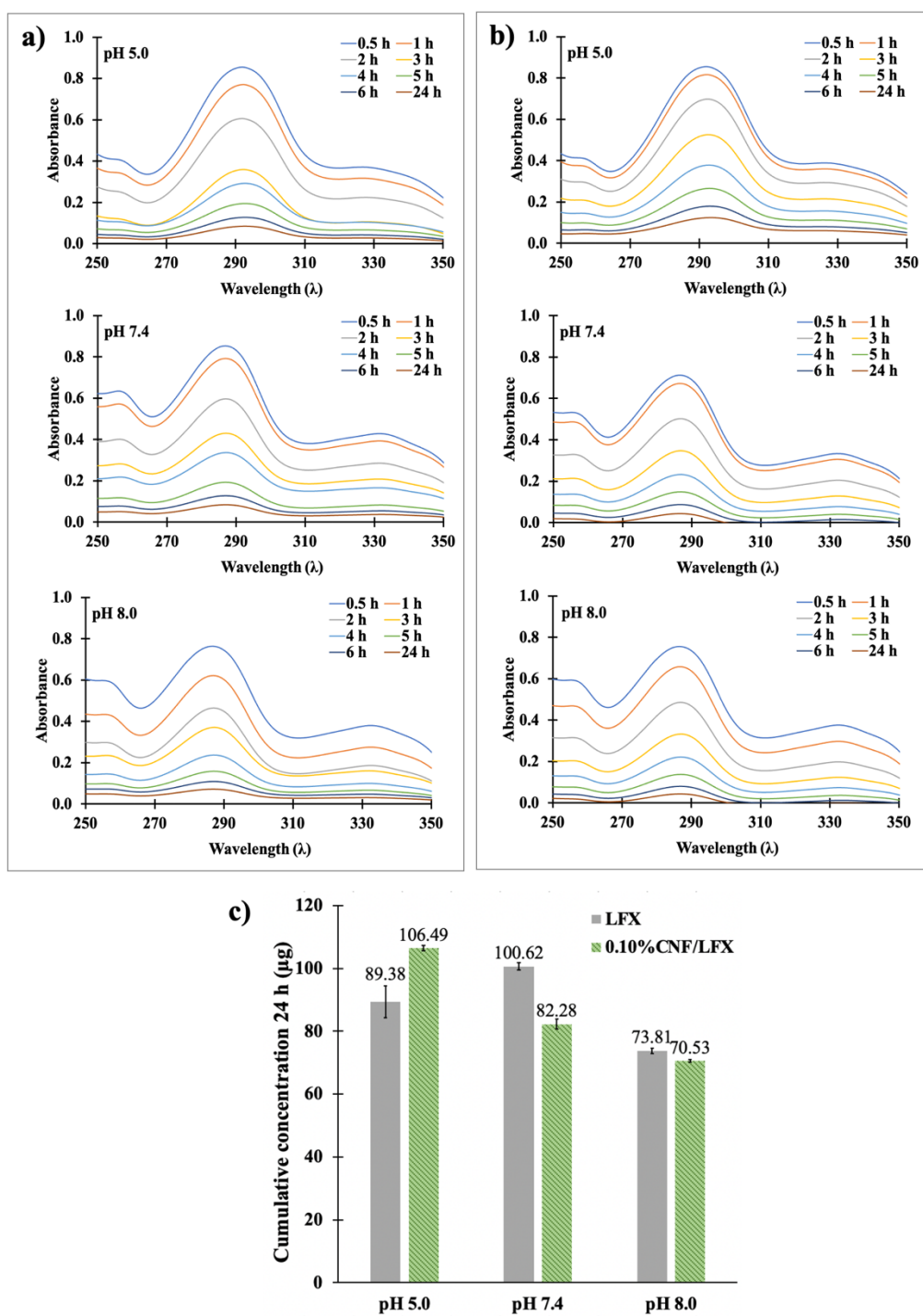
Figure 5.9 UV-visible spectra of levofloxacin released from a) LFX-loaded, b) theranostic contact lens at different pH, and c) total cumulative release (μg) of LFX and 0.10% CNF/LFX loaded contact lens at 24 h (n = 3).

The noticeable pH-responsive characteristics 0.10% CNF/LFX loaded contact lens was related to the interaction between CNF and zwitterionic forms of LFX. According to its structure, LFX is zwitterionic compound with pK_{a1} of 5.7 and pK_{a2} of 7.9 suggesting that the most stable form of LFX was approximately at pH 7.4 [219], which is related to the highest releasing drug of LFX loading lens. In case of 0.10% CNF/LFX loaded contact lens, the presence of CNF led to high amount of released LFX compared with the LFX loaded lens since hydrogen bond between CNF and LFX was created.

In addition, the significant reduction in LFX cumulative concentration over 24 h for the 0.10% CNF/LFX loaded contact lens when pH increased was affected by electrostatic interaction of the functional groups of LFX and CNF. LFX that contains carboxylic group moiety having pK_a around 6.24 [205] exhibited deprotonated form and became negative charge which form the repulsive interaction with the cellulose nanofibrils carrying abundant hydroxyl groups at high pH (7.4 and 8.0). In the preparation process, the pH of the LFX and CNF/LFX solutions were approximately 7.0 -7.1. This created high repulsive force between CNF and LFX attached onto the contact lens surface, which higher pH provides higher repulsive interaction. In consequence, the drug and CNF were hard to bind together, and the entrapped drug was easily removed by blotting process while the network of the nanofibrils was expanding in wet condition. This resulted in low releasing behavior and low LFX cumulative concentration at pH 8.0 which this behavior both drug-loaded contact lenses. It is possible that the high cumulative concentration of antibacterial drug from the proposed theranostic contact lens compared with other works [220, 221] might be related to the nanofibrous structure of CNF providing high surface area and aspect ratio for facilitating drug interaction.

Furthermore, binding energies of LFX with CNF was calculated using Density Functional Theory or DFT. The calculated binding energy of protonated LFX and deprotonated LFX with CNF was -2825.614 and -2687.894 kcal/mol, respectively. This indicated that at pH 8.0 exhibited low drug binding. The optimized structure of CNF-LFX complex was displayed in **Figure 5.10**.
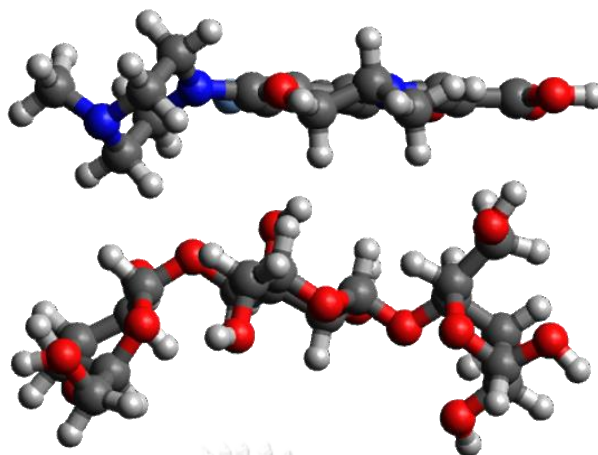
Figure 5.10 The optimized structure of Levofloxacin with cellulose nanofibrils complex.

Additionally, the relatively high standard deviation of total cumulative release of LFX loaded contact lens compared with the CNF/LFX loaded contact lens at 24 h was observed verifying that LFX-CNF interaction helped slow down the drug releasing, as previously described in FT-IR discussion.

3.7 Cytotoxicity

The cytotoxicity of theranostic contact lens for ocular bacterial infection was investigated by MTT assay to verify the biocompatible of the theranostic contact lens. According to ISO 0993-5, the viability of fibroblast cells tested with the sample extract that is higher than 70% compared to the blank indicates non-cytotoxic response production of cells. For theranostic contact lens, %viability was found to be 85%, which suggested that our proposed theranostic contact lens based on CNF/LFX nanocomposite can be a potential theranostic wearable lens for applying with real patients facing oscular bacterial infection. The viability of samples was demonstrated in **Table 5.1**.

Table 5.1 Cell viability evaluated by MTT cytotoxicity assay based on ISO 10993-5

Sample	The average of	
	OD 570 nm	Viability (%)
Blank	1.017	100
Negative control	1.024	100
Positive control	0.000	0
Unmodified contact lens	1.002	98
Developed theranostic contact lens	0.865	85

3.8 Commercial eye drop media

The performance of the developed theranostic contact lens was investigated in preservative-free commercial eye drop media in order to confirm the ability to measure tear pH and releasing drug of the theranostic contact lens. As shown in **Figure 5.11**, the color of the lens indicated that the pH of eye drop was neutral. For the LFX release study, the theranostic contact lens exhibited ability to prolong LFX release, which the LFX concentration increased rapidly at $0 - 1$ h then continued to release to 6 h of releasing time. It was found that the cumulative concentration of LFX was 110.88 ± 0.77 µg at 24 h of releasing time. These results confirmed the theranostic performance of the developed contact lens to be used in real matrix.
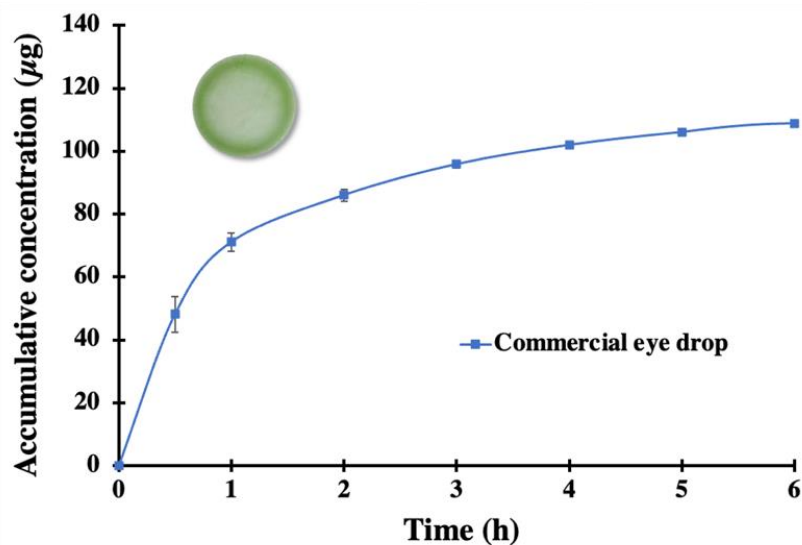
Figure 5.11 Cumulative drug releasing (μg) from LFX-loaded and theranostic contact lens including the changing of color toward commercial eye drop (n = 3).

Conclusion

Theranostic contact lens for oscular bacterial infection were successfully prepared by incorporating CNF/LFX nanocomposite for tuning pH-responsive drug release behavior. CNF/LFX nanocomposite containing theranostic contact lens exhibited the pH-responsive levofloxacin releasing, which the highest cumulative concentration of drug was presented at pH 5.0, 7.4, and 8.0, respectively. This obtained contact lens provided high drug content at low pH (106.49 ± 0.77 μg at pH 5.0 over 24 h) and the longer drug residence time compared with conventional eye drops, leads to an improved treatment of the infection since it enhanced drug bioavailability. Meanwhile, the contact lens also displayed sensitive and vivid color change from green to orange when tear pH decreased corelated with eye infection that is useful for the disease diagnosis. These functions were provided by cellulose nanofibrils that increased hydrophilicity, surface area and functional groups on the contact lens surface leading to pH-responsive drug release behavior with high drug entrapment. Furthermore, this developed contact lens was fabricated from the commercial contact lens with biocompatible reagents and non-cytotoxic confirmed by MTT testing.

Consent to participate

Not applicable

Consent to publish

Not applicable

Availability of data and materials

Not applicable

Competing of interest

The authors have no competing interests to declare that are relevant to the content of this article.

Author Contributions

All authors contributed to the study conception and design. Material preparation, data collection, analysis, and first draft of the manuscript were performed and written by Tatiya Siripongpreda. Conceptualization and visualization were performed by Pear Pongsachareonnont, and funding acquisition, conceptualization, supervision, validation, review & editing were performed by Nadnudda Rodthongkum. All authors commented on previous versions of the manuscript including read and approved the final manuscript.

CHAPTER VI

Novel nanocomposite-chitosan film based on titanium dioxide/nitrogen-doped graphene nanocomposite for LDI-MS

Tatiya Siripongpreda [a], Russell J. Composto [b], Naddudda Rodthongkum [c,d*]

[a] *Nanoscience and Technology Interdisciplinary Program, Chulalongkorn University, Phayathai Road, Wangmai, Patumwan, Bangkok 10330, Thailand*
[b] *Department of Materials Science and Engineering, University of Pennsylvania, Philadelphia, Pennsylvania 19104, United States*
[c] *Metallurgy and Materials Science Research Institute, Chulalongkorn University, Phayathai Road, Wangmai, Patumwan, Bangkok 10330, Thailand*
[d] *Center of Excellence in Responsive Wearable Materials, Chulalongkorn University, Soi Chula 12, Phayathai Road, Pathumwan, Bangkok, 10330, Thailand*

*Corresponding author e-mail: Nadnudda.R@chula.ac.th

Abstract

Laser desorption-ionization mass spectrometry or LDI-MS is a powerful technique for quantitative and qualitative detection of biomolecules such as amino acids, peptides, proteins which can be used as the biomarkers for early disease diagnosis. Herein, titanium dioxide/nitrogen-doped graphene nanocomposite (TiO_2/NG) was synthesized and spin-coated on silicon wafer using chitosan as a polymeric support to create a polymeric nanocomposite thin film. The developed thin films were exploited as a self-matrix of LDI-MS for peptide detection without the use of conventional organic matric. The result showed that the developed thin film was able to determine various peptides (i.e., bradykinin, angiotensin I, angiotensin II, bombesin, renin substrate, adrenocorticotropic hormone) with high intensity and high signal to noise ratio. Thus, this novel polymeric nanocomposite thin film might be a potential LDI-MS self-matrix for biomarker determination for medical diagnosis.

Keywords: Titanium dioxide, Nitrogen-doped graphene, LDI-MS, Chitosan, Thin film, Peptide biomarkers

Graphical abstract
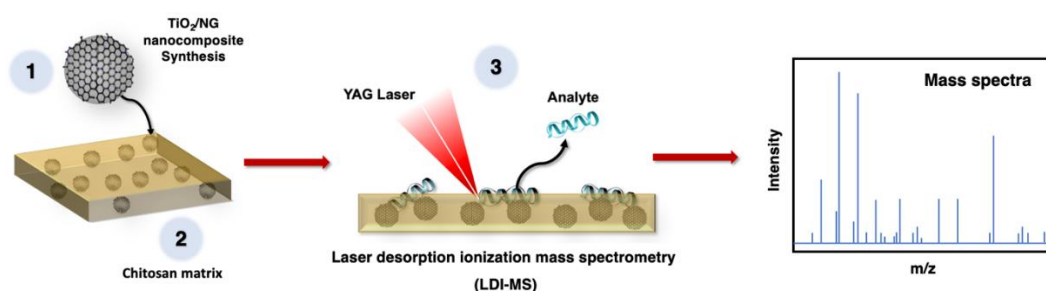
1. Introduction

Several peptide molecules have been used as biomarkers for disease diagnosis. For instance, bradykinin can indicate angioedema [222], cartilage degradation and inflammation in the synovial fluid [223], and etc. Renin-angiotensin system is composed of angiotensinogen, angiotensin I that is converted to angiotensin II by renin substrate, which angiotensin II triggers inflammation, coagulopathy, vasculopathy, fibrosis, oxidative stress, and thrombosis. According to previous report, it is related to pneumonia, sepsis, acute respiratory distress syndrome, diffuse thrombosis, and multi-organ damage in severe acute respiratory syndrome coronavirus-2019 (COVID-19) [224]. Thus, angiotensin I, II and renin, especially angiotensin II, can be used as COVID-19 biomarkers and severity prediction. Adrenocorticotropic hormone (ACTH) is a peptide hormone related to Cushing and Addison syndrome which resulting in high levels of secreted or circulating ACTH [225, 226]. Bombesin is another interesting peptide that is recently proposed as a biomarker for early detection of bronchopulmonary dysplasia in infants [227]. However, some peptides need complicated procedure like enzyme-linked immunosorbent assay (ELISA), for example, bradykinin. Hence, laser desorption-ionization mass spectrometry (LDI-MS) was chosen for the biomarker determination. LDI-MS is a soft ionization mass spectrometry that is selective to organic molecules since the signals are obtained from relative molecular mass, but this technique needs

laser-absorbing matrices, such as cyano hydroxycinnamic acid, sinapinic acidfor transferring energy to target molecules [109].

Titanium dioxide (TiO$_2$) is a promising for LDI-MS matrix and common semiconductor applied in the field of photocatalysis, because of its strong light absorption, chemical stability, low cost, and non-toxicity [228]. There are 3 different forms of TiO$_2$, which are anatase, rutile, and brookite that consist of interconnected TiO$_2$ octahedra with different degree of distortion [25]. Although, anatase form offers the most stability in the nanoscopic scale and exhibits photocatalytic activity over rutile. Therefore, anatase is considered more suitable for photocatalytic applications [229]. Graphene is an allotrope of carbon in the form of a single layered hexagonal lattice with sp^2 hybridization [230] having high conductivity, high stability, and a large specific surface. Doping nitrogen atoms into graphitic structure to create nitrogen-doped graphene (NG) provides functional groups, catalytic activity, with large surface area and increased free carrier density. From previous report, NG offers a clearer matrix background, better salt tolerance, and higher detection sensitivity compared with other graphene-based materials [33]. By integrating TiO$_2$ and NG nanomaterials together, the proposed hybrid nanomaterials having high surface area of nanostructures provide active sites for analyte desorption/ionization and signals with less background mass peaks related to the matrix molecules at low m/z [231]. Chitosan (CH), a cationic polymer which its charge density depends on the degree of acetylation and pH of the solvent [232], was selected for using as a polymeric support for the nanocomposites since it possesses biocompatibility, biodegradability and film-forming ability.

Herein, titanium dioxide/nitrogen-doped graphene nanocomposites (TiO$_2$/NG) were synthesized using simple hydrothermal reaction. The TiO$_2$/NG nanocomposites was combined with CH and spin-coated on silicon wafer to prepare TiO$_2$/NG-CH thin films. The TiO$_2$/NG nanocomposites was characterized and the TiO$_2$/NG-CH thin films utilized in as a substrate and self-matrix of LDI-MS for sensitive detection of disease biomarker facilitating the proper therapeutic decision.

2. Experimental

2.1 Materials and instrument

Titanium dioxide nanopowder (TiO$_2$, anatase with <25 nm particle size) was purchased from Sigma-Aldrich, USA. Nitrogen-doped graphene (NG) was obtained from ACS material, USA. Chitosan, Chitoclear® Cg-10 (Mw: 60 kDa and degree of deacetylation: 87%) was received from Primex ehf., Iceland. Glacial acetic acid, isopropanol (IPA), ethanol, methanol, and toluene were purchased from Fisher scientific, USA. N-type, oriented silicon wafers (dopant Ph, 10−20 Ω· cm resistivity, single side polished) were purchased from Silicon Quest International. Peptide calibration standard II was obtained from Bruker, Germany.

2.2 Characterization

Scanning transmission electron microscope (S/TEM, JEOL F200) was used for sizes and morphology observation of nanomaterials and elemental mapping to confirm the obtained nanocomposite composition.

2.3 Synthesis of the titanium dioxide/nitrogen-doped graphene (TiO2/NG) nanocomposites

TiO$_2$ nano-powder and 2.5% w·w^{-1} NG flakes were sonicated with ultrapure water for 8 h. Then, the dispersion was added to a 100 mL hydrothermal reactor and heat-treated at 180°C for 24 h. After the hydrothermal reaction, the obtained nanocomposite suspension was centrifuged at 8000 rpm for 15 min, and ethanol for 3 times. Then, the nanocomposite was dried at 60°C.

2.4 Preparation of chitosan films with TiO$_2$/NG nanocomposites

Chitosan power was dissolved in 50% v·v^{-1} acetic acid (1.0% v·v^{-1}) and IPA. TiO$_2$ or TiO$_2$/NG nanocomposites was added to the chitosan solution, sonicated for 3 h and filtrated with 0.22 μm filter. Silicon wafer was cut into 1.0 × 1.0 cm^2 and washed with methanol and toluene then, dried with N$_2$. After that, 50 μL of the

prepared dispersion was dropped onto the clean silicon wafer and spin-coated using 5000 rpm for 1 min.

2.5 Laser desorption ionization mass spectrometry (LDI-MS) of chitosan film with TiO_2/NG

First, 2 µL of standard peptide solution (2 pM·µL^{-1}) was dropped onto the as-prepared spin-coated wafer and dried at a room temperature 25±5 °C prior to attaching to target plate and inserting into a mass spectrometer. All LDI-MS experiments were performed on a Bruker Autoflex Max MALDI-TOF mass spectrometer with 30% N_2 laser (337 nM) intensities and 30 laser shots.

3. Results and discussion

3.1 Characterization of TiO_2/NG nanocomposite

As shown in **Figure 6.1a**, the pristine TiO_2 were rod-shaped particles with hetero-dispersity, and the particle sizes were found to be 22-35 nm. However, it was found that the synthesized TiO_2/NG nanocomposite (**Figure 6.1b**) exhibited round-shaped with smaller particle size, approximately 20 nm in diameter, and also showed higher homo-dispersity compared to the pristine TiO_2. According to pervious report, the high temperature of the hydrothermal reaction affected to the shape and dimensional size of TiO_2 [233].
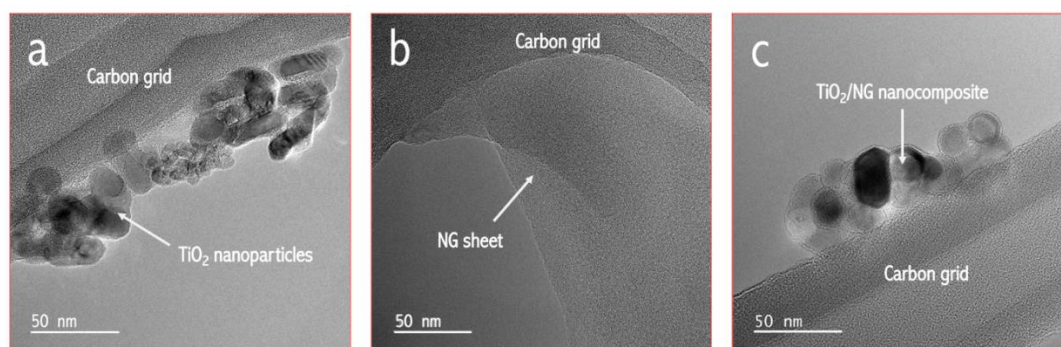
Figure 6.1 TEM images of a) TiO2 nanoparticles, b) NG sheet, and c) TiO2/NG nanocomposites with magnification of 250k.

EDX spectrum of TiO_2 and TiO_2/NG nanocomposites were shown in **Figure 6.2**. In **Figure 6.2a**. the spectra showed the peaks of Ti and O of pristine TiO_2 nanoparticles, which the inset displayed only Ti and O element. After the hydrothermal reaction with NG (**Figure 6.2b**), the high intensity of Ti and O with lower intensity of C and N verifies that there are NG successfully coated onto TiO_2 nanoparticles. This confirmed by the elemental mapping inset that illustrated C, and N from the introduced NG.

จุฬาลงกรณ์มหาวิทยาลัย

CHULALONGKORN UNIVERSITY
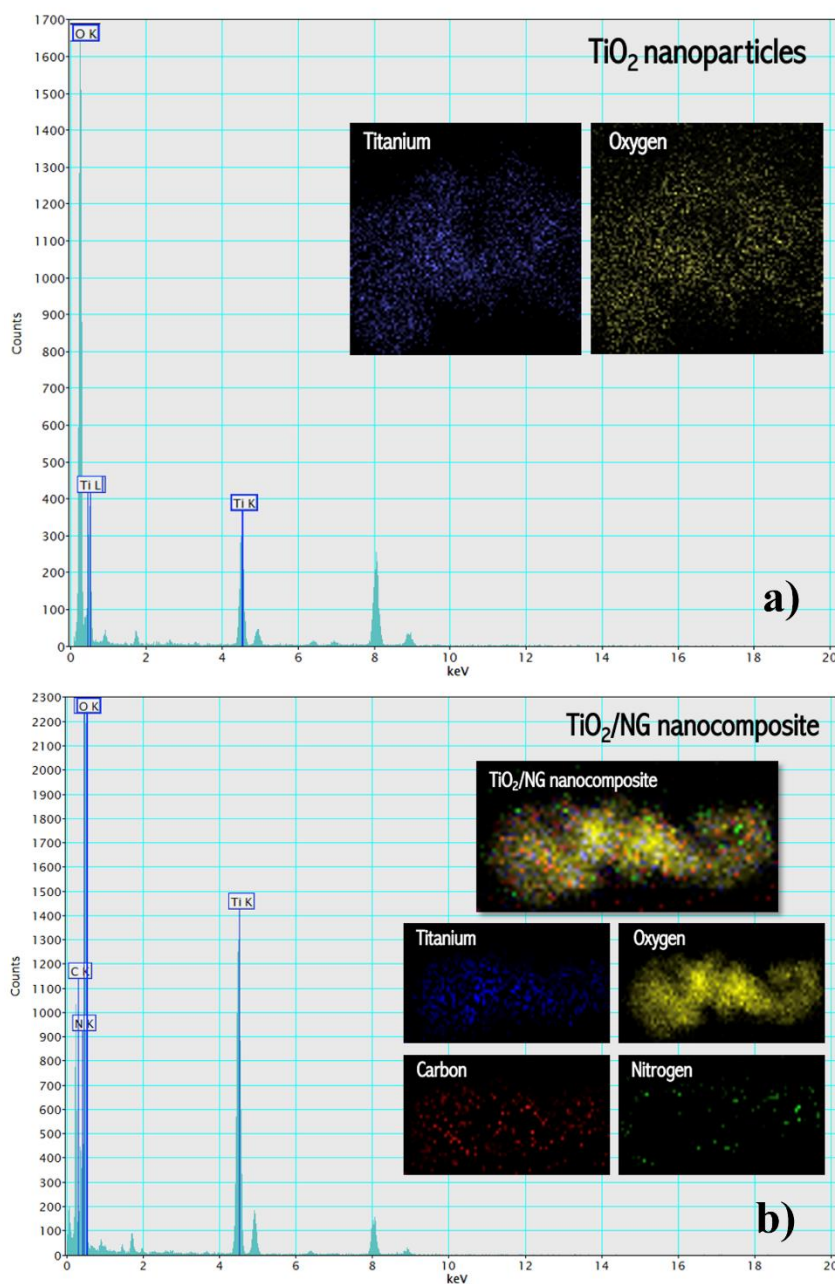
Figure 6.2 EDX analysis and elemental mapping of a) TiO_2 and b) TiO_2/NG nanocomposites.

3.2 Chitosan and chitosan with TiO_2/NG nanocomposites thin films

As shown in **Figure 6.3**, the solvent using for spin-coating chitosan affected the thin film formation. The spin-coated chitosan using 1% acetic acid as solvent

(**Figure 6.3a**) showed poor film quality and nonuniformity that might be caused by low viscosity of the chitosan solution. Since NG is well dispersed in IPA [234], IPA was selected to use in the solvent mixture (1% acetic acid with 50% IPA). It was found that the thin films of chitosan (**Figure 6.3b**) and chitosan with nanocomposite (**Figure 6.3c**) exhibited higher film quality with uniformity. The better film formation using the acetic acid/IPA solvent mixture was due to the gelation of chitosan by IPA.
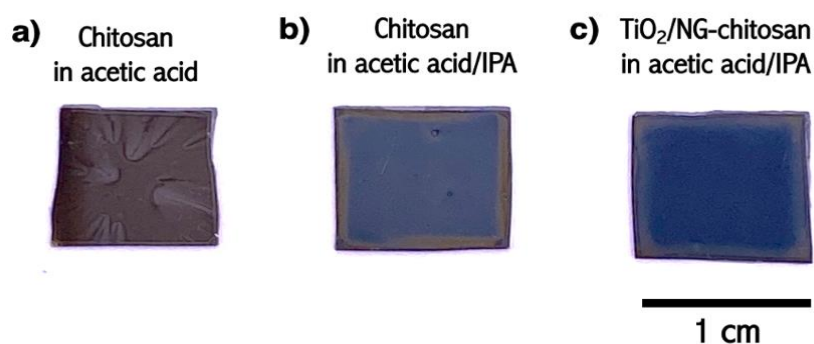
Figure 6.3 Photographs of spin-costed silicon wafer appearance of a) chitosan dissolved in acetic acid, b) chitosan dissolved in acetic acid/isopropanol, and c) chitosan with TiO$_2$/NG nanocomposite dispersed in acetic acid/isopropanol.

3.3 Laser desorption ionization mass spectrometry (LDI-MS) of chitosan film with TiO$_2$/NG

Figure 6.4 showed the performance of the TiO$_2$/NG in order to identify peptides using LDI-MS. As displayed in **Figure 6.4a**, the uncoated wafer showed relatively low S/N ratio (signal to noise ratio) compared to the TiO$_2$/NG nanocomposite-chitosan coated silicon wafer. The TiO$_2$/NG nanocomposite-chitosan coated silicon wafer was able to identify peptides which are bradykinin, angiotensin II, angiotensin I, bombesin, renin substrate, ACTH (18-39) with the molecular ion (M$^+$) of 791.276, 1017.094, 1294.569, 1633.144, 1757.133, and 2462.141, respectively (**Figure 6.4b**). Moreover, the silicon wafer with the developed nanocomposite-chitosan thin films provided high intensity of m/z with high S/N ratio with low background and interfering signals, implying that TiO$_2$/NG nanocomposite-

chitosan thin film can be used as a matrix for LDI-MS in order to determine biomarkers for medical diagnostic application.
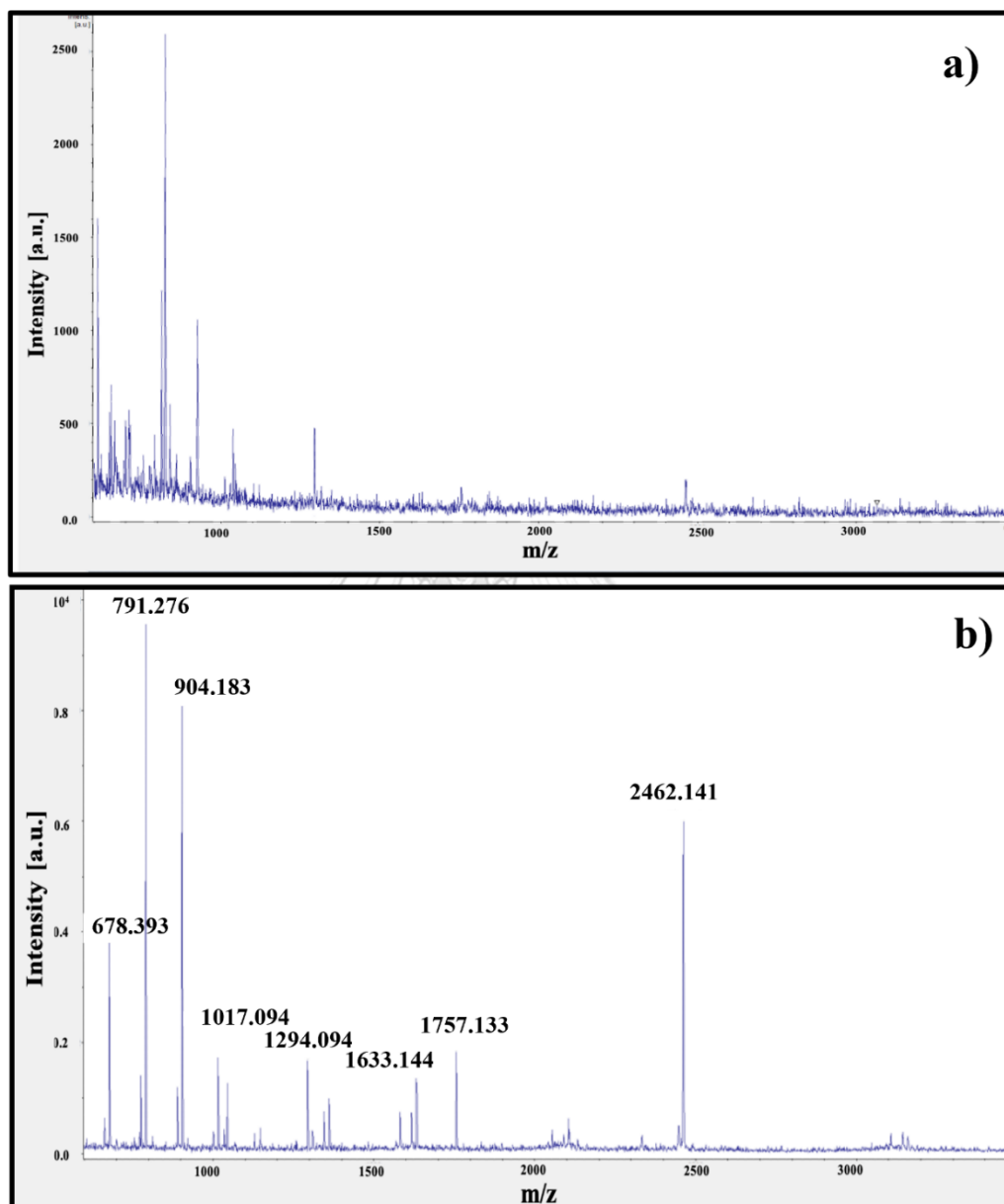
Figure 6.4 LDI-MS spectra of standard peptides determined using a) uncoated silicon wafer, and b) TiO$_2$/NG nanocomposite-chitosan coated silicon wafer.

Conclusion

Herein, TiO$_2$/NG nanocomposite-chitosan thin film was successfully fabricated on silicon wafer by spin-coating process for utilizing as LDI-MS matrix for peptide biomarker determination. The TiO$_2$/NG nanocomposite synthesized by hydrothermal method exhibited round-shaped with smaller particle size and higher homo-dispersity, compared to the pristine TiO$_2$. The developed thin film was subjected to LDI-MS to evaluate the peptide determination performance which the thin film can identify each type of peptides from standard peptide mixture with high intensity and S/N ratio. This might be concluded that the TiO$_2$/NG nanocomposite-chitosan thin film can be used as an alternative LDI-MS self-matrix for peptide biomarker determination for medical diagnosis.
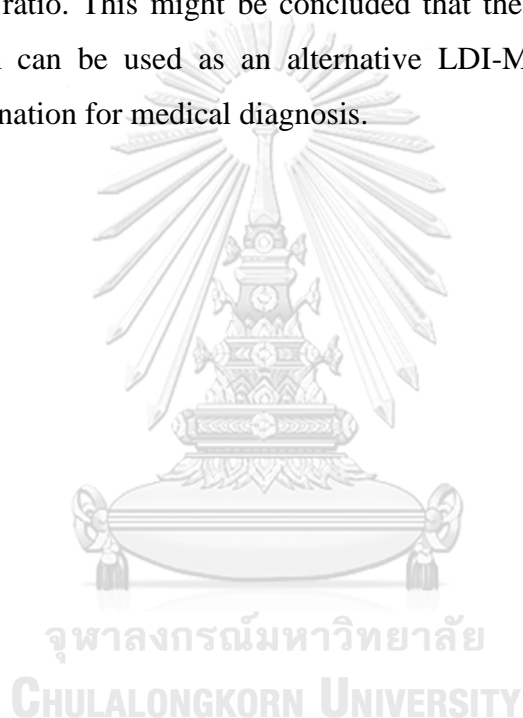
CHAPTER VII
CONCLUSIONS

In this dissertation, the properties of biopolymers (i.e., PLA, cellulose, chitosan) were altered by incorporating of nanomaterials (i.e., nanosized calcium carbonate calcium carbonate nanoparticles, graphene oxide and N-doped graphene) and bio-based nanomaterials. These biopolymer nanocomposites were applied for chemical sensors and substrates for laser desorption/ionization mass spectroscopy which can be exploited in food and healthcare application.

Part I: Colorimetric sensor and LDI-MS detection of biogenic amines in food spoilage based on porous PLA and graphene oxide

Highly porous PLA film was successfully fabricated by breath figure method integrated with nanosized calcium carbonate (NCC) addition. The NCC increased porosity of the film leading to higher entrapment efficiency for sensing element and higher color intensity of the colorimetric sensor towards putrescine and cadaverine. On the other side of dual platform, cellulose was employed as a substrate for LDI-MS by coating with GO providing specific and highly sensitive determination. The dual detection platform can be used for screening of food expiration date on smart packaging.

Part II: Bacterial cellulose-based hydrogel for colorimetric sensor of sweat pH and glucose

Bacterial nanocellulose (BC) was used for hydrogel preparation, then utilized as colorimetric sensor of sweat pH and glucose. Carboxymethyl cellulose (CMC) penetrated into bacterial nanocellulose network and coated on BC fibers resulting in high swelling ratio and re-swelling property. The colorimetric sweat pH and glucose sensors exhibited a rapid color change response, wide linearity with low LOD, and high accuracy. Hence, the BC/CMC hydrogel can be applied an alternative platform for non-invasive sensors for health monitoring.

Part III: Theranostic contact lens based on cellulose nanofibrils for ocular bacterial infection

Commercial contact lens, a polymeric substrate, was modified with cellulose nanofibrils-based composite and pH-sensitive dyes to create a theranostic contact lens

for ocular infection. Cellulose nanofibrils-levofloxacin nanocomposite was synthesized and deposited onto the tear pH-sensor based on commercial contact lens. The developed theranostic contact lens exhibited acid-responsive levofloxacin releasing with high drug content, and the contact lens displayed the vivid color change from green to orange when tear pH decreased corelated with infection severity that is useful for the disease diagnosis and treatment.

Part IV: Novel nanocomposite-chitosan film based on titanium dioxide/nitrogen-doped graphene nanocomposite for LDI-MS

Cationic chitosan thin films were prepared by spin-coating process on silicon wafer. By incorporating titanium dioxide/nitrogen-doped graphene nanocomposites (TiO_2/NG) having laser-absorbing property, which were readily synthesized using hydrothermal reaction, the obtained nanocomposite-chitosan thin films can be utilized in as a substrate of LDI-MS for sensitive and selective biomolecules determination.

Overall, incorporating of nanomaterials to biopolymers presented in this dissertation offers increased surface area, increased ionization efficiency and increased functionalities allowing for substantially improved detection efficiency in both chemical sensors and LDI-MS technique towards target analytes in food and healthcare.

REFERENCES

1.   Murariu, M. and P. Dubois, *PLA composites: From production to properties.* Advanced Drug Delivery Reviews, 2016. **107**: p. 17-46.

2.   Arrieta, M.P., et al. *On the Use of PLA-PHB Blends for Sustainable Food Packaging Applications*. Materials, 2017. **10**, DOI: 10.3390/ma10091008.

3.   Vandamme, E.J., et al., *Improved production of bacterial cellulose and its application potential.* Polymer Degradation and Stability, 1998. **59**(1): p. 93-99.

4.   Ullah, H., H.A. Santos, and T. Khan, *Applications of bacterial cellulose in food, cosmetics and drug delivery.* Cellulose, 2016. **23**(4): p. 2291-2314.

5.   Sharip, N.S. and H. Ariffin, *Cellulose nanofibrils for biomaterial applications.* Materials Today: Proceedings, 2019. **16**: p. 1959-1968.

6.   Soldano, C., A. Mahmood, and E. Dujardin, *Production, properties and potential of graphene.* Carbon, 2010. **48**(8): p. 2127-2150.

7.   Lee, C., et al., *Measurement of the Elastic Properties and Intrinsic Strength of Monolayer Graphene.* Science (New York, N.Y.), 2008. **321**: p. 385-8.

8.   Tiwari, S.K., et al., *Graphene research and their outputs: Status and prospect.* Journal of Science: Advanced Materials and Devices, 2020. **5**(1): p. 10-29.

9.   Loh, K.P., et al., *The chemistry of graphene.* Journal of Materials Chemistry, 2010. **20**(12): p. 2277-2289.

10.   Yu, W., et al., *Progress in the functional modification of graphene/graphene oxide: a review.* RSC Advances, 2020. **10**(26): p. 15328-15345.

11.   Dreyer, D.R., et al., *The chemistry of graphene oxide.* Chemical Society Reviews, 2010. **39**(1): p. 228-240.

12.   Zhang, Y., et al., *Interactions of graphene and graphene oxide with proteins and peptides.* 2013. **2**(1): p. 27-45.

13.   Hu, M. and B. Mi, *Layer-by-layer assembly of graphene oxide membranes via electrostatic interaction.* Journal of Membrane Science, 2014. **469**: p. 80-87.

14.   Wang, H., T. Maiyalagan, and X. Wang, *Review on Recent Progress in Nitrogen-Doped Graphene: Synthesis, Characterization, and Its Potential Applications.* ACS Catalysis, 2012. **2**(5): p. 781-794.

15.   Casanovas, J., et al., *Origin of the Large N 1s Binding Energy in X-ray*

Photoelectron Spectra of Calcined Carbonaceous Materials. Journal of the American Chemical Society, 1996. **118**(34): p. 8071-8076.

16.   Zhang, L. and Z. Xia, *Mechanisms of Oxygen Reduction Reaction on Nitrogen-Doped Graphene for Fuel Cells.* The Journal of Physical Chemistry C, 2011. **115**(22): p. 11170-11176.

17.   Simkiss, K., *Variations in the Crystalline Form of Calcium Carbonate precipitated from Artificial Sea Water.* Nature, 1964. **201**(4918): p. 492-493.

18.   Neikov, O.D., *Chapter 24 - Safety Engineering in the Production of Powders*, in *Handbook of Non-Ferrous Metal Powders*, O.D. Neikov, et al., Editors. 2009, Elsevier: Oxford. p. 551-595.

19.   Al Omari, M.M.H., et al., *Chapter Two - Calcium Carbonate*, in *Profiles of Drug Substances, Excipients and Related Methodology*, H.G. Brittain, Editor. 2016, Academic Press. p. 31-132.

20.   Trache, D., et al., *Nanocellulose: From Fundamentals to Advanced Applications.* Frontiers in Chemistry, 2020. **8**.

21.   Miyashiro, D., R. Hamano, and K. Umemura *A Review of Applications Using Mixed Materials of Cellulose, Nanocellulose and Carbon Nanotubes*. Nanomaterials, 2020. **10**, DOI: 10.3390/nano10020186.

22.   Gorgieva, S. and J. Trček *Bacterial Cellulose: Production, Modification and Perspectives in Biomedical Applications*. Nanomaterials, 2019. **9**,   DOI: 10.3390/nano9101352.

23.   Torres, F.G., J.J. Arroyo, and O.P. Troncoso, *Bacterial cellulose nanocomposites: An all-nano type of material.* Materials Science and Engineering: C, 2019. **98**: p. 1277-1293.

24.   Yi, T., et al. *From Cellulose to Cellulose Nanofibrils—A Comprehensive Review of the Preparation and Modification of Cellulose Nanofibrils*. Materials, 2020. **13**, DOI: 10.3390/ma13225062.

25.   Guo, Q., et al., *Fundamentals of TiO2 Photocatalysis: Concepts, Mechanisms, and Challenges.* Advanced Materials, 2019. **31**(50): p. 1901997.

26.   Zhao, Y., et al., *Synthesis and optical properties of TiO2 nanoparticles.* Materials Letters, 2007. **61**(1): p. 79-83.

27.   Reyes-Coronado, D., et al., *Phase-pure TiO$_2$ nanoparticles: anatase, brookite and rutile.* Nanotechnology, 2008. **19**(14): p. 145605.

28.   Chen, X. and A. Selloni, *Introduction: Titanium Dioxide (TiO2) Nanomaterials.* Chemical Reviews, 2014. **114**(19): p. 9281-9282.

29.   Topçu Şendoğdular, S., M. Pawar, and P. Gouma, *A Brief Overview of TiO 2 Photocatalyst for Organic Dye Remediation: Case Study of Reaction Mechanisms Involved in Ce-TiO 2 Photocatalysts System.* Journal of Nanomaterials, 2018. **2018**.

30.   Abdelhamid, H.N., *Nanoparticles Assisted Laser Desorption/Ionization Mass Spectrometry*, in *Handbook of Smart Materials in Analytical Chemistry*. 2019. p. 729-755.

31.   Abdelhamid, H.N., *Nanoparticle assisted laser desorption/ionization mass spectrometry for small molecule analytes.* Microchimica Acta, 2018. **185**(3): p. 200.

32.   Pomastowski, P. and B. Buszewski *Complementarity of Matrix- and Nanostructure-Assisted Laser Desorption/Ionization Approaches*. Nanomaterials, 2019. **9**, DOI: 10.3390/nano9020260.

33.   Shi, C.Y. and C.H. Deng, *Recent advances in inorganic materials for LDI-MS analysis of small molecules.* Analyst, 2016. **141**(10): p. 2816-2826.

34.   Chu, H.-W., et al., *Nanoparticle-based laser desorption/ionization mass spectrometric analysis of drugs and metabolites.* Journal of Food and Drug Analysis, 2018. **26**(4): p. 1215-1228.

35.   Wang, J., et al., *Recent progress in application of carbon nanomaterials in laser desorption/ionization mass spectrometry.* Analytical and Bioanalytical Chemistry, 2016. **408**(11): p. 2861-2873.

36.   de Sequeira, C.A. *Electrochemical Oxygen Sensors: A Preface to the Special Issue*. Oxygen, 2021. **1**, 73-76 DOI: 10.3390/oxygen1020008.

37.   Coyle, S., et al., *Chapter 2.1 - Wearable Bio and Chemical Sensors*, in *Wearable Sensors*, E. Sazonov and M.R. Neuman, Editors. 2014, Academic Press: Oxford. p. 65-83.

38.   Siripongpreda, T., N. Rodthongkum, and S. Ummartyotin, *A critical review on cellulose wastes as the novel substrates for colorimetric and electrochemical sensors.* Current Research in Green and Sustainable Chemistry, 2021. **4**: p. 100190.

39. Liu, B., J. Zhuang, and G. Wei, *Recent advances in the design of colorimetric sensors for environmental monitoring.* Environmental Science: Nano, 2020. **7**(8): p. 2195-2213.

40. Piriya V.S, A., et al., *Colorimetric sensors for rapid detection of various analytes.* Materials Science and Engineering: C, 2017. **78**: p. 1231-1245.

41. Kahlert, H., G. Meyer, and A. Albrecht, *Colour maps of acid–base titrations with colour indicators: how to choose the appropriate indicator and how to estimate the systematic titration errors.* ChemTexts, 2016. **2**(2): p. 7.

42. Abdessemed, A., et al., *Decolorization of methyl green and bromocresol purple in mono and binary systems by photochemical processes: direct UV photolysis, Acetone/UV and H2O2/UV. A comparative study.* 2016.

43. Rungsima, C., et al., *Hydrogel sensors with pH sensitivity.* Polymer Bulletin, 2021. **78**: p. 1-19.

44. Hemdan, S., A. Mansour, and F. Ali, *Importance of isosbestic point in spectroscopy: review.* 2019. **62**: p. 1-21.

45. Promphet, N., et al., *Non-invasive textile based colorimetric sensor for the simultaneous detection of sweat pH and lactate.* Talanta, 2019. **192**: p. 424-430.

46. Janošević, A., N. Paunovic, and N. Pejic, *Thermodynamics of micellization of hexadecyltrimethylammonium bromide in propylene glycol-water mixture: A conductivity study.* Facta universitatis - series: Physics, Chemistry and Technology, 2014. **12**: p. 17-26.

47. Lee, H., et al., *Enzyme-Based Glucose Sensor: From Invasive to Wearable Device.* Advanced Healthcare Materials, 2018. **7**(8): p. 1701150.

48. Liu, Y., L. Lei, and Z. Zhang, *An ultrasensitive colorimetric immunoassay based on glucose oxidase catalyzed cascade formation of blue–black iodine–starch complex.* Sensors and Actuators B: Chemical, 2017. **248**: p. 195-200.

49. Giri, B., *11 - Simultaneous Determination of Protein and Glucose in Urine Sample Using a Paper-Based Bioanalytical Device*, in *Laboratory Methods in Microfluidics*, B. Giri, Editor. 2017, Elsevier. p. 69-75.

50. Dang, W., et al., *Stretchable wireless system for sweat pH monitoring.* Biosensors and Bioelectronics, 2018. **107**: p. 192-202.

51.   Zhou, L. and R.W. Beuerman, *Tear analysis in ocular surface diseases.* Progress in Retinal and Eye Research, 2012. **31**(6): p. 527-550.

52.   Moreddu, R., et al., *Laser-inscribed contact lens sensors for the detection of analytes in the tear fluid.* Sensors and Actuators B: Chemical, 2020. **317**: p. 128183.

53.   Iyamu, E. and O. Enobakhare. *pH and Osmolality of Pre-corneal Tear Film and Commercially Available Artificial Tears.* 2019.

54.   Coles, W.H. and P.A. Jaros, *Dynamics of ocular surface pH.* Br J Ophthalmol, 1984. **68**(8): p. 549-52.

55.   Motelica, L., et al. *Smart Food Packaging Designed by Nanotechnological and Drug Delivery Approaches.* Coatings, 2020. **10**, DOI: 10.3390/coatings10090806.

56.   Kuswandi, B., et al., *Smart Packaging: Sensors for monitoring of food quality and safety.* Sensing and Instrumentation for Food Quality and Safety, 2011. **5**: p. 137-146.

57.   Drumright, R.E., P.R. Gruber, and D.E. Henton, *Polylactic Acid Technology.* Advanced Materials, 2000. **12**(23): p. 1841-1846.

58.   Galindo, S. and F. Ureña-Nuñez, *Enhanced surface hydrophobicity of poly(lactic acid) by Co60 gamma ray irradiation.* Revista Mexicana de Fisica, 2018. **64**: p. 1-7.

59.   Zhou, D., et al., *Effect of polar groups of polystyrenes on the self-assembly of breath figure arrays.* Journal of Polymer Science, 2022. **60**(15): p. 2371-2382.

60.   Zhang, A., H. Bai, and L. Li, *Breath Figure: A Nature-Inspired Preparation Method for Ordered Porous Films.* Chemical Reviews, 2015. **115**(18): p. 9801-9868.

61.   Siripongpreda, T., K. Siralertmukul, and N. Rodthongkum, *Colorimetric sensor and LDI-MS detection of biogenic amines in food spoilage based on porous PLA and graphene oxide.* Food Chemistry, 2020. **329**: p. 127165.

62.   Bormashenko, E. *Breath-Figure Self-Assembly, a Versatile Method of Manufacturing Membranes and Porous Structures: Physical, Chemical and Technological Aspects.* Membranes, 2017. **7**, DOI: 10.3390/membranes7030045.

63.   Santos, M.H.S., *Biogenic amines: their importance in foods.* International Journal of Food Microbiology, 1996. **29**(2): p. 213-231.

64.   Doeun, D., M. Davaatseren, and M.-S. Chung, *Biogenic amines in foods.* Food Science and Biotechnology, 2017. **26**(6): p. 1463-1474.

65.   del Rio, B., et al., *The biogenic amines putrescine and cadaverine show in vitro cytotoxicity at concentrations that can be found in foods.* Scientific Reports, 2019. **9**(1): p. 120.

66.   Erdag, D., O. Merhan, and B. Yıldız, *Biochemical and Pharmacological Properties of Biogenic Amines.* 2019.

67.   Deligkaris, K., et al., *Hydrogel-based devices for biomedical applications.* Sensors and Actuators B: Chemical, 2010. **147**(2): p. 765-774.

68.   Park, H. and K. Park, *Hydrogels in Bioapplications*, in *Hydrogels and Biodegradable Polymers for Bioapplications*. 1996, American Chemical Society. p. 2-10.

69.   Lim, T.M., M. Ulaganathan, and Q. Yan, *Chapter 14 - Advances in membrane and stack design of redox flow batteries (RFBs) for medium- and large-scale energy storage*, in *Advances in Batteries for Medium and Large-Scale Energy Storage*, C. Menictas, M. Skyllas-Kazacos, and T.M. Lim, Editors. 2015, Woodhead Publishing. p. 477-507.

70.   Fang, J.-H., *Chapter 7 - Polyimide Proton Exchange Membranes*, in *Advanced Polyimide Materials*, S.-Y. Yang, Editor. 2018, Elsevier. p. 323-383.

71.   Sievers, J., et al., *Determination of hydrogel swelling factors by two established and a novel non-contact continuous method.* Journal of Applied Polymer Science, 2021. **138**(18): p. 50326.

72.   Ahmed, E.M., *Hydrogel: Preparation, characterization, and applications: A review.* Journal of Advanced Research, 2015. **6**(2): p. 105-121.

73.   Benchabane, A. and B. Karim, *Rheological properties of carboxymethyl cellulose (CMC) solutions.* Colloid and Polymer Science, 2008. **286**: p. 1173-1180.

74.   Watcharamul, S., et al., *Effects of Carboxymethyl Cellulose/Nano-Calcium Carbonate Hydrogel Amendment of Loamy Sand Soil for Maize Growth.* ACS Agricultural Science & Technology, 2022. **2**(5): p. 1071-1080.

75.   Rahman, M.S., et al., *Recent Developments of Carboxymethyl Cellulose.* Polymers, 2021. **13**(8): p. 1345.

76.   Saiful, M., et al., *Biopolymer Electrolyte Based on Derivatives of Cellulose from Kenaf Bast Fiber.* Polymers, 2014. **6**: p. 2371-2385.

77.   Moreddu, R., D. Vigolo, and A.K. Yetisen, *Contact Lens Technology: From Fundamentals to Applications.* Advanced Healthcare Materials, 2019. **8**(15): p. 1900368.

78.   NICHOLS, J.J., *A status quo remains for much of the contact lens industry.* Contact Lens Spectrum, 2017. **32**: p. 22-25, 27, 29, 55.

79.   Farandos, N.M., et al., *Contact Lens Sensors in Ocular Diagnostics.* Advanced Healthcare Materials, 2015. **4**(6): p. 792-810.

80.   Musgrave, C.S. and F. Fang *Contact Lens Materials: A Materials Science Perspective.* Materials, 2019. **12**, DOI: 10.3390/ma12020261.

81.   Kim, E., M. Saha, and K. Ehrmann, *Mechanical Properties of Contact Lens Materials.* Eye & Contact Lens: Science & Clinical Practice, 2017. **44 Suppl 2**: p. 1.

82.   ChemicalBook, *Hilafilcon B*, ChemicalBook, Editor. 2022.

83.   Lim, E.-K., et al., *Nanomaterials for Theranostics: Recent Advances and Future Challenges.* Chemical Reviews, 2015. **115**(1): p. 327-394.

84.   Jeelani, S., et al., *Theranostics: A treasured tailor for tomorrow.* J Pharm Bioallied Sci, 2014. **6**(Suppl 1): p. S6-8.

85.   Anderson, V.R. and C.M. Perry, *Levofloxacin.* Drugs, 2008. **68**(4): p. 535-565.

86.   Lambert, A., J.-B. Regnouf-de-Vains, and M.F. Ruiz-López, *Structure of levofloxacin in hydrophilic and hydrophobic media: Relationship to its antibacterial properties.* Chemical Physics Letters, 2007. **442**(4): p. 281-284.

87.   Wang, W., et al., *Chitosan Derivatives and Their Application in Biomedicine.* International Journal of Molecular Sciences, 2020. **21**(2): p. 487.

88.   Kas, H.S., *Chitosan: Properties, preparations and application to microparticulate systems.* Journal of Microencapsulation, 1997. **14**(6): p. 689-711.

89.   Qin, Y., P. Li, and Z. Guo, *Cationic chitosan derivatives as potential antifungals: A review of structural optimization and applications.* Carbohydrate Polymers, 2020. **236**: p. 116002.

90.   Dodane, V. and V.D. Vilivalam, *Pharmaceutical applications of chitosan.* Pharmaceutical Science & Technology Today, 1998. **1**(6): p. 246-253.

91.   Hu, Y., et al., *Concentrations of biogenic amines in fish, squid and octopus and their changes during storage.* Food Chemistry, 2012. **135**(4): p. 2604-2611.

92.   Prester, L., *Chapter 22 - Biogenic amines in ready-to-eat foods.* Food Hygiene and Toxicology in Ready-to-Eat Foods, 2016: p. 397-416.

93.   Vinci, G. and M.L. Antonelli, *Biogenic amines: quality index of freshness in red and white meat.* Food Control, 2002. **13**(8): p. 519-524.

94.   Suzzi, G. and S. Torriani, *Editorial: Biogenic amines in foods.* Frontiers in Microbiology, 2015. **6**: p. 472.

95.   Kuswandi, B. and A. Nurfawaidi, *On-package dual sensors label based on pH indicators for real-time monitoring of beef freshness.* Food Control, 2017. **82**: p. 91-100.

96.   Lee, Y.-C., et al., *Determination of histamine in milkfish stick implicated in food-borne poisoning.* Journal of Food and Drug Analysis, 2016. **24**(1): p. 63-71.

97.   Sudalaimani, S., et al., *Colorimetric Sensing of Putrescine and Cadaverine Using Ninhydrin as a Food Spoilage Detection Reagent.* Food Analytical Methods, 2020. **13**(3): p. 629-636.

98.   Min, J.-S., et al., *Relationship between the Concentration of Biogenic Amines and Volatile Basic Nitrogen in Fresh Beef, Pork, and Chicken Meat.* 2007. **20**.

99.   Huang, X.-w., et al., *Determination of pork spoilage by colorimetric gas sensor array based on natural pigments.* Food Chemistry, 2014. **145**: p. 549-554.

100.   Farah, S., D.G. Anderson, and R. Langer, *Physical and mechanical properties of PLA, and their functions in widespread applications — A comprehensive review.* Advanced Drug Delivery Reviews, 2016. **107**: p. 367-392.

101.   Rodríguez-Hernández, J., *Chapter 4 - Nano-microporous structured surfaces prepared by the breath figures approach and their biorelated applications A2 - Grumezescu, Alexandru Mihai.* Surface Chemistry of Nanobiomaterials, 2016: p. 107-133.

102.   Rukchon, C., et al., *Development of a food spoilage indicator for monitoring freshness of skinless chicken breast.* Talanta, 2014. **130**: p. 547-554.

103.   Pablos, J.L., et al., *Solid Polymer Substrates and Coated Fibers Containing 2,4,6-Trinitrobenzene Motifs as Smart Labels for the Visual Detection of Biogenic Amine Vapors.* Chemistry – A European Journal, 2015. **21**(24): p. 8733-8736.

104.   Zhong, X., et al., *Rapid and ultrasensitive detection of biogenic amines with colorimetric sensor array.* Sensors and Actuators B: Chemical, 2018. **274**: p. 464-471.

105.   Zaragozá, P., et al., *Development of a colorimetric sensor array for squid spoilage assessment.* Food Chemistry, 2015. **175**: p. 315-321.

106.   Morsy, M.K., et al., *Development and validation of a colorimetric sensor array for fish spoilage monitoring.* Food Control, 2016. **60**: p. 346-352.

107.   Ahmad, A.N., et al., *A Colorimetric pH Sensor Based on Clitoria sp and Brassica sp for Monitoring of Food Spoilage Using Chromametry.* Sensors, 2019. **19**(21).

108.   Ding, L., et al., *A naked-eye detection polyvinyl alcohol/cellulose-based pH sensor for intelligent packaging.* Carbohydrate Polymers, 2020. **233**: p. 115859.

109.   Karas, M., et al., *Principles and applications of matrix-assisted UV-laser desorption/ionization mass spectrometry.* Analytica Chimica Acta, 1990. **241**(2): p. 175-185.

110.   Montesinos, I., et al., *Graphene-coated cotton fibers as a sorbent for the extraction of multiclass pesticide residues from water and their determination by gas chromatography with mass spectrometry.* Journal of Separation Science, 2014. **38**(5): p. 836-843.

111.   Wei, S.-C., et al., *Graphene oxide membrane as an efficient extraction and ionization substrate for spray-mass spectrometric analysis of malachite green and its metabolite in fish samples.* Analytica Chimica Acta, 2018. **1003**: p. 42-48.

112.   Liang, K., et al., *Graphene oxide aggregate-assisted LDI-MS for the direct analysis of triacylglycerol in complex biological samples.* Analytica Chimica Acta, 2018. **1035**(108118).

113.   Kong, X. and Y. Huang, *Applications of Graphene in Mass Spectrometry.* Journal of Nanoscience and Nanotechnology 2014. **14**(7): p. 4719-4732.

114.   Ding, L., et al., *Multi-length scale porous polymer films from hypercrosslinked breath figure arrays.* Journal of Colloid and Interface Science, 2016. **461**: p. 179-184.

115.   Sun, D., et al., *High performance supercapacitor electrode based on graphene paper via flame-induced reduction of graphene oxide paper.* Journal of Power Sources, 2013. **222**: p. 52-58.

116.   Park, S., et al., *Hydrazine-reduction of graphite- and graphene oxide.* Carbon, 2011. **49**(9): p. 3019-3023.

117.   Standardization, I.O.f., *ISO 10993-5:2009 Biological evaluation of medical devices - Part 5: Tests for in vitro cytotoxicity.* 2009.

118.   Cannella, V., et al., *Cytotoxicity Evaluation of Endodontic Pins on L929 Cell Line.* BioMed research international, 2019. **2019**: p. 3469525-3469525.

119.   Kim, Y.-K., et al., *Synergistic Effect of Graphene Oxide/MWCNT Films in Laser Desorption/Ionization Mass Spectrometry of Small Molecules and Tissue Imaging.* ACS Nano, 2011. **5**(6): p. 4550-4561.

120.   Gulbakan, B., et al., *A Dual Platform for Selective Analyte Enrichment and Ionization in Mass Spectrometry Using Aptamer-Conjugated Graphene Oxide.* Journal of the American Chemical Society, 2010. **132**(49): p. 17408-17410.

121.   Liu, Y., et al., *Graphene and graphene oxide: two ideal choices for the enrichment and ionization of long-chain fatty acids free from matrix-assisted laser desorption/ionization matrix interference.* Rapid Communications in Mass Spectrometry, 2011. **25**(21): p. 3223-3234.

122.   Oh, S.Y., et al., *Skin-Attachable, Stretchable Electrochemical Sweat Sensor for Glucose and pH Detection.* ACS Applied Materials & Interfaces, 2018. **10**(16): p. 13729-13740.

123.   Toghill, K.E. and R.G. Compton, *Electrochemical Non-enzymatic Glucose Sensors: A Perspective and an Evaluation.* International Journal of ELECTROCHEMICAL SCIENCE, 2010. **5**: p. 1246 - 1301.

124.   Hwang, E.T. and M.B. Gu, *Enzyme stabilization by nano/microsized hybrid materials.* Engineering in Life Sciences, 2013. **13**(1): p. 49-61.

125.   Zhang, Y., et al., *Passive sweat collection and colorimetric analysis of biomarkers relevant to kidney disorders using a soft microfluidic system.* Lab on a Chip, 2019. **19**(9): p. 1545-1555.

126.   Caldara, M., et al., *Optical monitoring of sweat pH by a textile fabric wearable sensor based on covalently bonded litmus-3-glycidoxypropyltrimethoxysilane coating.* Sensors and Actuators B: Chemical, 2016. **222**: p. 213-220.

127.   Khattab, T.A., et al., *Smart microfibrillated cellulose as swab sponge-like aerogel for real-time colorimetric naked-eye sweat monitoring.* Talanta, 2019. **205**: p. 120166.

128.   Corrie, S.R., et al., *Blood, sweat, and tears: developing clinically relevant protein biosensors for integrated body fluid analysis.* Analyst, 2015. **140**(13): p. 4350-4364.

129.   Xiao, G., et al., *A wearable, cotton thread/paper-based microfluidic device coupled with smartphone for sweat glucose sensing.* Cellulose, 2019. **26**(7): p. 4553-4562.

130.   Jadoon, S., et al., *Recent Developments in Sweat Analysis and Its Applications.* International Journal of Analytical Chemistry, 2015. **2015**: p. 1-7.

131.   Saxena, I.M. and R.M. Brown, *Biosynthesis of Cellulose*, in *Progress in Biotechnology*, N. Morohoshi and A. Komamine, Editors. 2001, Elsevier. p. 69-76.

132.   Boobphahom, S., et al., *A copper oxide-ionic liquid/reduced graphene oxide composite sensor enabled by digital dispensing: Non-enzymatic paper-based microfluidic determination of creatinine in human blood serum.* Analytica Chimica Acta, 2019. **1083**: p. 110-118.

133.   Ruecha, N., et al., *Kenaf cellulose-based 3D printed device: a novel colorimetric sensor for Ni(II).* Cellulose, 2020. **27**(9): p. 5211-5222.

134.   Pircher, N., et al., *Reinforcement of bacterial cellulose aerogels with biocompatible polymers.* Carbohydrate Polymers, 2014. **111**: p. 505-513.

135.   de Oliveira Barud, H.G., et al., *A multipurpose natural and renewable polymer in medical applications: Bacterial cellulose.* Carbohydrate Polymers, 2016. **153**: p. 406-420.

136.   Korhonen, J.T., et al., *Inorganic Hollow Nanotube Aerogels by Atomic Layer Deposition onto Native Nanocellulose Templates.* ACS Nano, 2011. **5**(3): p. 1967-1974.

137.   Chen, H.-H., et al., *In situ modification of bacterial cellulose nanostructure by adding CMC during the growth of Gluconacetobacter xylinus.* Cellulose, 2011. **18**(6): p. 1573-1583.

138.   de Lima Fontes, M., et al., *Effect of in situ modification of bacterial cellulose with carboxymethylcellulose on its nano/microstructure and methotrexate release properties.* Carbohydrate Polymers, 2018. **179**: p. 126-134.

139.   Huang, H.-C., et al., *In situ modification of bacterial cellulose network structure by adding interfering substances during fermentation.* Bioresource Technology, 2010.

101(15): p. 6084-6091.

140. Bellasio, C., A. Fini, and F. Ferrini, *Evaluation of a high throughput starch analysis optimised for wood.* PloS one, 2014. **9**(2).

141. Foster, L.S. and I.J. Gruntfest, *Demonstration experiments using universal indicators.* Journal of Chemical Education, 1937. **14**(6): p. 274.

142. Nakayama, A., et al., *High Mechanical Strength Double-Network Hydrogel with Bacterial Cellulose.* Advanced Functional Materials, 2004. **14**(11): p. 1124-1128.

143. Roy, J.C., et al., *Chitosan‑Carboxymethylcellulose-Based Polyelectrolyte Complexation and Microcapsule Shell Formulation.* International journal of molecular sciences, 2018. **19**(9): p. 2521.

144. Zhijiang, C. and Y. Guang, *Bacterial cellulose/collagen composite: Characterization and first evaluation of cytocompatibility.* Journal of Applied Polymer Science, 2011. **120**(5): p. 2938-2944.

145. Dayal, M.S. and J.M. Catchmark, *Mechanical and structural property analysis of bacterial cellulose composites.* Carbohydrate polymers, 2016. **144**: p. 447-453.

146. Cheng, K.-C., J.M. Catchmark, and A. Demirci, *Effects of CMC addition on bacterial cellulose production in a biofilm reactor and its paper sheets analysis.* Biomacromolecules, 2011. **12**(3): p. 730-736.

147. Ben-Hayyim, G. and I. Ohad, *Synthesis of cellulose by Acetobacter xylinum: VIII. On the formation and orientation of bacterial cellulose fibrils in the presence of acidic polysaccharides.* The Journal of cell biology, 1965. **25**(2): p. 191-207.

148. El-Sakhawy, M., et al., *THERMAL PROPERTIES OF CARBOXYMETHYL CELLULOSE ACETATE BUTYRATE.* CELLULOSE CHEMISTRY AND TECHNOLOGY, 2019. **53**(7-8): p. 667-675.

149. Zhang, J., et al., *Immobilization of lecithin on bacterial cellulose nanofibers for improved biological functions.* Reactive and Functional Polymers, 2015. **91-92**: p. 100-107.

150. Kuswandi, B., et al., *A Novel On-Package Sticker Sensor Based on Methyl Red for Real-Time Monitoring of Broiler Chicken Cut Freshness.* Packaging Technology and Science, 2014. **27**(1): p. 69-81.

151. Kuswandi, B., et al., *A novel colorimetric food package label for fish spoilage*

based on polyaniline film. Food Control, 2012. **25**(1): p. 184-189.

152. Kuswandi, B., et al., *Real time on-package freshness indicator for guavas packaging.* Journal of Food Measurement and Characterization, 2013. **7**(1): p. 29-39.

153. Pourjavaher, S., et al., *Development of a colorimetric pH indicator based on bacterial cellulose nanofibers and red cabbage (Brassica oleraceae) extract.* Carbohydrate Polymers, 2017. **156**: p. 193-201.

154. Lu, K., et al., *Removal of color from textile dyeing wastewater by foam separation.* Journal of hazardous materials, 2010. **182**(1-3): p. 928-932.

155. Rottman, C., et al., *Doped sol-gel glasses as pH sensors.* Materials Letters, 1992. **13**(6): p. 293-298.

156. El-Ashgar, N., et al., *Sol-Gel Thin Films Immobilized with Bromocresol Purple pH-Sensitive Indicator in Presence of Surfactants.* ISRN Analytical Chemistry, 2012. **2012**.

157. Carlsson, S., et al., *Effects of pH, Nitrite, and Ascorbic Acid on Nonenzymatic Nitric Oxide Generation and Bacterial Growth in Urine.* Nitric Oxide, 2001. **5**(6): p. 580-586.

158. Bono, M.J. and W.C. Reygaert, *Urinary Tract Infection.* 2020, StatPearls Publishing LLC.

159. Abelson, M.B., I.J. Udell, and J.H. Weston, *Normal Human Tear pH by Direct Measurement.* JAMA Ophthalmology, 1981. **99**(2): p. 301-301.

160. Roblegg, E., A. Coughran, and D. Sirjani, *Saliva: An all-rounder of our body.* European Journal of Pharmaceutics and Biopharmaceutics, 2019. **142**: p. 133-141.

161. Baliga, S., S. Muglikar, and R. Kale, *Salivary pH: A diagnostic biomarker.* Journal of Indian Society of Periodontology, 2013. **17**(4): p. 461-465.

162. Wan, Y., et al., *Mechanical, moisture absorption, and biodegradation behaviours of bacterial cellulose fibre-reinforced starch biocomposites.* Composites Science and Technology, 2009. **69**(7-8): p. 1212-1217.

163. Bruen, D., et al., *Glucose Sensing for Diabetes Monitoring: Recent Developments.* Sensors, 2017. **17**: p. 1866.

164. Garcia, B.H., et al., *Antibody microarray analysis of inflammatory mediator release by human leukemia T-cells and human non small cell lung cancer cells.* Journal

of biomolecular techniques : JBT, 2007. **18**(4): p. 245-251.

165. Koh, A., et al., *A soft, wearable microfluidic device for the capture, storage, and colorimetric sensing of sweat.* Science Translational Medicine, 2016. **8**: p. 366ra165-366ra165.

166. Liu, M.-M., et al., *A colorimetric assay for sensitive detection of hydrogen peroxide and glucose in microfluidic paper-based analytical devices integrated with starch-iodide-gelatin system.* Talanta, 2019. **200**: p. 511-517.

167. Aksorn, J. and S. Teepoo, *Development of the simultaneous colorimetric enzymatic detection of sucrose, fructose and glucose using a microfluidic paper-based analytical device.* Talanta, 2020. **207**: p. 120302.

168. Uddin, K.M.A., et al., *Disposable Microfluidic Sensor Based on Nanocellulose for Glucose Detection.* Global Challenges, 2019. **3**(2): p. 1800079.

169. Moreddu, R., et al., *Integration of paper microfluidic sensors into contact lenses for tear fluid analysis.* Lab on a Chip, 2020. **20**(21): p. 3970-3979.

170. Norn, M.S., *Human Tear pH.* 1977. **95**(1): p. 170-170.

171. Iyamu, E. and O. Enobakhare, *pH and Osmolality of Pre-corneal Tear Film and Commercially Available Artificial Tears.* 2019, EC Ophthalmology. p. 17-25.

172. Badugu, R., et al., *Contact lens to measure individual ion concentrations in tears and applications to dry eye disease.* Analytical Biochemistry, 2018. **542**: p. 84-94.

173. Coles, W.H. and P.A. Jaros, *Dynamics of ocular surface pH.* The British journal of ophthalmology, 1984. **68**(8): p. 549-552.

174. Stephanie, W., C.-A. Maria, and K. Pauline, *Common eye infections.* 2018, A ustralian prescriber

175. Attisano, C., et al., *Severe Ocular Bacterial Infections: A Retrospective Study Over 13 Years.* Ocular Immunology and Inflammation, 2017. **25**(6): p. 825-829.

176. Patel, A., et al., *Ocular drug delivery systems: An overview.* World journal of pharmacology, 2013. **2**(2): p. 47-64.

177. Bandello, F., et al., *One week of levofloxacin plus dexamethasone eye drops for cataract surgery: an innovative and rational therapeutic strategy.* Eye, 2020. **34**(11): p. 2112-2122.

178. Paradiso, P., et al., *Controlled Release of Antibiotics From Vitamin E–Loaded*

Silicone-Hydrogel Contact Lenses. Journal of Pharmaceutical Sciences, 2016. **105**(3): p. 1164-1172.

179.   Torres-Luna, C., et al., *Extended delivery of non-steroidal anti-inflammatory drugs through contact lenses loaded with Vitamin E and cationic surfactants.* Contact Lens and Anterior Eye, 2019. **42**(5): p. 546-552.

180.   Jung, H.J. and A. Chauhan, *Temperature sensitive contact lenses for triggered ophthalmic drug delivery.* Biomaterials, 2012. **33**(7): p. 2289-2300.

181.   Silvera-Tawil, D., M.S. Hussain, and J. Li, *Emerging technologies for precision health: An insight into sensing technologies for health and wellbeing.* Smart Health, 2020. **15**: p. 100100.

182.   Promphet, N., et al., *Non-invasive wearable chemical sensors in real-life applications.* Analytica Chimica Acta, 2021: p. 338643.

183.   Xu, J., et al., *A comprehensive review on contact lens for ophthalmic drug delivery.* Journal of Controlled Release, 2018. **281**: p. 97-118.

184.   Mutlu, Z., S. Shams Es-haghi, and M. Cakmak, *Recent Trends in Advanced Contact Lenses.* Advanced Healthcare Materials, 2019. **8**(10): p. 1801390.

185.   Shetty, Y., P. Prabhu, and B. Prabhakar, *Emerging vistas in theranostic medicine.* International Journal of Pharmaceutics, 2019. **558**: p. 29-42.

186.   Shete, M.B., et al., *Current trends in theranostic nanomedicines.* Journal of Drug Delivery Science and Technology, 2022. **71**: p. 103280.

187.   Choi, K.Y., et al., *Theranostic nanoplatforms for simultaneous cancer imaging and therapy: current approaches and future perspectives.* Nanoscale, 2012. **4**(2): p. 330-342.

188.   Smyth, M., et al., *Tunable Structural and Mechanical Properties of Cellulose Nanofiber Substrates in Aqueous Conditions for Stem Cell Culture.* Biomacromolecules, 2017. **18**(7): p. 2034-2044.

189.   Chinga-Carrasco, G., *Potential and Limitations of Nanocelluloses as Components in Biocomposite Inks for Three-Dimensional Bioprinting and for Biomedical Devices.* Biomacromolecules, 2018. **19**(3): p. 701-711.

190.   Sakwises, L., N. Rodthongkum, and S. Ummartyotin, *SnO2- and bacterial-cellulose nanofiber-based composites as a novel platform for nickel-ion detection.*

Journal of Molecular Liquids, 2017. **248**: p. 246-252.

191. Teekayupak, K., et al., *Flexible cotton-AuNP thread electrode for non-enzymatic sensor of uric acid in urine.* Cellulose, 2021. **28**(16): p. 10501-10515.

192. Phamonpon, W., et al., *Development of electrochemical paper-based analytical sensor from UHT milk packaging waste.* Journal of Materials Science: Materials in Electronics, 2020. **31**(13): p. 10855-10864.

193. Promphet, N., et al., *Cotton thread-based wearable sensor for non-invasive simultaneous diagnosis of diabetes and kidney failure.* Sensors and Actuators B: Chemical, 2020. **321**: p. 128549.

194. Promphet, N., et al., *Thread-Based Wristwatch Sensing Device for Noninvasive and Simultaneous Detection of Glucose and Lactate.* Advanced Materials Technologies, 2022. **7**(6): p. 2101684.

195. Passornraprasit, N., et al., *γ-Irradiation crosslinking of graphene oxide/cellulose nanofiber/poly (acrylic acid) hydrogel as a urea sensing patch.* International Journal of Biological Macromolecules, 2022. **213**: p. 1037-1046.

196. Du, H., et al., *Cellulose nanocrystals and cellulose nanofibrils based hydrogels for biomedical applications.* Carbohydrate Polymers, 2019. **209**: p. 130-144.

197. Durand, H., et al., *Pure cellulose nanofibrils membranes loaded with ciprofloxacin for drug release and antibacterial activity.* Cellulose, 2020. **27**(12): p. 7037-7052.

198. Anirudhan, T.S., V. Manjusha, and V. Chithra Sekhar, *A new biodegradable nano cellulose-based drug delivery system for pH-controlled delivery of curcumin.* International Journal of Biological Macromolecules, 2021. **183**: p. 2044-2054.

199. Sampath Udeni Gunathilake, T.M., et al., *Recent advances in celluloses and their hybrids for stimuli-responsive drug delivery.* International Journal of Biological Macromolecules, 2020. **158**: p. 670-688.

200. Dong, H., et al., *Cation-Induced Hydrogels of Cellulose Nanofibrils with Tunable Moduli.* Biomacromolecules, 2013. **14**(9): p. 3338-3345.

201. Raghav, N., M.R. Sharma, and J.F. Kennedy, *Nanocellulose: A mini-review on types and use in drug delivery systems.* Carbohydrate Polymer Technologies and Applications, 2021. **2**: p. 100031.

202.   Orasugh, J.T., et al., *Jute cellulose nano-fibrils/hydroxypropylmethylcellulose nanocomposite: A novel material with potential for application in packaging and transdermal drug delivery system.* Industrial Crops and Products, 2018. **112**: p. 633-643.

203.   Hivechi, A., S.H. Bahrami, and R.A. Siegel, *Drug release and biodegradability of electrospun cellulose nanocrystal reinforced polycaprolactone.* Materials Science and Engineering: C, 2019. **94**: p. 929-937.

204.   Li, J., et al., *Nanocellulose-Based Antibacterial Materials.* Advanced Healthcare Materials, 2018. **7**(20): p. 1800334.

205.   Chen, T., et al., *Synthesis and drug delivery properties of Ibuprofen-Cellulose nanofibril system.* International Journal of Biological Macromolecules, 2021. **182**: p. 931-937.

206.   Long, W., et al., *Simultaneous surface functionalization and drug loading: A novel method for fabrication of cellulose nanocrystals-based pH responsive drug delivery system.* International Journal of Biological Macromolecules, 2021. **182**: p. 2066-2075.

207.   Raghav, N. and M.R. Sharma, *Usage of nanocrystalline cellulose phosphate as novel sustained release system for anti-inflammatory drugs.* Journal of Molecular Structure, 2021. **1233**: p. 130108.

208.   Qu, P., et al., *Surface modification of cellulose nanofibrils for poly(lactic acid) composite application.* Journal of Applied Polymer Science, 2012. **125**(4): p. 3084-3091.

209.   Sarkar, G., et al., *Cellulose nanofibrils/chitosan based transdermal drug delivery vehicle for controlled release of ketorolac tromethamine.* New Journal of Chemistry, 2017. **41**(24): p. 15312-15319.

210.   Dafale, N.A., et al., *Development and validation of microbial bioassay for quantification of Levofloxacin in pharmaceutical preparations.* Journal of Pharmaceutical Analysis, 2015. **5**(1): p. 18-26.

211.   Bhardwaj, V., et al., *Drug–surfactant interaction: thermo-acoustic investigation of sodium dodecyl sulfate and antimicrobial drug (levofloxacin) for potential pharmaceutical application.* RSC Advances, 2014. **4**(47): p. 24935-24943.

212.   Saher, O., D. Ghorab, and N. Mursi, *Preparation and in vitro/in vivo evaluation*

of antimicrobial ocular in situ gels containing a disappearing preservative for topical treatment of bacterial conjunctivitis. Pharmaceutical development and technology, 2015. **21**: p. 1-11.

213. Davis, R. *Fourier tansform infrared (FT-IR) spectroscopy: A rapid tool for detection and analysis of foodborne pathogenic bacteria.* 2010.

214. Lai, C.-F., et al., *UV and blue-light anti-reflective structurally colored contact lenses based on a copolymer hydrogel with amorphous array nanostructures.* RSC Advances, 2018. **8**(8): p. 4006-4013.

215. Siripongpreda, T., et al., *Bacterial cellulose-based re-swellable hydrogel: Facile preparation and its potential application as colorimetric sensor of sweat pH and glucose.* Carbohydrate Polymers, 2021. **256**: p. 117506.

216. Abelson, M.B., I.J. Udell, and J.H. Weston, *Normal Human Tear pH by Direct Measurement.* Archives of Ophthalmology, 1981. **99**(2): p. 301-301.

217. Norn, M.S., *HYDROGEN ION CONCENTRATION OF TEAR FLUID.* Acta Ophthalmologica, 1968. **46**(2): p. 189-200.

218. McLaughlin, R.P., *Spectroscopy: Overview* ☆, in *Encyclopedia of Dairy Sciences (Third Edition)*, P.L.H. McSweeney and J.P. McNamara, Editors. 2022, Academic Press: Oxford. p. 591-599.

219. Hirano, T., et al., *Mechanism of the inhibitory effect of zwitterionic drugs (levofloxacin and grepafloxacin) on carnitine transporter (OCTN2) in Caco-2 cells.* Biochimica et Biophysica Acta (BBA) - Biomembranes, 2006. **1758**(11): p. 1743-1750.

220. Paradiso, P., et al., *Controlled Release of Antibiotics From Vitamin E–Loaded Silicone-Hydrogel Contact Lenses.* Journal of Pharmaceutical Sciences, 2016. **105**.

221. Maulvi, F.A., et al., *Contact lenses with dual drug delivery for the treatment of bacterial conjunctivitis.* International Journal of Pharmaceutics, 2018. **548**(1): p. 139-150.

222. Kaplan, A.P. and C. Maas, *The Search for Biomarkers in Hereditary Angioedema.* Frontiers in Medicine, 2017. **4**.

223. Bellucci, F., et al., *Synovial fluid levels of bradykinin correlate with biochemical markers for cartilage degradation and inflammation in knee osteoarthritis.* Osteoarthritis and Cartilage, 2013. **21**(11): p. 1774-1780.

224. Ozkan, S. and A. Ipekci, *Serum Angiotensin II as a Biomarker in COVID-19*, in *Biomarkers in Trauma, Injury and Critical Care*, R. Rajendram, V.R. Preedy, and V.B. Patel, Editors. 2022, Springer International Publishing: Cham. p. 1-24.

225. Rhodes, M.E., *Chapter 10 - Adrenocorticotropic Hormone*, in *Stress: Neuroendocrinology and Neurobiology*, G. Fink, Editor. 2017, Academic Press: San Diego. p. 109-116.

226. Carroll, B.J., et al., *Pathophysiology of hypercortisolism in depression.* Acta Psychiatrica Scandinavica, 2007. **115**(s433): p. 90-103.

227. Bhandari, A. and V. Bhandari, *Biomarkers in Bronchopulmonary Dysplasia.* Paediatric Respiratory Reviews, 2013. **14**(3): p. 173-179.

228. Rangarajan, G., et al., *Present applications of titanium dioxide for the photocatalytic removal of pollutants from water: A review.* Journal of Environmental Management, 2020. **270**.

229. Piler, K., et al., *Chapter Two - Lattice disorders of TiO2 and their significance in the photocatalytic conversion of CO2*, in *Advances in Catalysis*, C. Song, Editor. 2020, Academic Press. p. 109-233.

230. Zhen, Z. and H. Zhu, *1 - Structure and Properties of Graphene*, in *Graphene*, H. Zhu, et al., Editors. 2018, Academic Press. p. 1-12.

231. Kim, M.-J., et al., *Coffee Ring Effect Free TiO2 Nanotube Array for Quantitative Laser Desorption/Ionization Mass Spectrometry.* ACS Applied Nano Materials, 2020. **3**(9): p. 9249-9259.

232. Aranaz, I., et al. *Chitosan: An Overview of Its Properties and Applications*. Polymers, 2021. **13**, DOI: 10.3390/polym13193256.

233. Hidayat, R., G. Fadillah, and S. Wahyuningsih, *A control of TiO_2 nanostructures by hydrothermal condition and their application: a short review.* IOP Conference Series: Materials Science and Engineering, 2019. **578**(1): p. 012031.

234. Pace, G., et al., *Nitrogen-doped graphene based triboelectric nanogenerators.* Nano Energy, 2021. **87**: p. 106173.

VITA

NAME   Tatiya Siripongpreda

DATE OF BIRTH   22 August 1993

PLACE OF BIRTH   Bangkok

INSTITUTIONS   Bachelor of Environmental Science (with honors) in 2016
ATTENDED   Faculty of Science, Chulalongkorn University, Bangkok,
                                 Thailand

HOME ADDRESS   122 Banmo Rd., Phranakorn, Bangkok, 10200 Thailand

PUBLICATION   1. Siripongpreda, T., Siralertmukul, K., & Rodthongkum,
                                 N. (2020). Colorimetric sensor and LDI-MS detection of
                                 biogenic amines in food spoilage based on porous PLA
                                 and graphene oxide. Food Chemistry, 329, 127165. (2019
                                 Impact factor: 6.306, Q1, T1)

                                 2. Siripongpreda, T., Somchob, B., Rodthongkum, N., &
                                 Hoven, P.V. (2021). Bacterial cellulose-based re-swellable
                                 hydrogel: Facile preparation and its potential application
                                 as colorimetric sensor of sweat pH and glucose.
                                 Carbohydrate polymers, 256, 117506. (2019 Impact factor:
                                 7.182, Q1, T1)

                                 3. Boobphahom, S., Siripongpreda, T., Zhang, D., Qin, J.,
                                 Rattanawaleedirojn, P., & Rodthongkum, N. (2021).
                                 TiO2/MXene-PVA/GO hydrogel based electrochemical
                                 sensor for neurological disorder screening via urinary
                                 norepinephrine detection. Microchimica acta, 188, 387.
                                 (2020 Impact factor: 5.833, Q1)

                                 4. Phookum, T., Siripongpreda, T., Rodthongkum, N., &
                                 Ummartyotin, S. (2021) Development of cellulose from
                                 recycled office waste paper-based composite as a platform
                                 for the colorimetric sensor in food spoilage indicator.
                                 Journal of Polymer Research, 28, 416. (2021 Impact
                                 factor: 3.097, Q2)

                                 5. Siripongpreda, T., Rodthongkum, N., & Ummartyotin,
                                 S. (2021). A critical review on cellulose wastes as the
                                 novel substrates for colorimetric and electrochemical
                                 sensors. Current Research in Green and Sustainable
                                 Chemistry, 100190. (2021 Impact factor 4.714, Q2)

                                 6. Nuisin, R., Siripongpreda, T., Watcharamul, S.,

Siralertmukul, K., & Kiatkamjornwong, S. (2022). Facile syntheses of physically crosslinked carboxymethyl cellulose hydrogels and nanocomposite hydrogels for enhancing water absorbency and adsorption of Sappan wood dye. ChemistrySelect, 7, e202104598. (2021 Impact factor 2.109, Q2)

7. Passornraprasit, N., Siripongpreda, T., Ninlapruk, S., Rodthongkum, N., & Potiyaraj, P. (2022). γ-Irradiation crosslinking of graphene oxide/cellulose nanofiber/poly (acrylic acid) hydrogel as a urea sensing patch. International Journal of Biological Macromolecules, 213, 1037-1046. (2021 Impact factor 8.025, Q1, T1)

8. Watcharamul, S., Lerddamrongchai, S., Siripongpreda, T., Rodtassana, C., Nuisin, R., & Kiatkamjornwong, S. (2022). Effects of Carboxymethyl Cellulose/Nano-Calcium Carbonate Hydrogel Amendment of Loamy Sand Soil for Maize Growth. ACS Agricultural Science & Technology, 2 (5), 1071–1080. Published

AWARD RECEIVED   1. Best Poster Award - RSC Tokyo International Conference 2022, Tokyo, Japan

2. Selected participant : Global Young Scientists Summit 2021,
National Research Foundation, Prime Minister Office, Singapore

จุฬาลงกรณ์มหาวิทยาลัย

CHULALONGKORN UNIVERSITY